

INFORMATION TO USERS

This manuscript has been reproduced from the microfilm master. UMI films the text directly from the original or copy submitted. Thus, some thesis and dissertation copies are in typewriter face, while others may be from any type of computer printer.

The quality of this reproduction is dependent upon the quality of the copy submitted. Broken or indistinct print, colored or poor quality illustrations and photographs, print bleedthrough, substandard margins, and improper alignment can adversely affect reproduction.

In the unlikely event that the author did not send UMI a complete manuscript and there are missing pages, these will be noted. Also, if unauthorized copyright material had to be removed, a note will indicate the deletion.

Oversize materials (e.g., maps, drawings, charts) are reproduced by sectioning the original, beginning at the upper left-hand corner and continuing from left to right in equal sections with small overlaps. Each original is also photographed in one exposure and is included in reduced form at the back of the book.

Photographs included in the original manuscript have been reproduced xerographically in this copy. Higher quality 6" x 9" black and white photographic prints are available for any photographs or illustrations appearing in this copy for an additional charge. Contact UMI directly to order.

UMI

**A Bell & Howell Information Company
300 North Zeeb Road, Ann Arbor, MI 48106-1346 USA
313/761-4700 800/521-0600**

NORTHWESTERN UNIVERSITY

Morphology Transformations In Nanoparticles

A DISSERTATION

SUBMITTED TO THE GRADUATE SCHOOL

IN PARTIAL FULFILLMENT OF THE REQUIREMENTS

for the degree of

DOCTOR OF PHILOSOPHY

Field of Materials Science and Engineering

By

Doraiswamy Narayanaswamy, D.

Evanston, Illinois

June 1995

Ph.D.

UMI Number: 9537483

**Copyright 1995 by
Narayanaswamy, Doraiswamy
All rights reserved.**

**UMI Microform 9537483
Copyright 1995, by UMI Company. All rights reserved.**

**This microform edition is protected against unauthorized
copying under Title 17, United States Code.**

UMI

**300 North Zeeb Road
Ann Arbor, MI 48103**

© Copyright by Doraiswamy Narayanaswamy 1995

All Rights Reserved

ABSTRACT

Morphology Transformations in Nanoparticles

Doraiswamy Narayanaswamy

Small particles exhibit a wide variety of structures which range from the well-known single crystals to the multiply twinned particles, such as the decahedral and icosahedral multiply twinned configurations. Interestingly, all these structures have very little energy differences between them and easily transform from one to the other. This thesis addresses the nature of these morphology transformations.

In the first part, morphological transformations of Au particles supported on SiO were observed by real time High Resolution Electron Microscopy (HREM). The data were analyzed quantitatively to extract the relative probabilities of different morphologies and compared with a probability model to understand the role of the different parameters that affect the transformations. The experimental data and probability model are consistent and reveal several interesting trends.

The single crystal (Sc) population dominates over the icosahedral multiply twinned particles (Ic) and the decahedral multiply twinned particles (Dc) over the observed size regimes of 2nm to 8nm. The Ic shows a maximum in relative probability of occurrence at smaller sizes whereas the Dc probability increases with size leading to a

transition region centered at 6.5nm particle diameter at which the Dc and Ic show almost equal relative probabilities. The morphology transformations are also affected by the surface stress and anisotropy of the surface free energies. A means of obtaining the rate of kinetic transformations in small particles was also formulated and applied to the Au/SiO system.

These analytical and experimental techniques were then applied to the Ag/Si(100) system and a quantitative morphology analysis revealed that the Ag islands do not have the conventionally accepted single crystal morphology. Instead they exhibit a mixed morphology state. The morphology populations are strongly affected by the substrate-particle interaction. The Sc population showed a rapid increase with size while the Dc content decreased with size. Under Ultra High Vacuum conditions, the Ics were almost non-existent and appeared only after the samples were exposed to air.

Prof. Laurence D. Marks

Department of Materials Science and Engineering

Northwestern University, Evanston Il 60208

Dedicated to my parents
Dr. M. Narayanaswamy and Mrs. R. Narayanaswamy

ACKNOWLEDGEMENTS

The completion of this dissertation is a milestone in my life. At this point, nothing would be more pleasurable than expressing my sincere gratitude and thanks to the people who have contributed to the improvement of my professional and personal development.

My coming to Northwestern University would have been impossible if it were not for Prof. Kishore (IISc). His kind advice and mentoring have helped me hurdle several problems. The contributions of C. R. Ragnath and Ranjit Jobe will also be remembered.

I am deeply indebted to Prof. Laurence Marks for his continual support and patience. His contributions as a guru and honest friend are invaluable assets. I am also very grateful to him for buying a stable workhorse microscope (the H-9000).

It was a lot of fun to collaborate with Ganesh Jayaram and Richard Plass on the Ultra High Vacuum experiments. Their understanding, along with those of Jin Ping Zhang, Brad Storey, Donna Kroening, Derren Dunn, Rebecca Ai, Peirong Xu, Bob Passeri and Hong Zhang helped me remain optimistic through the lean months when the small particle demons refused to let me perform a census. In the last few months, I have had the opportunity to collaborate with Dan Grozea in static morphology experiments which have further reinforced my understanding of small particles.

During my stay at Evanston, innumerable wonderful people gave me a lot of support, love and care. Their kinship will always be cherished.

TABLE OF CONTENTS

CHAPTER 1: INTRODUCTION

1.1 Introduction	1
1.2 Electron microscopy of small particles	4
1.3 Small particle structures	11
1.3.1 The Wulff Construction	11
1.3.2 Structure of Multiply Twinned Particles	15
1.4 Structural stability of multiply twinned particles	19
1.4.1 Elastic Continuum Approach to Determine Structural Stability	19
1.4.2 Cluster Studies Using Ab-Initio Approaches	22
1.5 Growth and twinning	25
1.6 Structural fluctuations and quasimelting	31

CHAPTER 2: EXPERIMENTAL MORPHOLOGY MAP (Au/SiO)

2.1 Introduction	34
2.2 Sample preparation	42
2.3 Data acquisition	46
2.3.1 Data reduction scheme	46
2.3.2 The Basis Set	47
2.4 Results and discussion	65

CHAPTER 3: ANALYTICAL MORPHOLOGY MAP

3.1 Introduction	72
3.2 Analytical model	72
3.3 Potential energy surface	77
3.4 Results and discussion	78
3.5 Comparison with experimental results	83

CHAPTER 4: MORPHOLOGY TRANSFORMATION KINETICS

4.1 Introduction	91
4.2 Liquid droplet model	91
4.3 Activation energy	93
4.4 Discussion	98

CHAPTER 5: APPLICATION TO Ag/Si(100)

5.1 Introduction	103
5.2 Sample preparation	107
5.3 Results and discussion	109

CHAPTER 6: SUMMARY AND SUGGESTIONS

6.1 Summary	127
6.2 Suggestions for future work	129

APPENDIX 1: WULFF CONSTRUCTS

1.1 The Wulff Construct	132
1.2 The Modified Wulff Construct	135

APPENDIX 2: LIQUID DROPLET

139

REFERENCES

143

TABLE OF ILLUSTRATIONS

- Figure 1.2.1: A schematic of the profile imaging technique. The electron beam direction is perpendicular to the edge of the surface. 9
- Figure 1.3.1: (a) An HREM image of a cuboctahedral particle of gold supported on an amorphous carbon substrate. (b) Schematic of the general three dimensional shape of a cuboctahedral particle with only {111} and {100} facets. 12
- Figure 1.3.2: An HREM image showing the variety of different structures present in small particles of gold deposited onto an amorphous carbon substrate. 14
- Figure 1.3.3: (a) An HREM image of a decahedral multiply twinned particle clearly showing the 5 different tetrahedral units. The directions of the twins are indicated by arrows. (b) A schematic of the five fold symmetry orientation of the decahedral multiply twinned particle in relation to the substrate and the electron beam. 16
- Figure 1.3.4: (a) An HREM image of an icosahedral multiply twinned particle exhibiting a three fold symmetry with the twins indicated by arrows. (b) A schematic of the three fold symmetry orientation of the icosahedral multiply twinned particle in relation to the substrate and the electron beam. 17
- Figure 1.3.5: A polyparticle exhibiting a mixture of twinned regions. 20
- Figure 1.5.1: A schematic to illustrate the successive twinning mechanism proposed by Hall and Fawzi (1986) to explain the occurrence of five fold twins during large scale electrodeposition. 27
- Figure 1.5.2: The successive twinning mechanism suggested by Allpress and Sanders (1967) leading to the formation of MTPs. 27
- Figure 1.5.3: The layer by layer growth mechanism in a multilayer icosahedral MTP. (a) An icosahedral nucleus of 55 atoms (Mackay icosahedron). (b) The external face of one of the tetrahedrons when covered by an additional regular Fcc layer. (c) The resultant 3-layer icosahedron formed from the Mackay icosahedron (when it is completely covered by an additional layer)(Adapted from Farges et al 1984). 30
- Figure 1.5.4: The nucleation and subsequent growth of a decahedral embryo from a liquid droplet, as proposed by Iijima 1987. 30
- Figure 2.1.1: Schematic of a two dimensional section of a hypothetical potential energy

surface (contour map of the free energy as a function of only the morphology of the particle). Ic, Dh, Sc, St are icosahedral MTP, decahedral MTP, single crystal and single twin respectively. 35

Figure 2.1.2: Diagram of a hypothetical potential energy surface for a twinned particle. Energy contours correspond to non-equilibrium values of the relative volumes of tetrahedra and the fraction (α) of twin boundary energy shared by two adjacent segments. The dotted lines trace two possible paths X and Y representing single crystals. The point O is a constrained minima. Note that even though OX and OY are low energy paths, the twin boundary constrains the particle to move along OZX (reproduced from Marks 1981). 36

Figure 2.1.3: The two dimensional change in crystal structure corresponding to the movement of the disclination in one direction, where β represents the distance of the disclination from the center of the particle (adapted from Dundurs et al. 1988). 38

Figure 2.1.4: Schematic of the index of quasimelting shown as a function of particle radius and temperature. An index close to 1 implies lower activation energies and higher probability of structural fluctuations (reproduced from Ajayan 1989). 38

Figure 2.1.5: Phase map showing the stable structures and the quasimolten phase. Stability regimes are: the liquidus state L, the quasimolten state QM. Dh, Ic, Sc are the decahedral MTP, icosahedral MTP and the single crystal regimes respectively. 40

Figure 2.2.1: Pillar formed beneath a particle. 45

Figure 2.2.2: A linear plot of the pillar height as a function of particle radius (from Ajayan 1989). 45

Figure 2.3.1: The experimental setup 48

Figure 2.3.2: The data reduction scheme. 48

Figure 2.3.3: (a)HREM image of a cubooctahedral particle in a [110] orientation. (b) Schematic of the [110] oriented cubooctahedral particle. 50

Figure 2.3.4: (a)HREM image of a cubooctahedral particle in a [100] orientation. (b) Schematic of a [100] oriented cubooctahedral particle. 50

Figure 2.3.5: (a) A single crystal showing only one set of {111} fringes. 51

Figure 2.3.6: An asymmetrical decahedral MTP with the disclination located very close to the crystal edge. 51

Figure 2.3.7: A single twinned crystal.	53
Figure 2.3.8: (a)HREM image of a decahedral MTP in the fivefold orientation. Note the clearly resolved twins.(b) Schematic of the five fold symmetric decahedral MTP orientation.	54
Figure 2.3.9: (a) HREM image of a decahedral MTP lying on a (111) face.(b) Schematic of the orientation.	54
Figure 2.3.10: (a) An HREM image of a decahedral MTP tilted by an angle of 77.6 degrees from the five fold orientation. (b) Schematic of the orientation.	56
Figure 2.3.11: (a) An HREM image of a decahedral MTP at an angle of 0 degrees azimuthal, 36 degrees declination from the five fold orientation.	56
Figure 2.3.12: (a) A decahedral MTP that is commonly mistaken to be a single twin.(b) Schematic of the orientation.	57
Figure 2.3.13: (a) A five fold symmetric orientation of the icosahedral MTP is seen in this HREM image.(b) A schematic of the orientation.	58
Figure 2.3.14: (a) HREM image of a fivefold symmetric icosahedral MTP on an amorphous background.	58
Figure 2.3.15: (a) HREM image of a two fold oriented icosahedral MTP. (b) Schematic of the two fold oriented icosahedral MTP.	60
Figure 2.3.16: (a) HREM image of a three fold oriented icosahedral MTP. (b) Schematic of the three fold oriented icosahedral MTP.	60
Figure 2.3.17: HREM images of decahedral MTPs which are misoriented from the fivefold axis.	61
Figure 2.3.18: HREM images of icosahedral MTPs which are misoriented from the twofold axis.	62
Figure 2.3.19: HREM images of icosahedral MTPs which are misoriented from the threefold axis.	63
Figure 2.3.20: An unidentifiable HREM image.	64
Figure 2.4.1: Plot of the time sequence evolution of the morphologies for a 6nm particle at a) 3A/cm² b) 6A/cm² c) 11A/cm². Each type of morphology has been assigned an	

arbitrary value. 1 is for the decahedral MTP, 2 for Icosahedral MTP, 3 for Single Crystal, 4 for single twins, 6 for indistinguishable and 7 for unknowns. The x-axis represents the time in seconds spent in a morphology. 66

Figure 2.4.2: The mean residence time in seconds has been plotted as a function of the beam flux in A/cm^2 for various sizes in Angstroms. 67

Figure 2.4.3: The mean residence time in seconds plotted as a function of particle diameter in angstroms at constant fluxes of 3, 6, 11, 20 A/cm^2 respectively for the three morphologies (a) Dc (b) Ic (c) Sc. The lines are drawn to guide the eye in observing the trend. 69

Figure 2.4.4: The experimental probability measured as fractional residence time in percent been plotted as a function of particle diameter in Angstroms for beam fluxes of 3, 6, 11, 20 A/cm^2 respectively shows the downward trend in probability for the (a) Ic and the upward trends for (b) Dc and (c) Sc. The lines help guide the eye in observing the trend. 70

Figure 3.4.1: A typical set of relative probability maps of the morphologies at a driving energy of 10eV and the remaining constants determined from the standard values tabulated in Table 1. The contour lines define the probability as a function of the temperature and particle radius. The depression in melting point [Buffat and Borel 1976] curve separates the liquid and solid phases. (a) Ic relative probability map, (b) Dc relative probability map, (c) Sc relative probability map. 80

Figure 3.4.2: The variation of the relative probability of (a) Ic (b) Dc (c) Sc with driving energy is illustrated for driving energies of 2, 10, 18eV. The graphs are isothermal sections at 300K of a relative probability versus temperature, particle diameter in angstroms map. 82

Figure 3.4.3: An isothermal section at 300K of a 3D morphology map of relative probability versus temperature, particle diameter in angstroms illustrating the variation of the relative probability with surface stress (in N/m^2) for (a) Dc (b) Ic (c) Sc at a driving energy of 10eV. 84

Figure 3.4.4: An isothermal section at 300K of a 3D morphology map of relative probability versus temperature, particle diameter in angstroms illustrating the variation of the relative probability with anisotropy [defined as $\beta = 1 - (\gamma_{100} / (\sqrt{3}\gamma_{111}))$] for (a) Dc (b) Ic (c) Sc at a driving energy of 10eV. 85

Figure 3.5.1: The best fit morphology sections, of (a) Ic, (b) Dc, (c) Sc at 300K of the probability model compared with the experimental data reveals the crossover regime centered at 6.5nm. The surface stress is $0.8N/m^2$ and the anisotropy is such that $\gamma_{100} =$

1.15 γ_{111} at a driving energy of 10eV.	87
Figure 4.2.1: Values of the vibration frequency as a function of the particle size of gold.	94
Figure 4.3.1: Schematic of the energy barrier to a disclination as it moves from a single crystal structure ($x=-1$) to a symmetrical decahedral MTP ($x=0$) to a single twin structure ($x=1$).	94
Figure 4.3.2: Movement of a disclination by the generation of an edge dislocation. The figure illustrates an intrinsic disclination of rotation $\pi/2$ acting as the source of two dislocations. The first dislocation leaves along glide line G_1 , resulting in the displacement of the disclination from 1 in (a) to the center of the triangle formed by 1,2 and 3 in (b). A second dislocation, shown in (c), glides along the same glide line, the disclination is displaced to 2 in (d). G_2 in (a) is a second possible glide line for the dislocations (Reproduced from Harris and Scriven 1971).	95
Figure 4.3.3: Torsional rotation between two pentagonal faces of an icosahedral particle resulting in the formation of a strained decahedral MTP.	97
Figure 4.4.1: Rate of fluctuations for a) Dislocation model. b) Shear model assuming a shear modulus softening by a factor of 10.	99
Figure 4.4.2: The experimental average transition frequency plotted against particle diameter.	101
Figure 5.1.1: Three modes of epitaxial growth.	104
Figure 5.1.2: A schematic of the Si(100)-2x1 structure for a six-layer relaxation model; the dimer bond lies in the plane of the paper. Arrows show the direction of dimerization while the numbers denote the magnitude (in Å) of atom displacements (along the "2" direction of the reconstruction, i.e., the y-axis in the calculations) from the bulk positions (from Jayaram et al 1993).	106
Figure 5.1.3: Section through the symmetric (2x1) dimer surface. The dimer bond is in the plane of the paper, the dimer rows run perpendicular to the plane of the paper. The arrows indicate the directions of displacements of the atoms away from their bulk positions and the numbers give the magnitude of these displacements as a fraction of the lattice constant (5.29 Å) (from Roberts and Needs 1990).	106
Figure 5.2.1: The UHV-HREM facility (courtesy of Dr. J. E. Bonevich).	108

- Figure 5.2.2: A TED of a clean 2x1 Si(100) surface. Arrows indicate the surface spots. 110
- Figure 5.3.1: A typical TED pattern following Ag deposition on a Si(100)-2x1 surface; arrowed surface reconstruction spots coexist with the (111) and (220) ring of Ag, denoted by the letters A and B. All the features can be interpreted by a combination of silicon, silver and moiré spacings. 111
- Figure 5.3.2: An on-zone filtered image showing the moiré contrast arising from the interference between the bulk Si and the small particles. 113
- Figure 5.3.3: HREM micrograph illustrating the occurrence of a structure that appears to be an incomplete layer of Ag. 114
- Figure 5.3.4: UHV-HREM micrograph of a <110> oriented single crystal; the cross fringes in the single crystal image are due to the (111) planes. 115
- Figure 5.3.5: The aspect ratios of Ag single crystals plotted as function of the length of one edge of the crystals. 115
- Figure 5.3.6: The aspect ratios of Ag single crystals plotted as functions of the area of the crystals. 116
- Figure 5.3.7: A single crystal with a long aspect ratio. 116
- Figure 5.3.8: UHV-HREM micrograph of a <110> oriented decahedral MTP with arrows indicating the five twins separating {111} facets. 118
- Figure 5.3.9: UHV-HREM micrograph of a <112> oriented icosahedral MTP. 118
- Figure 5.3.10: The plot of the percent yield of decahedral MTPs as a function of the average size of the Ag particles. 120
- Figure 5.3.11: The plot of the percent yield of single crystal as a function of the average size of the Ag particles. 120
- Figure 5.3.12: Plan view of a structural model illustrating the adsorption site for Ag atoms on Si(100)-2x1 (from Samsavar et al. 1989). The circles, large filled circles and small filled circles represent Ag adatoms, Si dimer atoms and the Si atoms just below the dimer layer. 121
- Figure 5.3.13: A cluster model for Ag adsorption and migration on Si(100)-2x1, as well

- as the possible adsorption sites (from Ru-Hong Zhou et al. 1993). 121
- Figure 5.3.14: UHV-HREM (off-zone image) showing chain like adsorption sites. The chains are indicated by arrows. 123
- Figure 5.3.15: An atypical pentagonal Ag single crystal on a Si(100)-2x1 surface indicating inter-morphology conversion via grain boundary migration. 124
- Figure A1.1: A $\langle 110 \rangle$ section of the Wulff construct for a particle with only $\{111\}$ and $\{100\}$ facets. 134
- Figure A1.2: Schematic of the geometrical construction used to prove the Wulff construct using the Brunn-Minkowski inequality (Reproduced from Herring 1953). 134
- Figure A1.3: The shape of the $\langle 110 \rangle$ sectioned single crystal segment derived from the modified Wulff construct for a perfectly symmetrical decahedral MTP (from Marks 1980). 136
- Figure A2.1: The vibrational modes of a dense sphere (a) the repeated contraction and expansion mode (b) the spheroidal mode and (c) the torsional mode. 140
- Figure A2.2: An oscillating droplet. (a) spherical equilibrium shape, (b) departure from equilibrium described by Legendre polynomials. 142

CHAPTER 1: INTRODUCTION

1.1 INTRODUCTION

The basic physical phenomena of many materials are often interpreted in terms of the periodic arrangement of atoms within them. At small sizes, atoms experience interactions that differ from the bulk and compensate for these changes by reconfiguring themselves. Atoms at and near two dimensional features such as surfaces try to attain minimal energy configurations by surface reconstructions and lattice contractions. In three dimensionally limited aggregates these effects become even more pronounced and the deviations from the bulk lead to entirely new structures which show gradual size dependent transitions in physical properties from the bulk to those of molecular dimensions.

These aggregates can be broadly classified as clusters (5 atoms to 1000 atoms) and small particles (1.5nm to 500nm diameter). The boundaries are not rigidly defined and there is considerable overlap between the two classes. Small particles are also known as nanoparticles. Small particles greater than 500nm in diameter are usually termed as ultrafine particles.

The unique properties of these small aggregates are, perhaps, best illustrated by the "quantum size effect". The quantum size effect [Kubo 1962] arises when the dimensions of the small particle become small enough to show discrete quasi-continuous

electron energy bands. As a consequence, particles may exhibit a temperature and size dependent transition from an insulating to a metallic state with increasing cluster size. A case in point is the behavior of small alkali metal clusters, which have the outer electrons in states delocalized over the entire cluster [Knight et al 1984]. These clusters do not become metallic until the states are so dense that they overlap thermally. Kubo also argued that the details of the energy spectrum would depend on the geometry of the small particles, although particles of the same size would have the same average level spacing. In contrast to the volume dependent quantum size effect, deviation from the bulk of the magnetic susceptibility is attributed to an increase in surface area known as the finite size phenomenon [Kimura 1990].

Another manifestation of size dependent properties is in the lattice vibration spectra of small particles [Dickey and Paskin 1968, Burton and 1970, Matsubara et al 1977, Hasegawa et al 1980] which have low frequency surface modes instead of the normal bulk transverse and longitudinal peaks. It has been suggested that the two dimensional nature of the phonon spectrum is also responsible for the increase in the superconducting transition temperature [Khlyustikov and Buzdin 1987]. The optical properties of small particles, being sensitive to the surface plasmon modes, are also significantly modified from those of the bulk. Fleischmann et al (1974) observed surface enhanced Raman intensity and a general theory has been based on the resonant excitation of surface plasmons [Agarwal et al 1982].

Among the well known phenomena related to small particles is the depression in melting point first observed by Takagi (1954). Later workers [Blackman and Sambles

1970, Couchman and Karasz 1977, Couchman and Jesser 1977, Couchman and Ryan 1978, Borel 1981, Ross and Andres 1981, Garrigos et al 1986, Nimtz et al 1989] also observed a similar phenomenon. Computer simulations [Briant and Burton 1975, Eters and Kaelberer 1977, Natanson et al 1983, Berry et al 1984, Honeycutt and Anderson 1987, Beck et al 1988, Stillinger and Stillinger 1990, Matsuoka et al 1992] show the existence of a range of melting leading to upper and lower critical melting points. Most of these properties can be ascribed to an average size dependent behavior, but even within a given size regime there exists a multitude of structural modifications [Gordon et al 1979, Woltersdorf et al 1981, Heinemann et al 1983, Penisson and Renou 1990], contractions of the surface layer [Takayanagi 1991] and surface reconstructions [Mitome, Takayanagi 1990] differing from those of bulk crystals. A large number of researchers have studied the size dependence of the lattice parameter [Apai et al 1979, Balerna et al 1985, Montano et al 1986, Crescenzi et al 1987]. Systems showed variable results from no lattice contractions [Montano et al 1986] to a strong lattice contraction [Apai et al 1979].

These interesting and exciting properties of small particles have spawned several decades of research. The most glamorous of such endeavors in recent years is the study and application of bucky balls [Kroto et al 1985] and carbon nano-tubes [Iijima 1991]. Other kinds of small particles and clusters of metals, nonmetals, semiconductors and compound materials are also available. These have been possible due to creative methods of synthesis ranging from the simple vaporization of metals heated by a resistive boat to methods employing lasers or arc-discharges to vaporize the species of interest. An

interesting development is the creation of "optical molasses" which trap the vapors of relatively volatile metals in the gas phase and hold them in an essentially motionless condition. This is achieved by the use of focussed tunable lasers arranged to push back clusters that drift into the laser beam [Ertner 1987].

The development of these materials as single entities or consolidated aggregates, as in nanomaterials, has resulted in their possible application in areas as diverse as the commonly understood catalysts to the more esoteric quantum wells and quantum dots. Table 1.1.1 indicates the many areas in which these materials have become integral components or have potential applications. Several reviews give detailed accounts of the progress of our understanding of these novel materials [Ogawa and Ino 1971, Gillet 1977, Ajayan and Marks 1990, Gryaznov and Trusov 1993, Marks 1994a, Marks 1994b].

It is in the context of such breakthroughs and applications that the study of the evolution, growth and stability of small particle structures gains importance. The studies in this thesis are directed towards better understanding the kinetics of the morphological evolution in small particles by extensive experimental observations using high resolution electron microscopy and modelling of the observed phenomena.

1.2 ELECTRON MICROSCOPY OF SMALL PARTICLES

Small particles have been studied by a wide variety of techniques. The conventional TEM techniques allow for easy characterization of the particle sizes, shapes and particle size distributions [Renou and Gillet 1981, Bond 1991]. Special dark field techniques have also been used extensively to study the defects within small particles [Ino 1966, Yacaman and Dominguez 1980, Marks 1985, Tholen 1986]. X-ray and electron

TABLE 1.1.1: Applications of small particles and clusters

PROPERTY	APPLICATION
Reactivity	Gas sensors
	Combustion catalyst for fuel
	Chemical Catalyst
Conductivity	Resistive pastes
	Conductive fillers
Magnetic	High performance magnetic tapes
Surface Area	Colloidal emulsions in paint
	Heat exchanger walls for ultra low temperature
	Micro filters
	Sintering accelerator
Mechanical	Cermets
	Nanoceramics
	Nanocomposites
	Nanometals
Precursor	Nanomaterials
	Thin film synthesis
	Bioceramics
Optical	Data storage
	Radioactive detectors
	Photography
Isolation	Quantum dots
Site specificity	Protein sequencing
Directional growth inducers	Nanowires
	Bucky tubes

diffraction [Hall et al 1991] techniques give average information on the structure, size and interparticle spacings. STEM [Pennycook et al 1983, Retchkiman et al 1984, Cowley 1984] analyses have been used in nanodiffraction to obtain structural information about small particles. With the advent of higher resolution instruments in the early 80s, high resolution electron microscopy (HREM) has almost become a universal tool to study the atomic nature of supported small particles. While conventional TEM is based on separately considering the amplitude contrast information contained in each of the transmitted and diffracted beams, HREM relies more on the phase contrast between the transmitted and diffracted beams.

An HREM image is obtained by allowing an accelerated electron beam to penetrate through a thin material. While passing through the specimen the electrons are scattered due to their interactions with the lattice potential, formed by the electrons and nuclei. The scattered exit beam consists of the transmitted beam and different diffracted beams which on recombination form an interference pattern. The interference pattern (HREM) image is a complex function of the phases and amplitudes of the recombined beams. Its decomposition would then yield the form of the interacting specimen potential and the structure of the specimen. However, the information is altered by the aberrations of the imaging electromagnetic lenses.

There is a vast amount of literature [Cowley 1981, Spence 1988, Self and O'Keefe 1988, Reimer 1993, Marks 1990] devoted to the process of information retrieval from an HREM image. The most common approach treats the aberrations as the effect of a single lens which acts on the waves that exit the surface of the specimen after being

scattered. The aberrations of the lenses can be of two kinds. Coherent aberrations include defocus, astigmatism, beam tilt and spherical aberrations and incoherent aberrations arise from focal spread and convergence of the beam, drift and vibrations. The coherent aberrations introduce a phase shift to the transmitted waves and contribute to the phase term $\chi(u)$, expressed in linear imaging theory as

$$\chi(u) = \pi/\lambda(\Delta z\lambda^2u^2 + 1/2Cs\lambda^4u^4) \quad (1.2.1)$$

where the Δz is the defocus and Cs is the spherical aberration of the lens, u the spatial frequency in reciprocal space.

The incoherent aberrations act as a soft aperture called the envelope that limit the spatial frequencies one can obtain in a image. It is usually represented as $E(u)$ and is given (in linear imaging theory) by

$$E(u) = S(\nabla\chi(u)/2\pi)F(\lambda u^2/2) \quad (1.2.2)$$

where S and F are the fourier transforms of the convergence and focal spread distributions of the electron beam.

The objective aperture, on the other hand, is usually considered as a hard aperture which abruptly cuts off spatial frequencies (An objective aperture is rarely used to form HREM images, in current practice). The net effect of the aberrations and the aperture is a contrast transfer function (CTF) which operates by weighting the spatial frequencies of the final image. In this sense, the microscope is an imaging device with a built in spatial

frequency filter. The sensitivity of the image to imaging parameters requires extensive simulations to accurately determine the structure of the materials under observations. Methods to decipher small particle structure can be found in the works of Flueli et al (1989), Buffat et al (1991), Nihoul (1992) and Kirkland et al (1991). HREM images have been interpreted to an accuracy of 0.1-0.2 Angstroms [Marks and Smith 1983, Saxton and Smith 1985] and have even resolved single atoms [Iijima 1977] to obtain, not only the local crystallographic information at the external surfaces of small particles but also the detailed structure of entire small particles. The accuracy of the numerical simulations and quantitative HREM have been limited only by the speed and storage of computers. Fortunately, only the contrast and amplitude of the fringe spacings of the lattice planes vary with imaging conditions. This allows local crystallographic information to be identified, in many cases, without resorting to image simulations.

Samples of supported small particles are often imaged along with their substrate. Sometimes the noise from the substrate can be comparable to the structure of the small particle [Gai et al 1986], making it difficult to differentiate between substrate and particle. Filtering techniques applied, with extreme caution, to crystalline substrates can partially alleviate the problem by removing the periodic component of the substrate [Nihoul 1992]. However, a simpler approach is to use the "profile imaging technique" [Marks and Smith 1983, Marks 1986, Smith et al 1986]. The geometry of the imaging is shown in figure 1.2.1. A variant of the technique images single particles on the edge of the particles and for the lack of a term it is still called "profile imaging". The technique places the particles on a background of vacuum and the noise contribution is reduced to that from

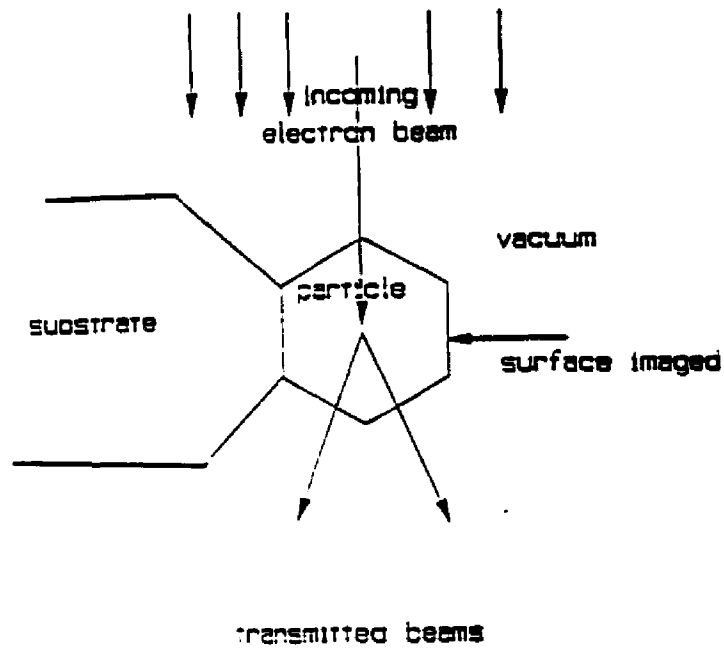


Figure 1.2.1: A schematic of the profile imaging technique. The electron beam direction is perpendicular to the edge of the surface.

the image acquisition system.

The use of TV imaging by fiber optically coupled or charge coupled devices has also greatly facilitated imaging small particles. In general, the phase contrast from a crystal depends strongly on orientation. When a crystal is tilted far away from a strongly excitable orientation, the internal structure information is lost and the particle shows only an outline due to differences in atomic scattering factors (amplitude contrast). Fortunately, samples prepared for HREM studies contain hundreds of small particles and the probability of finding a suitably oriented particle is high. A TV imaging system allows for quickly moving through the sample and selecting suitable particles for observation. The use of a suitable video recording device or an image grabber also allows for the real time observation of dynamic processes in small particles. The images are captured at NTSC or PAL-SECAM standards of 25-30 frames per second which places a limit on the lower time scales of detection. The images captured onto video tapes have a resolution of only 400 horizontal lines per inch, but adequate image processing can reveal very interesting results. An example is the observation [Bovin and Malm 1991] of the "atomic clouds" atop some particles fluctuating in structure under the electron beam. Single dislocations [Kamino et al 1990] at particle edges have also been seen. The system can also be used for the auto-alignment of the microscope but is limited in its applicability due to computer speed and memory.

The H-9000 microscope at Northwestern University is equipped with a fiber optically coupled TV camera system made by GATAN and the UHV H-9000 has a GATAN CCD camera which greatly simplified the study of the dynamics of small

particles and their structures.

1.3 SMALL PARTICLE STRUCTURES

1.3.1 The Wulff Construction

The shape of a crystal, in equilibrium with its vapor, can be determined by minimizing its surface free energy. Mathematically, as first formulated by Gibbs (1878), it can be expressed as minimizing

$$\int \gamma dS \quad (1.3.1)$$

where γ is the surface free energy which is integrated over the entire surface S .

A solution to the above equation is given by the Curie-Wulff construct (see Appendix A1.1). Most often, the low Miller index planes have low surface energy. In fcc metals the low Miller index planes $\{111\}$, $\{100\}$, $\{110\}$ are such that

$$\gamma_{111} < \gamma_{100} < \gamma_{110} \quad (1.3.2)$$

which, on application of the Wulff construct, leads to the cubooctahedral form with $\{111\}$ and $\{100\}$ facets as the equilibrium structure in these materials. An example is shown in figure 1.3.1. There have been several experimental verifications of the Wulff construction. Heyraud and Metois (1980),(1980b) demonstrated that micron sized particles of gold equilibrated with their own vapor have Wulff shapes independent of their actual size. Other analyzes of large single crystals ranging in the tens of nanometer size [Wang et al 1984, Flueli and Borel 1988, Marks 1990] are also consistent with the Wulff construction. Even under the constraint of a substrate the Wulff construct can be modified by adding in a component for the free energy of adhesion [Winterbottom 1967] and extended [Marks 1990] to include the effect of a non-rigid substrate. However, by

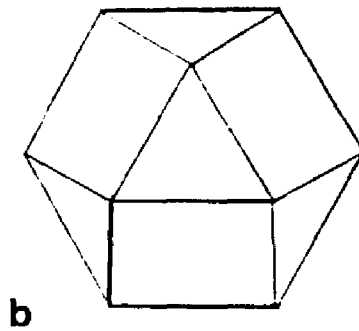


Figure 1.3.1: (a) An HREM image of a cuboctahedral particle of gold supported on an amorphous carbon substrate. (b) The schematic of the general three dimensional shape of a cuboctahedral particle with only $\{111\}$ and $\{100\}$ facets.

definition, the Wulff construct ignores all the kinetic effects and accounts only for the surface, but not the total energy. At smaller sizes, edges and corners could stabilize irregular polyhedra [Wang et al 1984] over the simple deformed Wulff construct. In fact, in a footnote to his paper [Gibbs 1878], Gibbs pointed out that the predictions of the equilibrium requirement are probably incorrect at edges and corner. Herring (1951) evaluated the rounding that would result if the surface free energies varied over a uniformly curved edge as a function of the surface free energies of the of the surfaces that meet at the edge. The model showed that rounding of a few tens of atom spacings could occur. But Herring concluded that the Wulff construct would hold true for fairly large sizes without any refinements. Searcy (1984), using a model based on the vacancy distribution necessary for dynamic equilibrium, observed that increasing the mole fraction of vacancies at edges and corners leads to metastable shapes other than the Wulff construct. In a discussion of the effect of packing corrections Marks (1985) showed that there are large deviations from the Wulff construction for particles as large as 10nm due to additional edge terms introduced by packing spheres leading to a drop in the fraction of surface {100} atoms with particle size. Experimental observations [Bonevich 1991] confirmed the size dependent trend. A molecular dynamics calculation [Cleveland and Landman 1991] showed a strong variation in facetting with size. Such deviations result in a wide range of twinned small crystals. (Figure 1.3.2) illustrates the fascinating number of different forms, often found in metals deposited onto oxide surfaces. Some structures occur with rather large frequency.

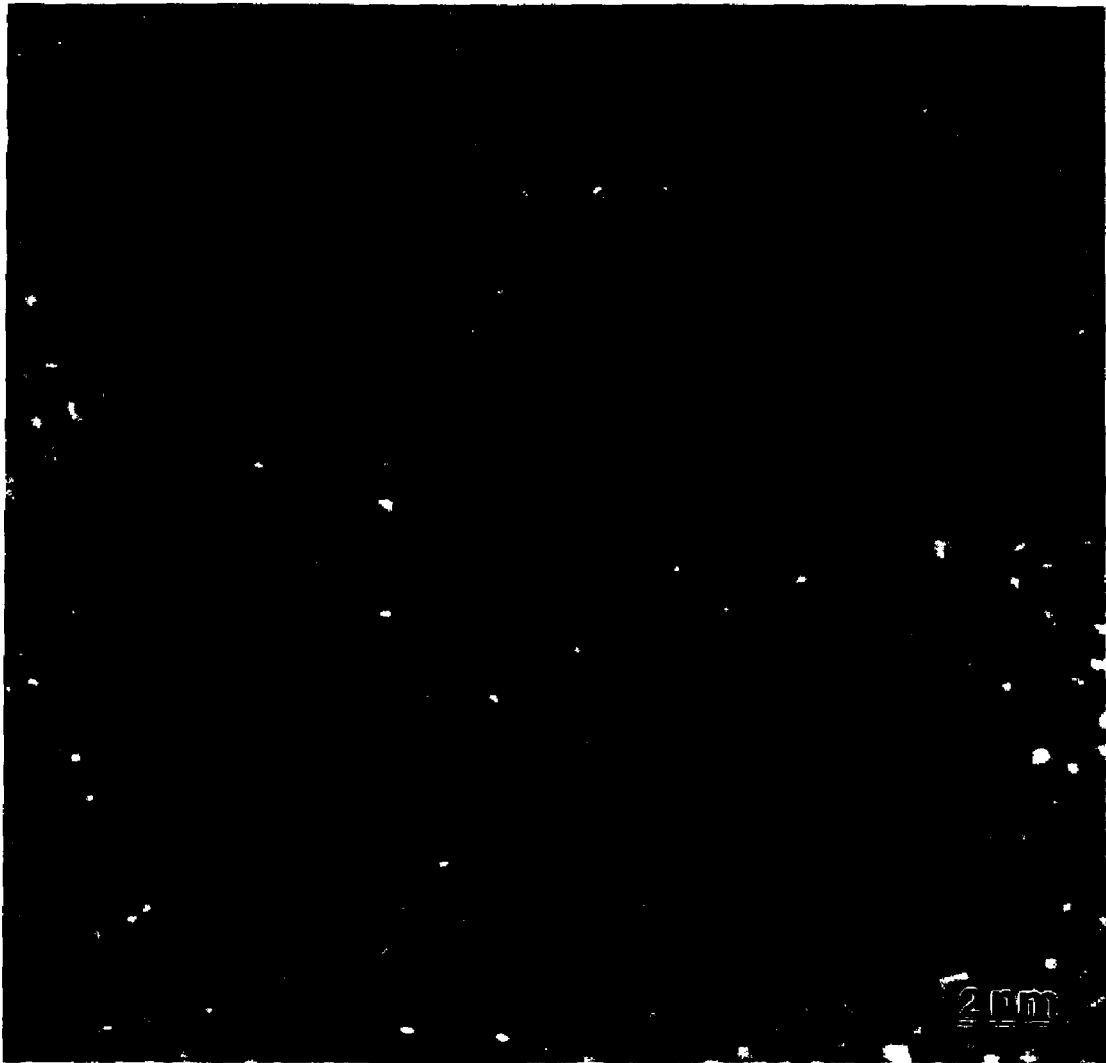


Figure 1.3.2: HREM micrographs showing a variety of structures which do not correspond to the single crystal structure.

1.3.2 Structure of Multiply Twinned Particles

In 1959, Melmed and Hayward (1959) observed five fold rotational symmetry by field emission microscopy in 5nm to 20nm diameter whiskers of iron, nickel and platinum. Similar five-fold symmetry structures were observed by means of optical microscopy [Wentorf 1963, Gedwill et al 1964] and in electrodeposited copper dendrites by X-rays [Ogburn et al 1964]. Electron microscopy studies of the nucleation of Au on a (001) single crystal film of silver [Allpress Sanders 1964] and on cleavage surface of rocksalt [Ino 1966] revealed the presence of twelve "abnormal" spots in the diffraction patterns. The nature of the "abnormal" spots was solved by Ino (1966) and independently by Allpress and Sanders (1967) using extensive darkfield techniques. According to Ino, the abnormal spots arise from a class of multiply twinned particles (MTPs). The MTPs consist of single crystal tetrahedra, twin related on their adjoining (111) faces. Common MTPs are the decahedral MTP(Dh) and the Icosahedral MTP(Ic). The decahedral MTP is assembled from five tetrahedra arranged symmetrically about an axis, sharing a common edge (Figure 1.3.3). The configuration has five fold symmetry. The icosahedral MTP is composed of 20 such tetrahedra sharing a common summit (Figure 1.3.4). When formed from perfect single crystal units, these models give rise to a spatial discontinuity formed by an angular misfit of $7^{\circ} 20'$ which is compensated by distortions. Experimental evidence show various defects such as partial dislocations [Smith and Marks 1981], stacking faults [Nepijko et al 1986], grain boundaries [Iijima (1987), (1987b)], microfacetting [Hofmeister 1991]. Conclusive experimental evidence by Marks (1985)

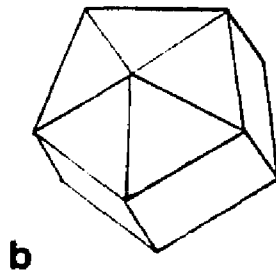
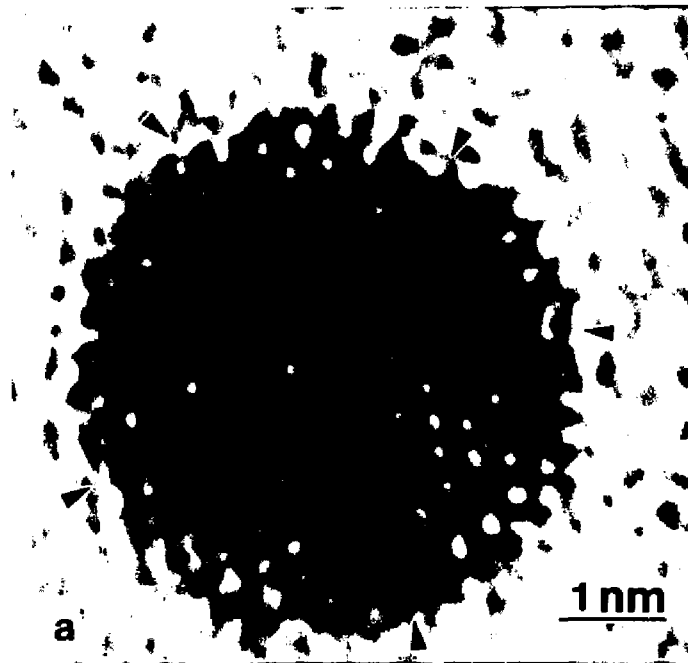


Figure 1.3.3: (a) An HREM image of a decahedral multiply twinned particle clearly showing the 5 different tetrahedral units. The directions of the twins are indicated by arrows. (b) A schematic of a decahedral multiply twinned particle.

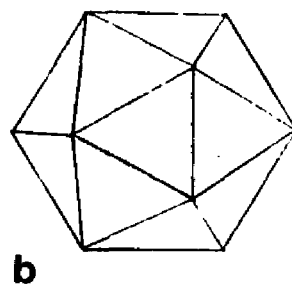
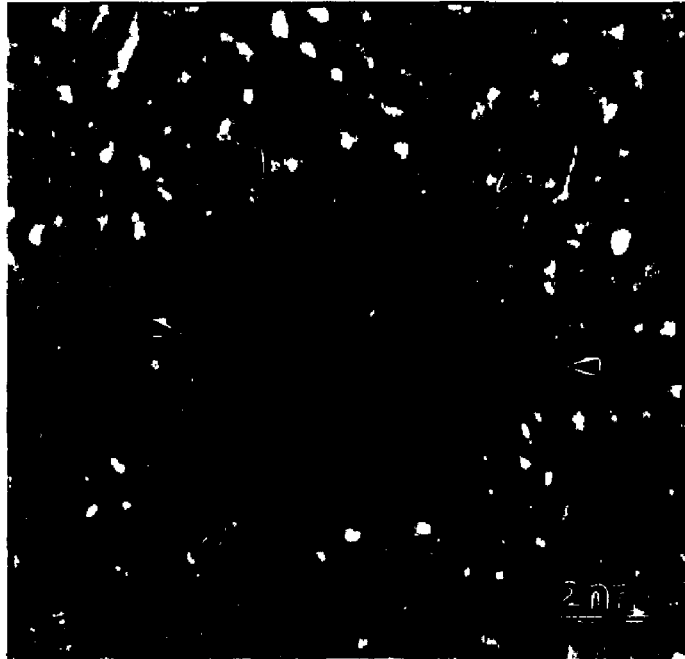


Figure 1.3.4: (a) An HREM image of an icosahedral multiply twinned particle exhibiting a three fold symmetry of the twins(indicated by arrows). (b) A schematic of an icosahedral multiply twinned particle.

showed that inhomogeneous strains have to be considered in any model of MTPs. Theoretical models accommodate the resultant strain in closing the misfit gap in various ways. Ino (1966) assumed a homogeneous distribution of the strain, Saito et al (1978) proposed a dislocation model and several workers based their models on a disclination approach [de Wit 1972, Howie and Marks 1984, Dundurs et al 1988, Gryaznov and Trusov 1993].

Geometrically equivalent dense sphere packing models were proposed by Bagley (1965) for the decahedron and by Mackay (1962) for the icosahedron. These models account for the misfit gap by assuming a homogeneous deformation. The decahedron has a body centered orthorhombic structure in these models. The icosahedral model can be considered to be composed of a rhombohedral structure resulting from the homogeneous deformation of the twinned tetrahedra towards their vertices along the $\langle 111 \rangle$ directions. The sphere packing models predict that clusters containing a certain "magic" number of atoms form almost spherical shapes with nearly close packed surfaces which have exceptional stability. Yang [Yang 1979, Yang et al 1979] conducted an extensive crystallographic analysis based on the sphere packing models and showed reasonable agreement between the models and experimental diffraction patterns. The ease of construction of sphere packing models has also lead to their extensive use in simulations of high resolution electron images of MTPs. Since their discovery, MTPs have been found to occur in almost all transition metals and semiconductors. They also form in some bimetallic compounds [Ajayan and Marks 1990].

The morphologies of small particles are not restricted only to the single crystal,

Ic and Dh. (Figure 1.3.5) shows a particle with a complex morphology of twins and are called polyparticles [Smith and Marks 1981]. These polyparticles usually occur through partial coalescence of two or more particles, as observed in room temperature growth of gold on KCl [Marks 1986] and dynamic HREM observations of coalescence [Flueli et al 1988]. Other structures such as lammellar twinned particles with a flat morphology, particles with a number of parallel twins [Iijima, 1987] are also common. Such large number of structures observed in small particles leads to the question whether these structures are only frozen transient kinetic structures. In fact, are any of the non-single crystal morphologies stable?

1.4 STRUCTURAL STABILITY OF MULTIPLY TWINNED PARTICLES

The stability of small particles and clusters have been studied by two main techniques: a) ab-initio approaches and b) elastic continuum theory. Ab-initio approaches are often computation intensive and have been limited to the study of clusters up to 1.5nm in diameter. The elastic continuum approach on the other hand is more applicable to larger particles. Apart from these two main methods, semi-continuum approaches such as packing corrections and capillarity considerations have also been employed by Griffin and Andres (1979), Martins et al 1981, Halicioglu and White (1981), Wang et al (1984), Marks (1985) and many others.

1.4.1 Elastic Continuum Approach to Determine Structural Stability

The first attempt to calculate the relative stabilities of single crystal f.c.c particles and MTPs, using continuum elasticity, was made by Ino (1966). In his model, the total free energy of a structure was evaluated by considering it to be the sum of the cohesive



Figure 1.3.5: A polyparticle exhibiting a mixture of twinned regions.

energy U_c , surface energies U_s of the particle, the particle-substrate adhesive energy U_a . In addition to these terms the MTPs included a twin energy term U_t and a homogeneous elastic strain U_e . The total free energy can be expressed as

$$U_n = -U_c + U_s - U_a + U_e + U_t \quad (1.4.1)$$

that is

$$U_n = -V(r)E_c + S(r)\gamma - A(r)\gamma_a + V(r)W + T(r)\gamma_t \quad (1.4.2)$$

where $V(r)$, $S(r)$, $A(r)$ are the volume, the surface area and the area adhering to the substrate, " r " is the radius of the particle, W is the elastic strain energy density and $T(r)$ is the twin boundary area. The surface energy per unit volume is given by γ , the adhesive energy per unit area is represented by γ_a . The twin boundary energy is characterized by γ_t , the twin boundary energy per unit area. E_c is the cohesive energy per unit volume. Energies of the tetrahedron, octahedron, Wulff polyhedron, Dh, Ic were computed. Comparison between structures were made assuming them to consist of the same number of atoms. Numerical values for the energies were derived from the bulk (The validity of such an extrapolation for small particles is in doubt). The results, however, were in general accord with the experimental observations. The icosahedron was found to be the most stable followed by the cubooctahedron at small sizes and a crossover to the cubooctahedron was observed at larger sizes. A drawback of the analysis was its inability to explain the stability of the Dh.

In order to explain the occurrence of decahedral Dhs, Howie and Marks (1984) proposed a strong surface facetting model using a modified Curie-Wulff construction (see

Appendix A1.2). The model included the twin boundary energies as re-entrant surface contributions and also introduced the effect of surface stresses. A comparison of the energies of the three structures placed stability of the decahedral MTP between the icosahedral MTP and the single crystal for a range of sizes. It also enumerated the conditions favorable for MTP formation as extensive faceting, small twin boundary energy and small surface stresses. In both the analyzes, the MTPs are stable at smaller sizes.

1.4.2 Cluster Studies Using Ab-Initio Approaches

A simple strategy to determine the stability of small clusters is to construct units of relatively high binding energy corresponding to close packed structures symmetric about a central atom with as little surface area as possible. This "spherical" cluster approach was introduced by Bernal in his studies on the short range order of liquids and is discussed in detail in his review [Bernal 1964]. A similar approach was applied to small clusters by Benson and Shuttleworth (1951). The sphere packing models showed the realization of the Werfelmeier series [Werfelmeier 1937] in which the atoms first form a tetrahedron, which in turn grows on to a decahedron and then finally forms an icosahedron. The variety of structures possible with different packings and external habits has been detailed by Van Hardeveld and Hartog (1969). Burton (1970) found that some of the compact cubooctahedra considered by Van Hardeveld and Hartog were actually metastable and could change over into the corresponding strained icosahedra. But, at best, the spherical packing model is a crude approximation of the real atomic potentials in a crystal.

An extension of the sphere packing models uses computer simulations employing Monte-Carlo or Molecular dynamics in conjunction with atomic potentials. The simulations [Nishioka et al 1971, McGinty 1971] using various kinds of pair potentials show the MTPs to be among the stable morphologies. Again, the drawbacks of simulations is the lack of an interatomic potential truly representative of the atomic interactions in small particles, specially that of metallic particles. The applicability of the different atomic potentials to clusters has been discussed in detail by Uppenbrink and Wales (1992).

In spite of the lack of a good atomic potential, early works showed several remarkable trends in small particles. Hoare and Pal (1971),(1972),(1979) examined the compact minimum configurations and small harmonic deviations from the minima of 4 to 70 atom clusters interacting through two body potentials and found a large number of minimal energy configurations with very small energy differences between them suggesting that the clusters had several coexisting configurations. Gordon et al (1979) calculated the cohesive energies of various size clusters with icosahedral and cubooctahedral geometries and found that for the same size but different geometries, the cohesive energy difference between the clusters is very small. Similarly, a series of studies by Berry, Wales and coworkers [Beck et al 1988, Berry et al 1984, Natanson et al 1983, Davis et al 1990, Wales and Berry 1990, Wales and Berry, 1990b, Wales, 1990] show that the clusters have a number of configurations and low energy transitions are sufficient to cause a change from one state of configuration to another.

In recent years, two models employing a many body term in addition to the

pairwise interaction terms have resolved many of the difficulties associated with simple pairwise interactions.

In the "glue model" proposed by Ercolessi et al (1991), the many body term is an energy associated with the local coordination number of each atom. It accounts for the cohesive character of the electronic d-bands in noble metals. However it is non-directional. This implies that the glue model would not be able to distinguish between structures whose coordination shells contain the same number of atoms and have the same interatomic spacings but vary only in the angular disposition of the atoms. Therefore, it would not distinguish between f.c.c and h.c.p structures.

The results of a simulated annealing procedure using the glue model [Ercolessi 1991] showed the relaxed f.c.c cubooctahedron to be most stable followed by the truncated decahedron, the icosahedron and finally a disordered "amorphous" structure. These results are in direct contradiction to that of the predictions of Ino (1966) and Howie and Marks (1984) as well as experimental results.

In contrast, a detailed numerical study [Cleveland and Landman 1991] of Ni cluster energetics and structure using many body interaction potentials gave the same stability sequence as found by Marks. The many body interaction potential was obtained by the embedded atom method(EAM) [Daw and Baskes 1984]. In the EAM method, the many body term is treated as arising out of the electron density around the atoms. The attractive force is provided by the local electron density and the repulsive term is considered to be from the pairwise interaction. The embedded atom method, however, has not been used to study the effect of temperature on small particle stability.

A common observation of all the simulations, irrespective of the technique or the potential used in the calculations, is the occurrence of a finite range of temperatures and sizes within which a number of structural configurations can coexist. The concept of a coexistence regime implies the lack of an absolute minimum energy structure and we shall discuss this in much greater detail in the following chapters.

1.5 GROWTH AND TWINNING

The thermodynamic stability analyzes of the particles indicate that Ics and Dhs would be absent at larger sizes. But experimental observations show that the MTPs persist to sizes as large as 1-2mm [Haluska et al 1993]. A possible explanation for the deviation is that the particles are frozen in a kinetic state which allows for the metastable phases to coexist with the lowest energy single crystal. This would imply a gradual decrease in the number density of MTPs with size. Again, experimental results do not reflect this trend [Solliard et al 1976].

Some of the earliest observations on small particles even show the occurrence of microtwins in evaporated thin films of transition metals. Burbank and Heidenreich (1960) suggested that the twins were formed to accommodate the displacement between the lattices of coalescing nuclei. Later Hall and Thompson (1961) explained the microtwins formation as a consequence of accidental wrong stacking of atoms in the {111} faces of growing nuclei. Matthews and Allinson (1963) argued that microtwins emerged as a result of misalignment of nuclei in the early stages of growth. Misalignment of nuclei leads neighboring nuclei to have lattices closer to a twin relationship than a parallel alignment. During coalescence, one of the nuclei could easily rotate and become a twin

of the other. Thicker films would have fewer number of misaligned nuclei resulting in a more uniform perfect film. Evidence for this proposal was found in their experiments on evaporated films with a thickness gradient where the thicker end was a perfect single crystals which gradually changed into increasing numbers of misaligned nuclei.

Another mechanism, suggested by Hall and Fawzi (1986) from their observations of the development of the structure of MTPs with thickness in electrodeposited Ni films, implies that the MTPs arise by a process of repeated twinning. In contrast to the earlier work of Matthews and Allinson (1963) they found that MTPs are better formed in the thicker than the thinner films. The repeated twinning process(Figure 1.5.1) occurs by the initial formation of a single twin boundary separating two twin orientations. Secondary twins then grow, one in each of the original twins having a common boundary along the line of the original twin boundary. Finally, another section of orientation is added to complete the MTP structure. The formation of MTPs by this mechanism is supported by the common occurrence of four-twin structures in the films.

Even though these models provide plausible accounts of the formation of twins in evaporated films they do not explain the occurrence of twins within individual small particles much before their coalescence. A model for twinned particles and their growth can be found in the initial works on epitaxial deposited thin films by Allpress and Sanders (1967). They based the growth of particles on the relative bonding between metal-substrate and metal-metal atoms. The most stable arrangement of two metals atoms then is a pair and of three a triangular array lying flat on the substrate. A fourth atom can either form a planar or a tetrahedral configuration. In the event of a strong metal-

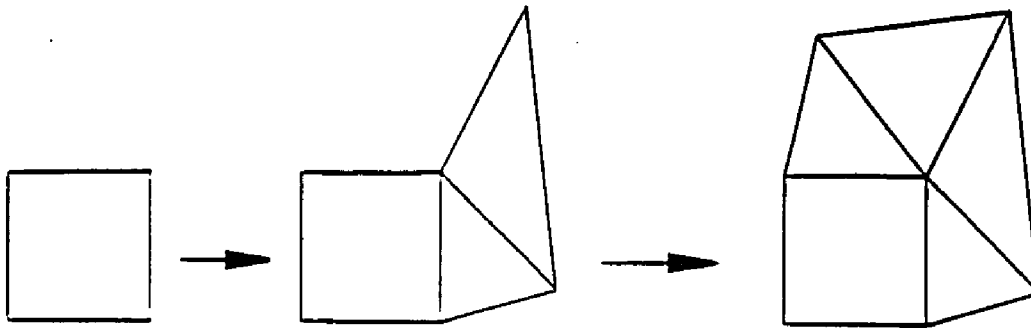


Figure 1.5.1: A schematic to illustrate the successive twinning mechanism proposed by Hall and Fawzi (1986) to explain the occurrence of five fold twins during large scale electrodeposition.

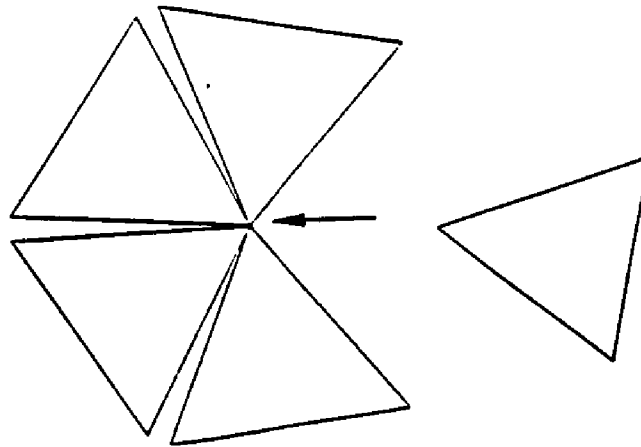


Figure 1.5.2: The successive twinning mechanism suggested by Allpress and Sanders (1967) leading to the formation of MTPs.

substrate bonding energy or a high energy atomically rough surface with many kink sites the planar configuration is preferred and forms sheets of atoms leading to lamellar structures. On the other hand, most epitaxial depositions are performed on atomically smooth substrates which allows for atoms to easily move on to the top of the planar islands to form three dimensional clusters. Renucleation of a layer on one of the exposed $\{111\}$ faces is then accompanied by a high probability of faulting leading to the eventual formation of primary twins (Figure 1.5.2). Further formation of secondary twins without renucleation would lead to a symmetrical pentagonal crystal, provided only two faces of the parent becomes twinned. If all the three faces of the parent crystal becomes twinned then an icosahedral crystal can be created. If the metal-metal bonding energy is very strong, the initial clusters will be highly faulted and the structure formed by continued growth would have most of the atoms in non-lattice sites. This would lead to a rearrangement of the atom positions into a perfect crystal which could then form MTPs by the successive twinning mechanism. They also suggest that coalescing particles can form new particles by retaining their original shapes or form new structures which have no relation to that of their predecessors. Fukano and Wayman (1969) advocated a sphere-packing sequence in which a central icosahedron undergoes a rotational displacement to become a pentagonal prism which grows about its symmetry axis.

An alternative model [Gillet and Gillet 1972], also proposed by Ogawa and Ino (1971), suggests that MTPs form from layer by layer addition to an existing nuclei. A nucleus of seven atoms exhibiting a five fold symmetry forms the decahedral MTP and a 12 atom nucleus forms icosahedral MTPs. Farges et al (1984), in a similar

model (Figure 1.5.3), proposed that an extra layer of atoms can be added onto an icosahedral nucleus either by the formation of an extra FCC layer or the formation of an additional twin. However, the potential energy of the latter arrangement is much higher and more unstable than the form for icosahedra more than three layers resulting in preferential layer by layer growth. Iijima (1987), from observations of small particles of Si formed by the arc-discharge method in an inert gas environment, concluded that decahedral MTPs can be formed from the nucleation (Figure 1.5.4) of a decahedral embryo on the surface of a liquid droplet. The embryo can then grow by subsequent crystallization of the droplet along the pentagonal symmetry axes into a decahedral MTP.

Almost all the models considered so far were suggested by observations of post deposition particles. While these observations did provide pointers on the nature of the growth process, a more definitive demonstration had to await the classic in-situ observations by cine film of Yagi et al (1975), who studied the growth processes of Ag and Au particles on MgO and clearly showed that MTPs form by successive twinning as well as by layer by layer growth. They also showed that MTPs can reform after coalescence. This was the first direct evidence of the stability of MTPs. An interesting observation made by them was that the dark field images showing the characteristic butterfly-like contrast changed continually in orientation and intensity during growth reflecting the dynamic mode of growth. This implies that MTPs could be crystallographically interrelated. In fact, Mackay (1962) and Marks (1980) suggested that the MTPs and single crystal forms are all crystallographically inter-related and thermal vibrational modes could induce structural transformations between them. Tholen (1981)

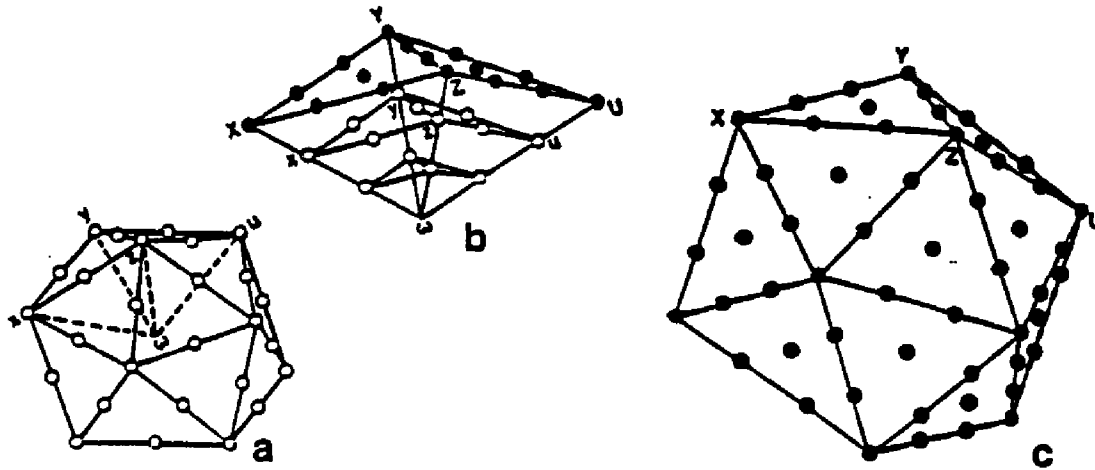


Figure 1.5.3: The layer by layer growth mechanism in a multilayer icosahedral MTP. (a) An icosahedral nucleus of 55 atoms (Mackay icosahedron). (b) The external face of one of the tetrahedrons when covered by an additional regular Fcc layer. (c) The resultant 3-layer icosahedron formed from the Mackay icosahedron (when it is completely covered by an additional layer)(Adapted from Farges et al 1984).

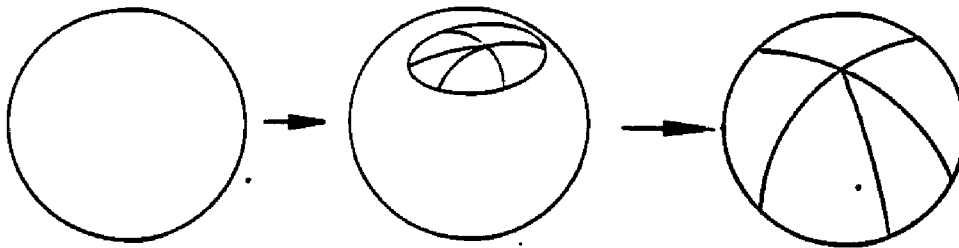


Figure 1.5.4: The nucleation and subsequent growth of a decahedral embryo from a liquid droplet, as proposed by Iijima 1987.

also showed that the particles can transform due to vibrational transformations from an analysis of Co particles aggregated by the arc-discharge method. As mentioned earlier, computer simulations also indicate that the all particles can grow and interconvert between a multitude of configurations.

1.6 STRUCTURAL FLUCTUATIONS AND QUASIMELTING

Interestingly, such coexistence regimes are not limited to small clusters. A series of electron microscopy observations [Iijima and Ichihashi 1986, Smith et al 1986, Wallenberg et al 1986, Malm et al 1988] using real time video recordings have shown that particles smaller than 5nm are structurally unstable in the presence of an intense electron beam. The particles fluctuate with high frequencies between single crystal structure and MTPs. In materials, such as Ru, which do not readily form MTPs the fluctuations took place between close packed structures of h.c.p, f.c.c and b.c.c [Malm et al 1988].

Iijima and Ichihashi (1986) observed during in situ studies that the structural fluctuations were enhanced by the electrical conductivity of the substrate. In some cases, the particles jumped away from the substrate. They discounted the effect of beam heating and suggested that the particles or local areas within them deviated temporarily from electrical neutrality. In such a case, the insulating substrate would impose Coulomb repulsive forces on the particle until it discharges. The translational and rotational motion would be affected by this force and the structural modifications would be caused by the strain induced by particle-substrate adhesion.

Howie (1986) hypothesized that the fluctuations are induced by an inner shell

excitation process. The process can be described as the removal of a core level electron which is then filled by electrons from higher energy levels followed by the simultaneous emission of X-rays and a secondary Auger cascade process due to emitted surplus energy.

An alternative mechanism considers the structural instability as a result of spikes in the temperatures of the particle. Williams (1987) speculated that rapid increases in temperature result when Auger electrons impart energy to a particle faster than the heat transferred away from the particle. The fluctuations in a 2nm cluster, at a beam flux of $20\text{A}/\text{cm}^2$ were calculated to be 10-20 times a second. This seems to be confirmed by observations, however, the occurrence of fluctuations at much lower beam fluxes [Ajayan and Marks 1989] implies that the process is driven by other mechanisms.

It has been found [Iijima and Ichihashi 1986] that heating the particle system to 500K produces similar effects as beam flux induced structural transformations. Theoretical results have also shown that heating can reduce surface anisotropy and cause structural fluctuations by reducing the activation barriers between shapes. However, calculations [Gale and Hale 1961] and experiments using energy loss spectroscopy [Rez and Glaisher 1991] of the temperature rise caused by beam heating show a maximum of only 100K. The particles are also found to be at almost the same temperature as the substrate. Such a small rise is not enough to cause the fluctuations. This discounts beam heating as the sole mechanism for structural fluctuations.

Small particles on a support are found to align themselves with a zone axis parallel to the electron beam. The particles show no correlation with the substrate orientation. The effect has been related to a direct momentum transfer due to scattering

of the electron beam. Marks and Zhang (1992) term it as an "electron wind effect". Karlan and Tholen (1988) found that such a momentum transfer can produce rotational frequencies as high as 6×10^6 rad/sec. They assume that the fluctuations in structure are produced by the elastic stresses induced by the rotations and particle-substrate adhesion. No extensive calculations were performed to show the exact relation between the fluctuations and rotations. Therefore the exact mechanism of energy transfer due to an electron beam continues to be unresolved.

Summarizing, the research on small particles indicate that the particles have numerous twinned configurations. Among the twinned configurations, the most common are the decahedral and icosahedral MTPs. The energy differences between the various configurations are very small and the particles have been observed to undergo rapid structural transformations under the beam. While the exact mechanism of energy transfer due to an electron beam remains unresolved, the temperature effect is negligible.

In the following chapters a unique method of obtaining information on the preferred occurrences of morphologies will be described and applied to material systems.

CHAPTER 2: EXPERIMENTAL MORPHOLOGY MAP (Au/SiO)

2.1 INTRODUCTION

The survey of studies on small particles and clusters in the last chapter indicated that clusters have a number of possible configurations and small particles tend to show a similar behavior. This implies that the idea of a potential energy surface introduced for very small clusters also applies to larger small particles [Marks 1983] as illustrated in figure 2.1.1. Many local minima exist corresponding to, for instance, multiply twinned particles or single crystals separated by energy barriers. If the energy differences between the wells are large and the kinetics for transitions are adequately fast the system tends to the lowest thermodynamic state. If either the kinetics are slow or the energy differences are small, a population of structures becomes feasible and with increasing energy in the system the particle would sample progressively larger areas of the potential energy surface. The critical issue then is the determination of the activation energies separating the particle morphologies.

An elegant approach to understand the nature of the potential energy surface between twinned particles of sizes larger than 10nm was suggested by Marks (1983). The basic procedure involved dividing up the twin boundaries and then minimizing the surface energy of each single crystal unit using a modified Wulff construction (see Appendix

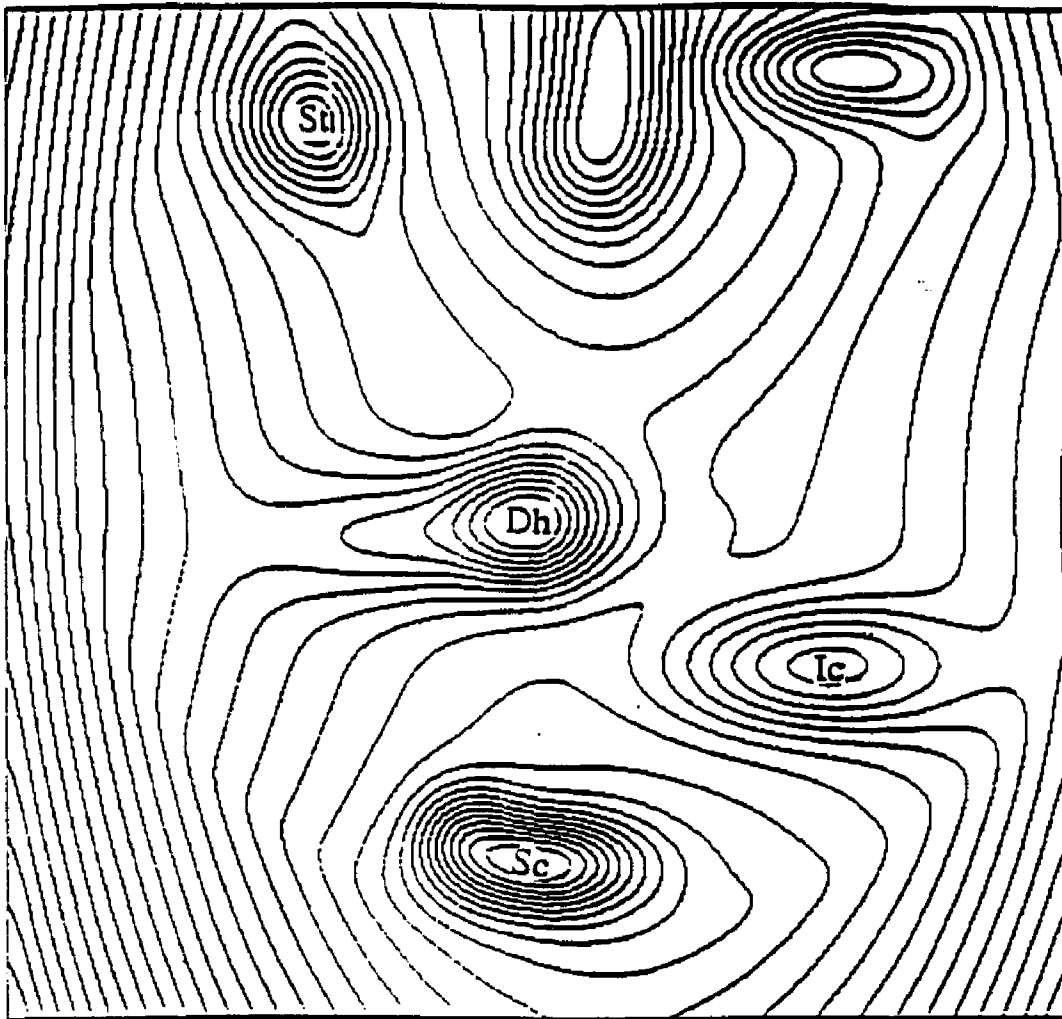


Figure 2.1.1: Schematic of a two dimensional section of a hypothetical potential energy surface (Contour map of the free energy as a function of only the morphology of the particle). Ic, Dh, Sc, St are icosahedral MTP, decahedral MTP, single crystal and single twin respectively

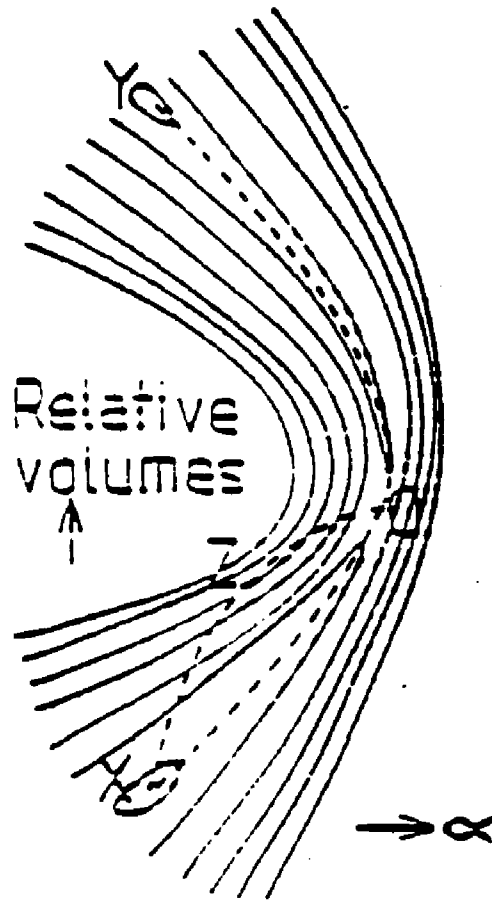


Figure 2.1.2: Diagram of a hypothetical potential energy surface for a twinned particle. Energy contours correspond to non-equilibrium values of relative volumes of tetrahedras and the fraction (α) of twin boundary energy shared by two adjacent segments. The dotted lines trace two possible paths X and Y representing single crystals. The point O is a constrained minima. Note that even though, OX and OY are low energy paths, the twin boundary constrains the particle to move along OZX (reproduced from Marks 1981).

A1.2) and then matching the partition fraction with an appropriate value of the relative volumes of the single crystal components. Each case of completely matched faces is a local minimum in the potential energy surface. Figure 2.1.2 represents the hypothetical potential energy surface. It illustrates the effect of surface faceting on the path taken by the small particle. In particular, the effect of temperature in reducing the surface faceting and inducing a shape change is seen. The model, while showing remarkable qualitative agreement with experimental observations lacks quantitative results for energy values as functions of the temperature, anisotropy and particle shape.

The effects of these parameters were studied in greater detail by Dundurs et al. (1988) by taking just one section of the n-dimensional potential energy surface. The section corresponds to a series of asymmetric decahedral MTPs. The total strain energy of a decahedral MTP was solved as a function of the distance of the 5-fold axis from the particle center in two-dimensions, followed by a constrained minimization of a (111) and (100) faceted set of five single crystal units with the same asymmetry. The structure of the crystal changes with the position of the disclination such that when $x=-1$ it is a single crystal, when $x=1$ a crystal with one twin boundary and when $x=0$ a symmetrical decahedral particle (Figure 2.1.3). The initial work by Dundurs et al. (1988) was for particles at absolute zero temperature; a later analysis included the temperature effects in terms of the entropy terms [Ajayan and Marks 1989]. The results, shown in figure 2.1.4, demonstrate that the activation energy barriers are surprisingly low even at very moderate temperatures.

From the free energy values as a function of particle size and shape, it is possible

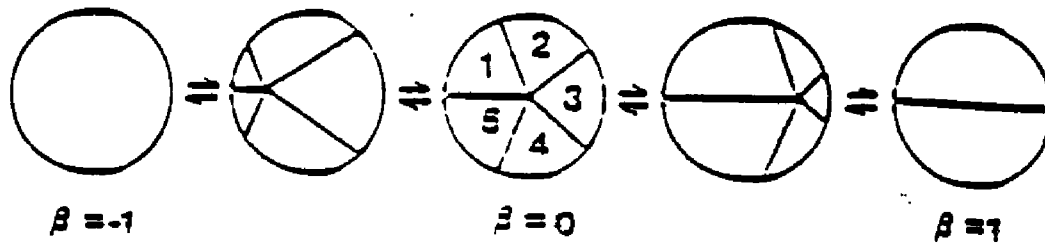


Figure 2.1.3: The two dimensional change in crystal structure corresponding to the movement of the disclination in one direction, where β represents the distance of the disclination from the center of the particle (adapted from Dundurs et al. 1988).

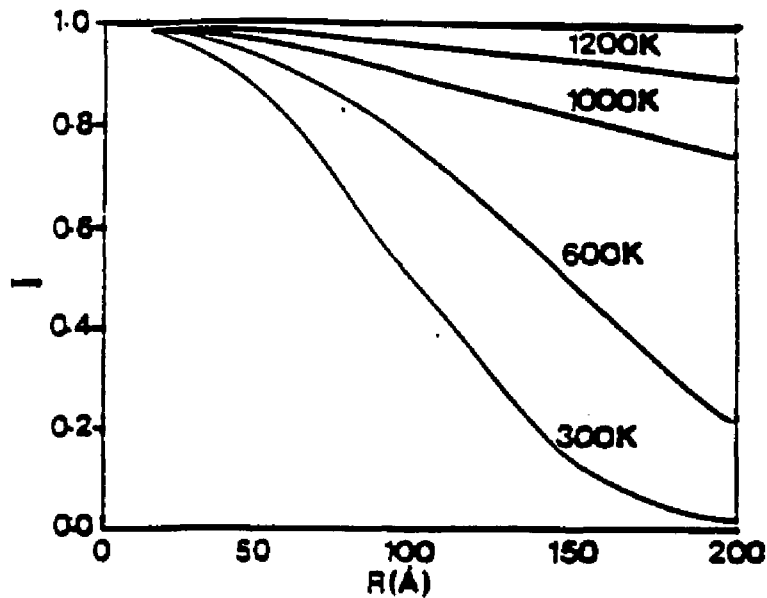


Figure 2.1.4: Schematic of the index of quasimelting shown as a function of particle radius and temperature. An index close to 1 implies lower activation energies and higher probability of structural fluctuations (reproduced from Ajayan 1989).

to estimate the conditions where a particle will start to fluctuate. This was done by taking the ratio (termed as the index of quasimelting) of the probabilities of the highest and lowest energy structures. When this was larger than 0.95, structural fluctuations were assumed to be possible. At low temperatures and moderate sizes the particles are static. Increasing temperatures closer to the melting point, on the other hand, lead to fluctuations. A phase diagram (Figure 2.1.5) constructed from the calculated free energies and the data for size dependent melting given by Couchman and Ryan (1978) was used to indicate the stability regimes for the icosahedral MTP, decahedral MTP, single crystal and the melt. The regimes include a region, referred to as "quasimelting", of unstable structures coexisting together. It corresponds to a region where the particles have an index of quasimelting larger than 0.95. Many molecular dynamics calculations of small clusters have observed the same phenomenon, which in some cases has been described as premelting [Heyraud et al. 1989, Ercolessi et al. 1991, Beaglehole 1991]. Because of the difficulties of handling large enough clusters to match the small particle data, and also long enough time periods, comparison is difficult. For instance, Sawada and Sugano (1991) attempted an extrapolation from their data but were unable to obtain reasonable results unless they hypothesized multiply ionized clusters, which is unreasonable.

As apparent from the real time observations and the theoretical calculations, particles occupy a variety of morphologies which can be considered as local minima in potential energies in a configurational space [Marks 1983]. The nucleation and growth of the particles follow a trajectory in this space decided by the probabilities of the morphologies at a given time for the local conditions around the particle. In this sense,

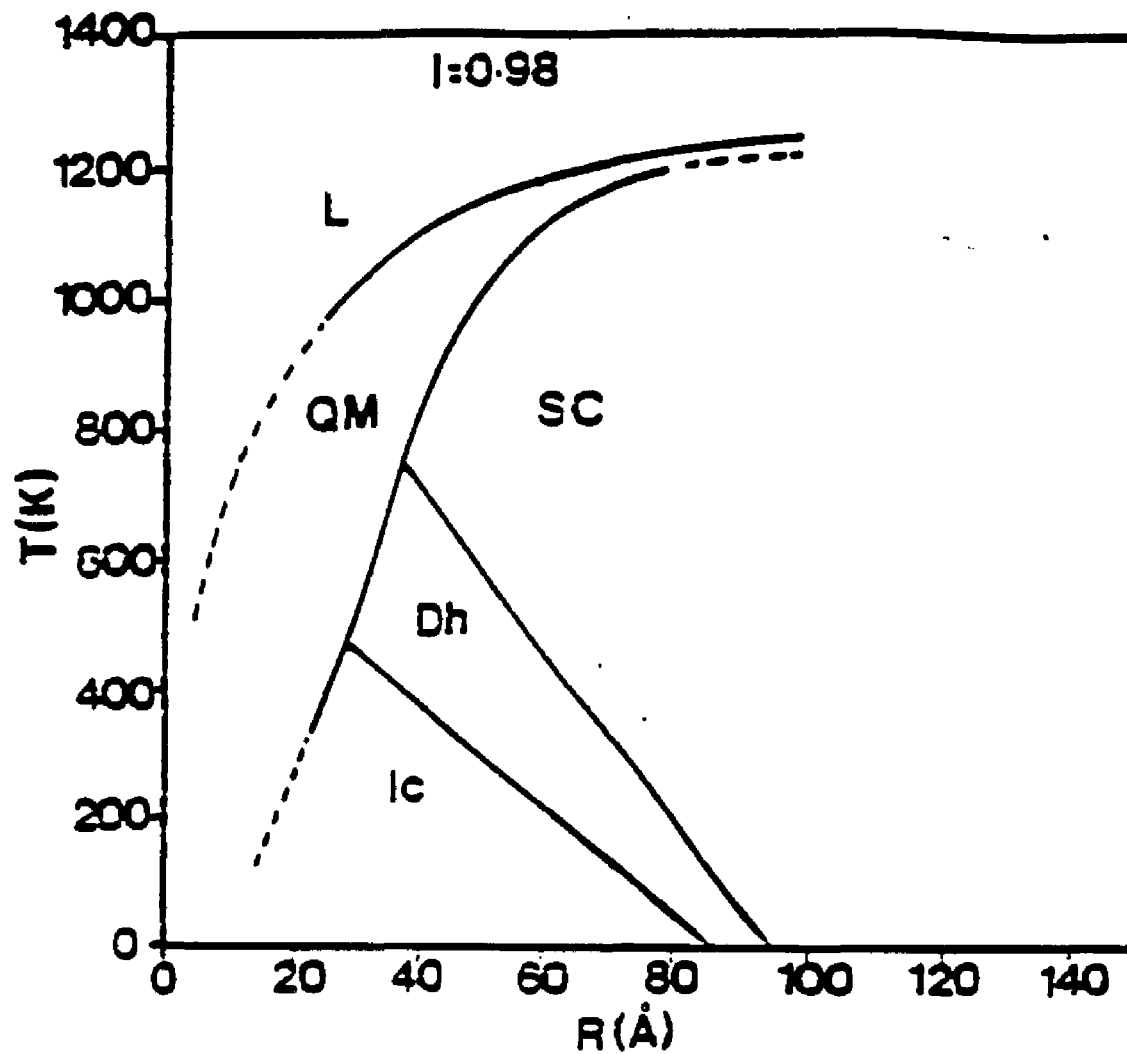


Figure 2.1.5: Phase map showing the stable structures and the quasimolten phase. Stability regimes are: the liquidus state L, the quasimolten state QM. Dh, Ic, Sc are the decahedral MTP, icosahedral MTP and the single crystal regimes respectively (Ajayan 1989).

the particle morphologies are history dependent and any real attempt to decipher the evolution of particle morphologies would have to consider the entire configurational space or at least a section of the space for a given controlled set of conditions.

At this juncture of studies on small particles, there is a bewildering amount of information collected on small particles. However, all the experiments, except the inert gas aggregation methods [Renou and Gillet 1981, Hall et al. 1991, Reinhard et al. 1993, Reinhard et al. 1994] and the static morphology study by Yagi et al. (1975), sample only single points of the configurational space.

Electron diffraction studies on free floating particles formed by the inert gas aggregation method form a systematic approach to verify the "phase diagram" experimentally. The studies also satisfy the assumption of a free floating cluster. The method [Yokozeki and Stein 1978] uses a hot vapor produced by evaporation from a molten source. This vapor then mixes with an inert gas, which is much cooler, causing the vapor to cool very quickly and condense into small particles. The mixture of small particles and gases are then directed along a beam of gas, by differential pumping of the chambers in the path of the electron beam. The data obtained from the method [Hall et al. 1991] using a modified inert gas system and a set of electron diffraction patterns for the three particle types in the phase diagram show qualitative agreement with the phase diagram. However, the inert gas aggregation method is strongly affected by the conditions at the evaporation source and the gradient in conditions below it. These parameters vary significantly with each experimental run, thereby reducing the quantitative application of the data to free floating particles. HREM imaging offers an

alternative solution, in being able to record the morphological fluctuations in real time. Again, experimental real time information has been largely limited to short time observations which only show the existence of structural transformation in small particles. Only two papers [Kizuka et al. 1993, Narayanaswamy and Marks 1993] identify and quantitatively differentiate the components of the real time observations in small particles. Kizuka et al. (1993) focussed on the orientation relationship between a fluctuating small Au particle and its substrate (MgO crystallite). Narayanaswamy and Marks (1993) showed that a fluctuating Au particle subjected to an electron beam has a high rate of rotations along with a much lower rate of transformations. In particular, real time high resolution electron microscopy (HREM) has not been used quantitatively to follow the time evolution of the transformations of a small particle for a range of sizes.

In this chapter, a method of obtaining quantitative information on the time evolution of morphological fluctuations will be discussed and applied to extract information to map the potential energy surface and to understand the nature of the kinetics of the fluctuations.

2.2 SAMPLE PREPARATION

Small particles can be deposited onto a variety of substrates. In order to conduct the real time studies, three such substrates were chosen. MgO is an electron transparent crystalline oxide which can be easily synthesized by "smoking" a Mg ribbon and collecting the "smoked" particles onto a grid. Holey amorphous carbon is also another ideal substrate for the imaging of small particles. Similarly, SiO is a stable amorphous oxide of Si commercially available in large quantities as mm size particles. When

suitably crushed it cleaves into wedge shaped, smaller particles with abundant thin material at the edge. The thin edge is electron transparent. The amorphous nature of SiO also ensures minimal substrate-particle effect, preventing any bias for a morphology due to preferred orientation relations. Moreover, Au does not react with all three of the substrates to form any subsidiary compounds at the interface. Au is an inert noble metal and is very stable even at atmospheric conditions. It also has a low sticking coefficient which reduces ambiguity in the experiment due to changes in surface energy from chemisorption. As a material for imaging, its high atomic scattering factor makes it easy to identify against the backdrop of SiO.

Small particles deposited on all three of the substrates showed morphological transformations. However, an amorphous substrate was preferred over a crystalline substrate to minimize any preferred morphology due to particle substrate orientations. Most of the experiments were conducted on SiO due to the ease of synthesis.

Au-SiO specimens were prepared by adding a drop of distilled H₂O containing fine crushed SiO onto a 1000 mesh, 3mm Cu grid. Au was then deposited from a resistively heated tungsten boat onto the dried grid in a Denton 501a evaporator maintained at a base pressure of 1×10^{-6} torr. The deposition was monitored by a crystal monitor sensitive to submonolayer coverages. The prepared specimen was then quickly transferred to a Hitachi H-9000 HREM routinely capable of a pressure of 1×10^{-7} torr.

Two different flux conditions are possible in the microscope. A low flux condition, in which the beam flux varied up to 60 amps/cm^2 , can be obtained by the insertion of a condenser aperture. In the absence of any aperture a high flux condition

of up to 150amps/cm^2 is obtainable at the cost of a small loss in resolution. The fluxes can be directly monitored by the insertion of a Faraday cup. Further sample preparation was conducted in the microscope. An initial anneal of the specimen at a beam flux of 50amps/cm^2 with a condensed beam for 15 minutes was performed to remove carbon contaminants from the surface.

One of the problems associated with studying supported particles is the often quoted "ambiguity" of the role of the substrate. Substrate particle interactions are known to cause encapsulation of particles as well as form pillars beneath the particle [Ajayan 1989]. Pillar formations have been observed in Au-MgO systems and the catalytic growth of bucky tubes [Amelinckx et al. 1994] has been attributed to the same mechanism. In fact, similar growth patterns have been found in the growth of Si, Ge whiskers and InP pillars [Bootsma and Gassen 1971, Givargizov 1975]. The process can be understood as a competitive mechanism between the surface diffusion of the substrate to encapsulate the particle and the volume diffusion promoted by the curvature and interfacial stresses at the particle substrate interface. The bulk diffusion can be enhanced by creating a large number of point defects [Itoh and Tanimura 1986, Murphy 1989]. In the microscope, this can be achieved by the use of an electron beam [Ajayan 1989]. Pillars readily form at high fluxes. In the Au-SiO system the pillars are more of the form of mounds tapering from the substrate towards the particle (Figure 2.2.1). Since the process involves only local diffusion and there is no renewal of mass to maintain a concentration gradient, the mass transport reduces with time and an equilibrium height is attained, depending on the beam flux and the radius of the particle. It has been shown [Ajayan 1989] that the height

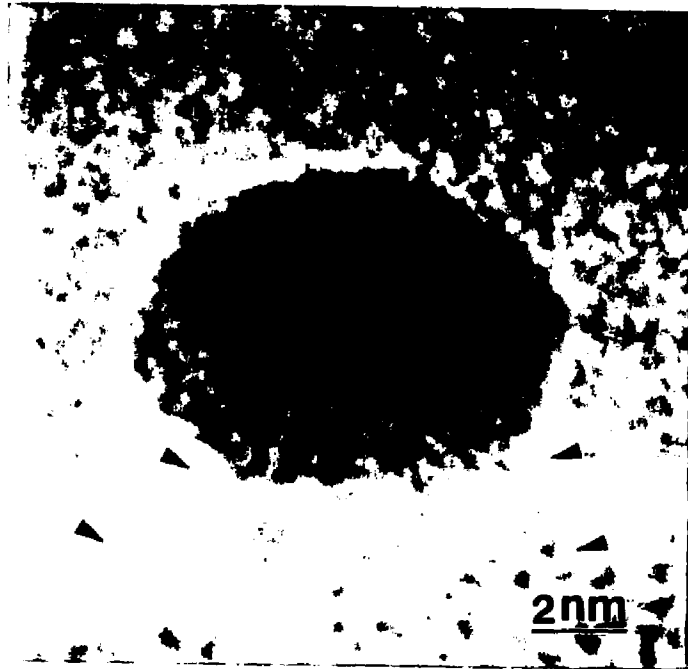


Figure 2.2.1: Pillar formed beneath a particle.

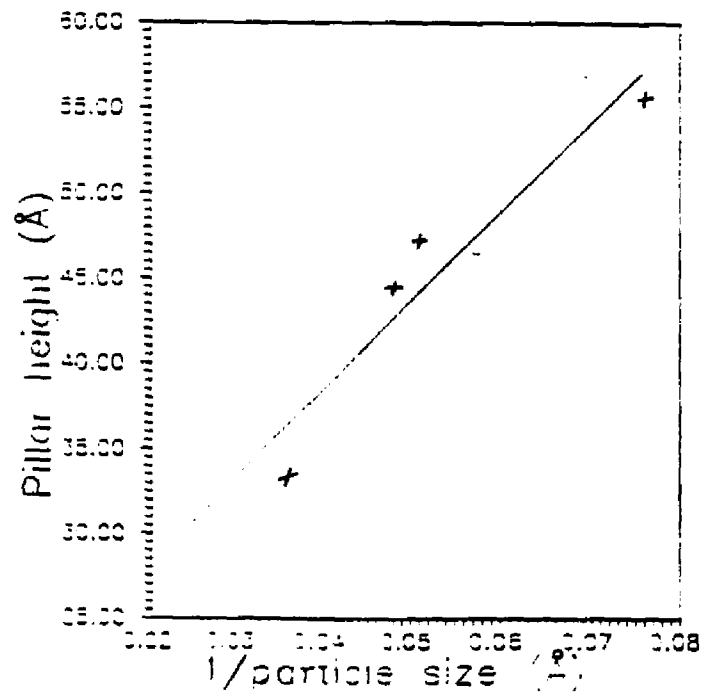


Figure 2.2.2: A linear plot of the pillar height as a function of particle radius (from Ajayan 1989).

of the pillar varies inversely with particle size (Figure 2.2.2). Substrate particle interactions were further minimized by a second annealing cycle, after selection of the particles of interest. The beam flux in the second cycle was controlled such that the substrates directly beneath the particles formed mounds which did not change in height during the observations. Further, high fluxes (22Amps/cm^2) are necessary to initiate the process of morphological transformations but the fluxes required to sustain it are much lower [Ajayan and Marks 1989]. Particles smaller than 5nm transformed between morphologies even at 3A/cm^2 , the minimum flux at which the particle fluctuations could be recorded. Sometimes, higher fluxes led to very rapid movement and rotation of the particles which displaced them off the mounds. After being displaced off the mounds the rate of structural transformations of the particles decreased until they once again rested atop pillars. All observations to map the evolution of morphologies were therefore conducted by first initiating the formation of pillars. Due to the sensitivity of the pillars and particles to these parameters and the variation of the upper and lower limits of flux conditions with size, only particles which formed stable pillars and remained on them for at least 5 minutes were used for the observations.

2.3 DATA ACQUISITION

2.3.1 Data Reduction Scheme

The morphological transformations in the selected particles were then observed, in real time, with a fiber optically coupled GATAN TV camera. Simultaneously, images were recorded onto Hi8mm video tapes using a Sony EVO9800 connected to the TV camera. The images in the tape were then individually scanned into an Apollo

workstation through an ITEX image grabber for further analysis by SEMPER, an image processing software (Figure 2.3.1).

To ensure a good statistical count, each observation lasted for more than three minutes. During this time several hundred image frames (each corresponding to an exposure of 1/30th of a second) were recorded. These images were then analyzed and pattern matched by using a data reduction scheme. A basis set of good images was selected from each recording and completely characterized using simulated images and experimental images obtained by earlier workers [for example: Marks and Smith (1981), Buffat et al. 1991, Kirkland et al. 1991, Altenheim et al. 1991, Giorgio et al. 1992, Giorgio et al. 1993]. Each basis set consisted of four distinct morphologies in various orientations, featureless structures were identified as indistinguishable and structures with features that could not be classified were categorized as unknowns (Figure 2.3.2).

The entire recording for that particle size was then processed frame by frame by matching all the images with the characterized basis set. The images were matched by comparing overall particle morphology, facetting and re-entrant faces. Cross correlation filtering with a Gaussian [Frank 1980, Buckett 1991], Fourier filtering and power spectra of single frame images were used to enhance the visibility of any fringes in the particle.

2.3.2 The Basis Set

The basis set comprised of the commonly occurring single crystals, single twins, icosahedral MTPs and decahedral MTPs. The images of the different structures vary with orientation and a complete classification requires image simulations at different orientations. Many researchers [Marks and Smith 1981, Buffat et al. 1991, Kirkland

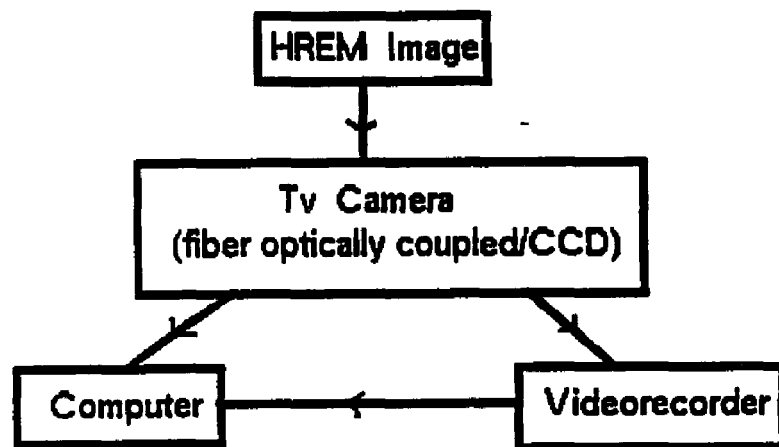


Figure 2.3.1: The experimental setup

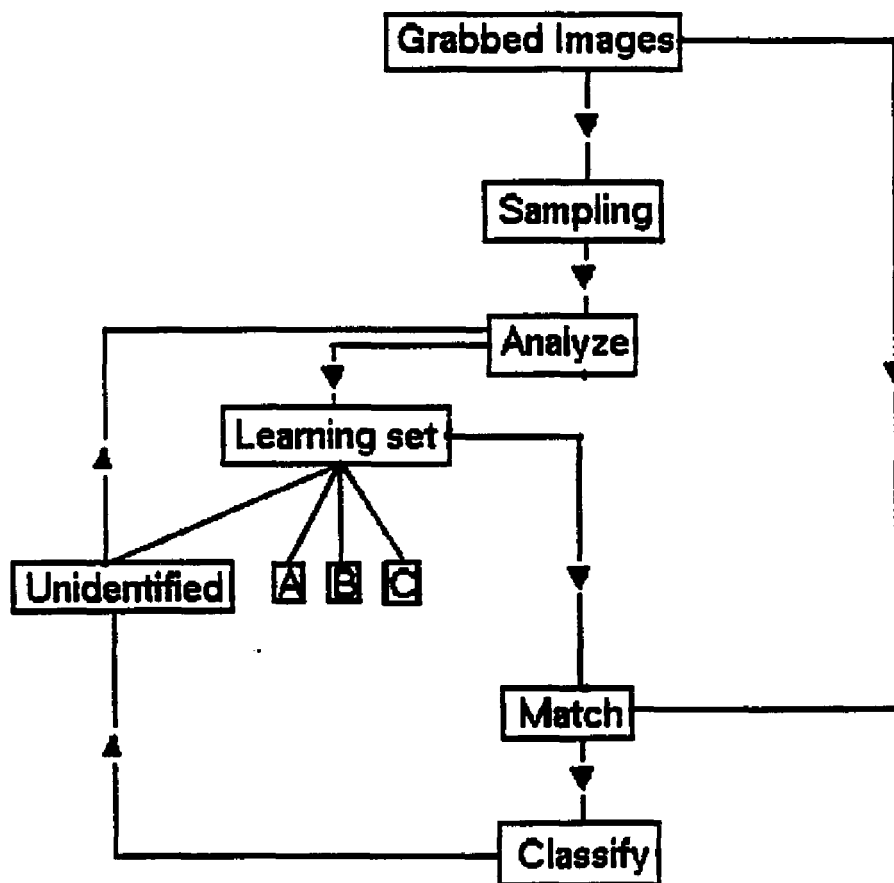


Figure 2.3.2: The data reduction scheme.

1991] have identified several different orientations. Some of the symmetric structures from these classes and their contrast variations are discussed below.

Cubooctahedral single crystal for fcc metals is an octahedron with (111) external facets, truncated by a cube having (100) facets and centered on the octahedron. Sometimes there is an additional truncation by a second cube with (110) type facets. The extent of the truncations is decided by the relative surface energies and in Au, the structure is closer to a cubooctahedron with regular hexagonal (111) facets.

The contrasts in most images result from the {111} and {200} type planes and in some cases there is a small contribution from the {220} sets. The most easily identifiable of the cubooctahedrons are the high symmetry axes, that is, the $\langle 110 \rangle$ and $\langle 100 \rangle$ orientations. These orientations give rise to "atomic column" contrasts of black and white dots. When viewed down the $\langle 110 \rangle$ axis, the contrast arises from two {111} and one {200} sets. The result is a series of black and white dots with an angular pattern (Figure 2.3.3). In the $\langle 100 \rangle$ orientation, two {200} sets of planes cross each other at right angles. The image consists of a rectangular mesh pattern (Figure 2.3.4). Most of the cubooctahedral images can be classified by considering just these orientations and taking care to note that the real time images do not necessarily have symmetrical particles and the orientations will mostly be at a small angle deviation from these axes (for example: Figure 2.3.5). Single crystals do not have any reentrant faces in the external morphology. By their definition, they have no planar defects which considerably simplifies their identification. Figure 2.3.6 illustrates a decahedral MTP which can be wrongly identified as a single crystal without careful scrutiny.

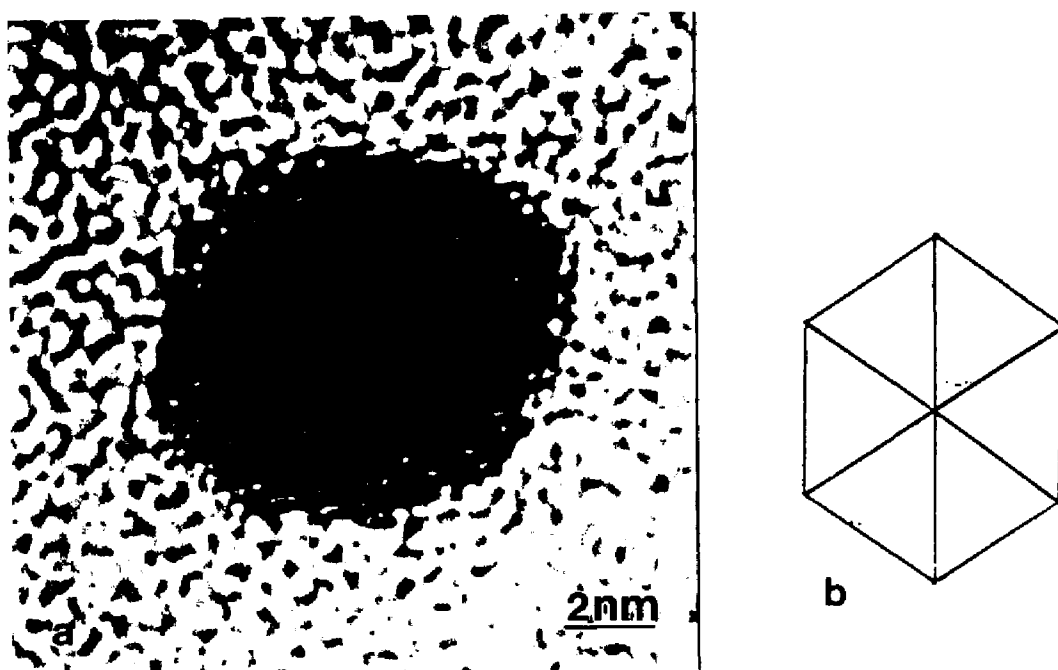


Figure 2.3.3: (a)HREM image of a cubooctahedral particle in the 110 orientation. (b) Schematic of the 110 oriented cubooctahedral particle.

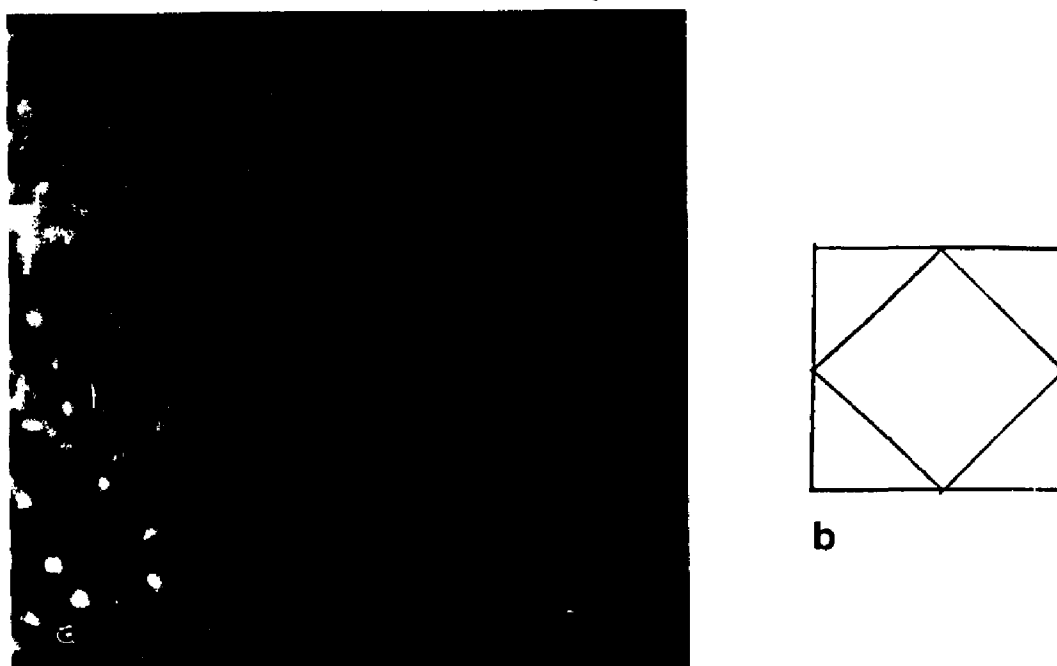


Figure 2.3.4: (a)HREM image of a cubooctahedral particle in the 100 orientation. (b) Schematic of the 100 oriented cubooctahedral particle.

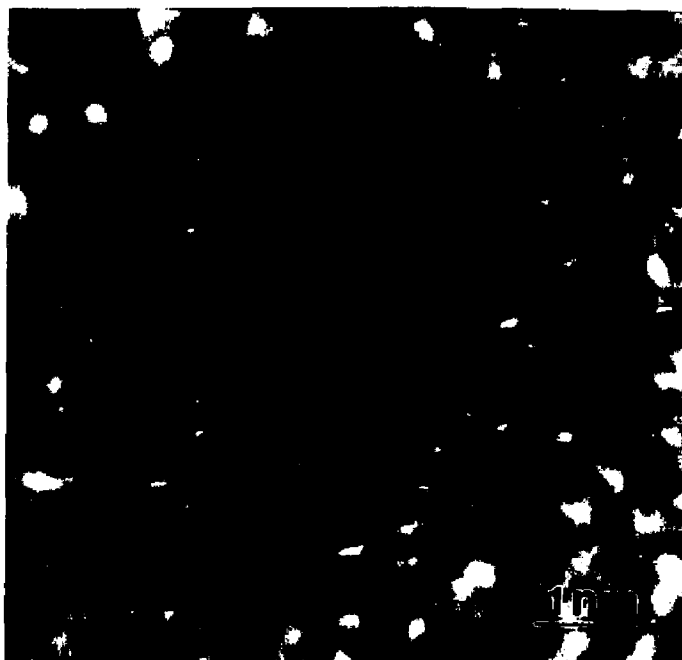


Figure 2.3.5: (a) A single crystal showing only one set of {111} fringes.



Figure 2.3.6: An asymmetrical decahedral MTP with the disclination located very close to the crystal edge.

Single twinned particles resemble single crystals in many respects. However, they can be distinguished by the presence of a single line of black and white dots separating two mirror symmetric regions. Often, the line of separation is not visible and the morphology is distinguished solely on the basis of the mirror symmetry of the contrast (Figure 2.3.7).

The contrast arising from MTPs can be qualitatively understood from the orientations of the individual tetrahedra within them. The tetrahedra have (111) external faces and the edges are always along the $\langle 110 \rangle$. A facet parallel to the direction of observation is, therefore, a set of {111} planes imaged as a set of fringe lines. One edge parallel to the beam induces atomic contrast. The final image can then be considered as a sum of these effects with the inclusion of the variation in thickness of the tetrahedra.

Perhaps the most easily recognizable structure in the basis set is the five fold symmetric $\langle 110 \rangle$ oriented decahedral morphology. In this orientation each of the five tetrahedra has an edge parallel to the axis of observation giving rise to atomic column contrast (Figure 2.3.8). The other high symmetry axes $\langle 100 \rangle$ and $\langle 111 \rangle$ also give an atomic column contrast. When the decahedral MTP rests on one of its faces, the resulting image (Figure 2.3.9) reveals only {111} fringes on one edge while the remaining twinned regions are seen only as dark contrast areas. At a tilt of 77.6 degrees from the fivefold axis, a rather unique structure is seen. Flueli et al. (1991) explain the contrast as one twin plane parallel to the beam produces one set of fringe lines extending over the image of the two tetrahedra joined by a twin. Then each external facet parallel to the axis of



Figure 2.3.7: A single twinned crystal (twin indicated by an arrow).

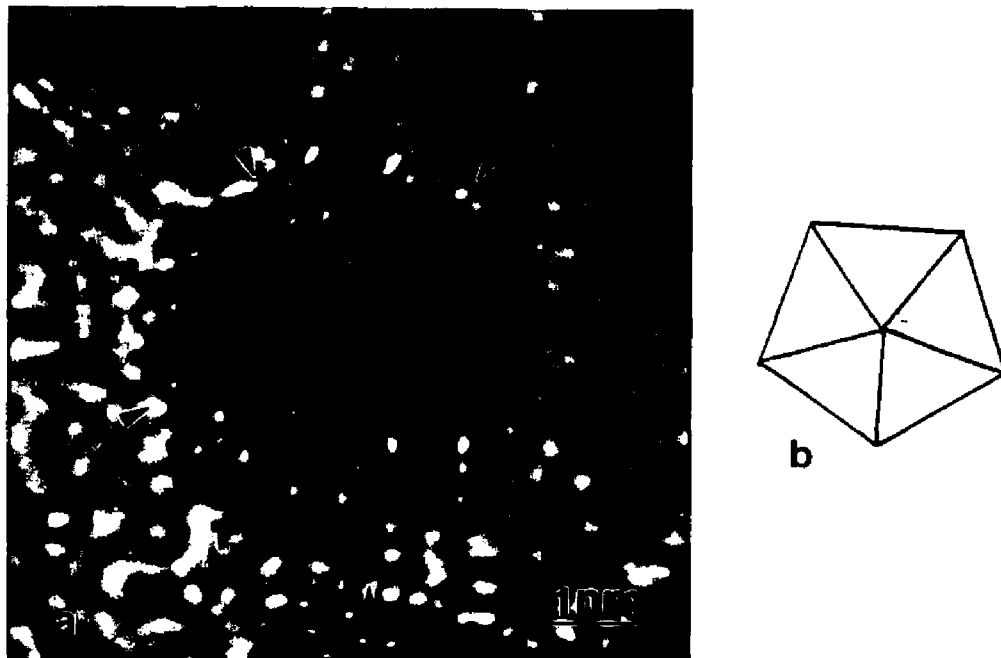


Figure 2.3.8: (a) HREM image of a decahedral MTP in the fivefold orientation. Note the clearly resolved twins. (b) Schematic of the orientation.

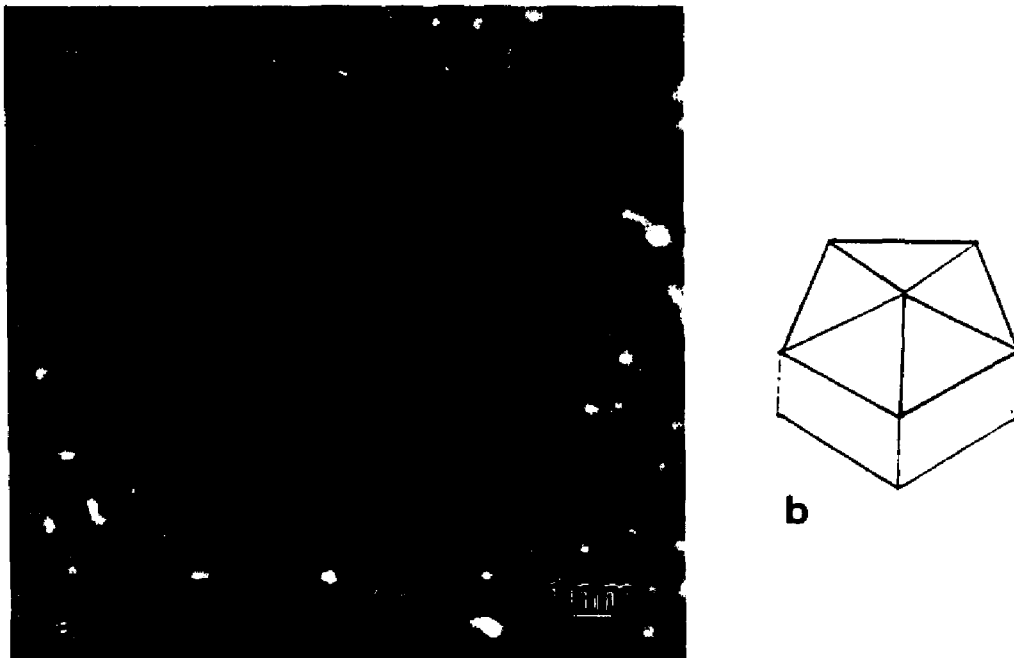


Figure 2.3.9: (a) HREM image of a decahedral MTP lying on a 111 face. (b) Schematic of the orientation.

observation generates one set of fringes which on superposition with the first set produces the contrast in figure 2.3.10. Another complex structure, which is often not considered as identifiable, is shown in figure 2.3.11. It is a decahedral MTP oriented at an azimuthal angle of 60 degrees and a declination of 18 degrees from the five fold axis. Simulations [Kirkland 1991] indicate that the image is composed of {111} fringes in $\langle 112 \rangle$ tetrahedra and crossed {111} and {200} fringes from $\langle 110 \rangle$ tetrahedra which overlap to produce Moire fringes extending over large parts of the particle image. Decahedral MTPs and single twinned morphologies present almost identical contrasts in some conditions. Figure 2.3.12 is one such case. It clearly shows two different planes and the appearance is similar to a $\langle 110 \rangle$ oriented crystal with a single twin on a {111} plane. Closer examination shows that the planes are not mirror symmetric, the "twinned region" ends with a ribbed structure which is characteristic of a decahedral MTP oriented at an azimuthal angle of 0 (or 36) degrees and at a declination of 60 degrees.

Figure 2.3.13 illustrates an icosahedral MTP in the five fold symmetric $\langle 110 \rangle$ orientation. The contrast arises from two decahedral domains observed along their five fold axis and rotated by half the tetrahedral apical angle ($\pi/10$) with respect to each other. The resulting Moire pattern shows a tenfold symmetry for a perfect icosahedral MTP. The image is extremely sensitive to distortions and misorientations from the ideal structure and the tenfold symmetry is rarely seen in experimental images. The orientation is extremely difficult to interpret in the presence of a strong amorphous background (Figure 2.3.14).

The image of an icosahedral MTP along the two fold symmetry axis ($\langle 112 \rangle$) is

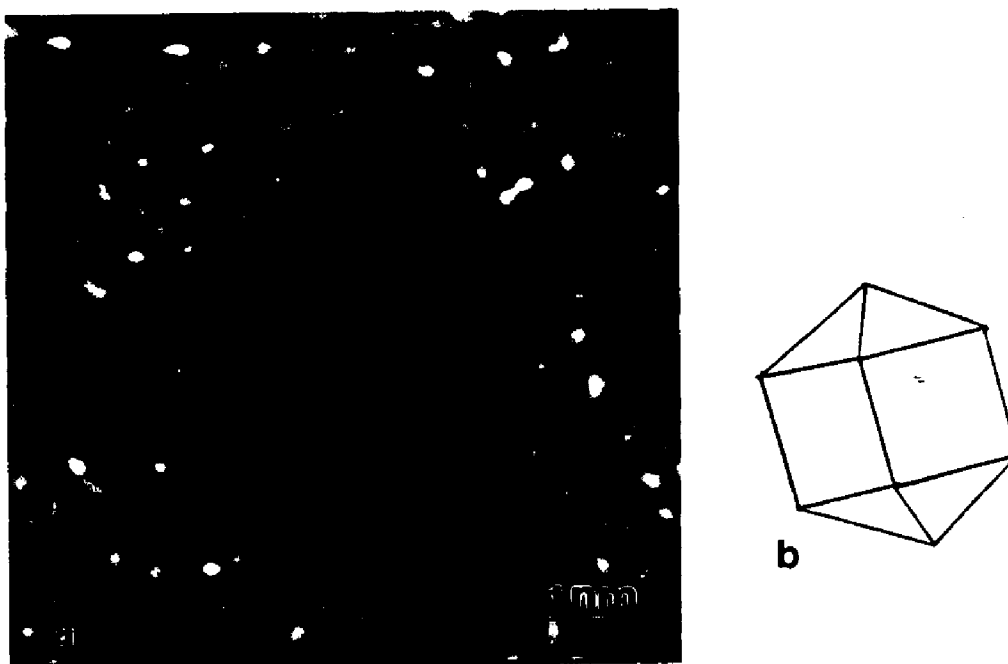


Figure 2.3.10: (a) An HREM image of a decahedral MTP tilted by an angle of 77.6 degrees from the five fold orientation. (b) Schematic of the orientation.

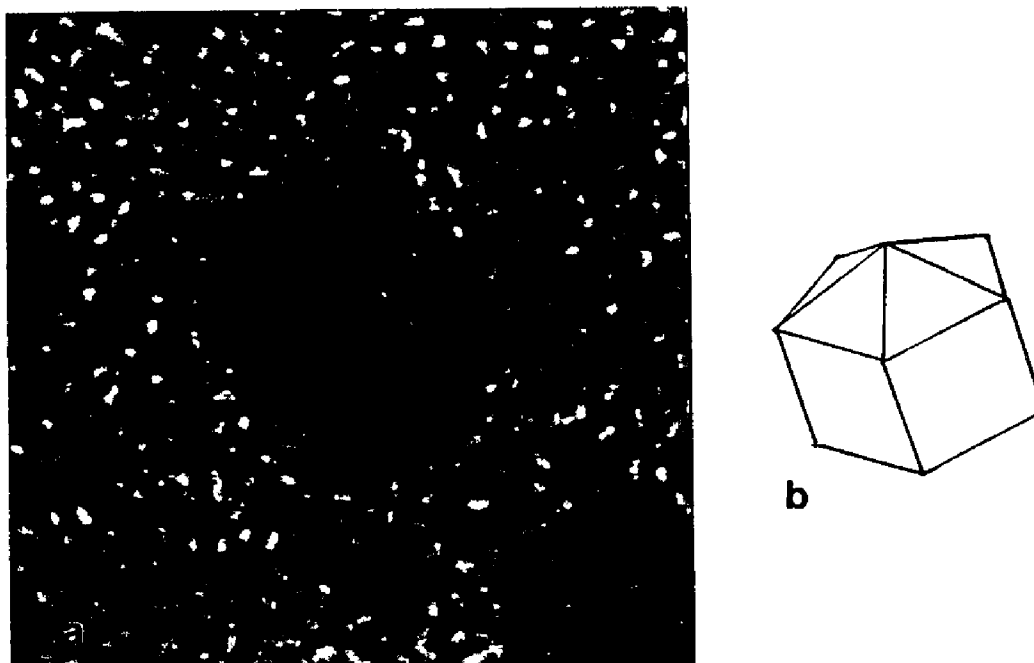


Figure 2.3.11: (a) An HREM image of a decahedral MTP at an angle of 60degrees azimuthal, 18 degrees declination from the five fold orientation.

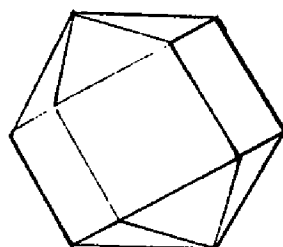
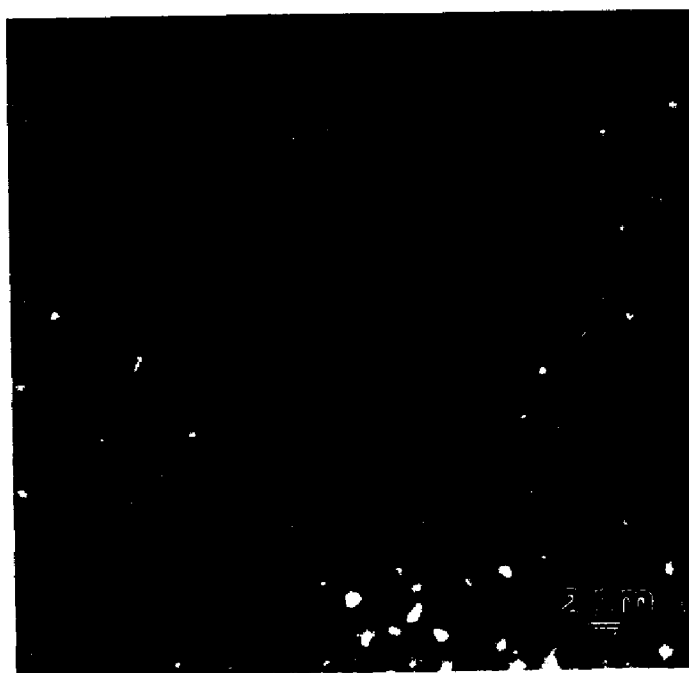
**b**

Figure 2.3.12: (a) A decahedral MTP that is commonly mistaken to be a single twin.(b) Schematic of the orientation.

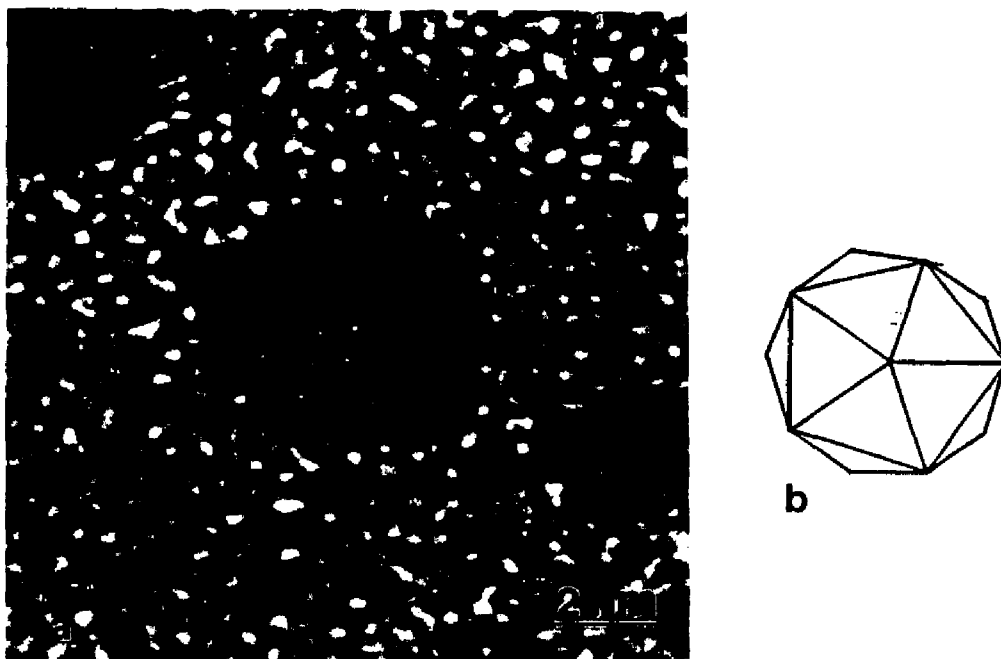


Figure 2.3.13: (a) A five fold symmetric orientation of the icosahedral MTP is seen in this HREM image.(b) A schematic of the orientation.

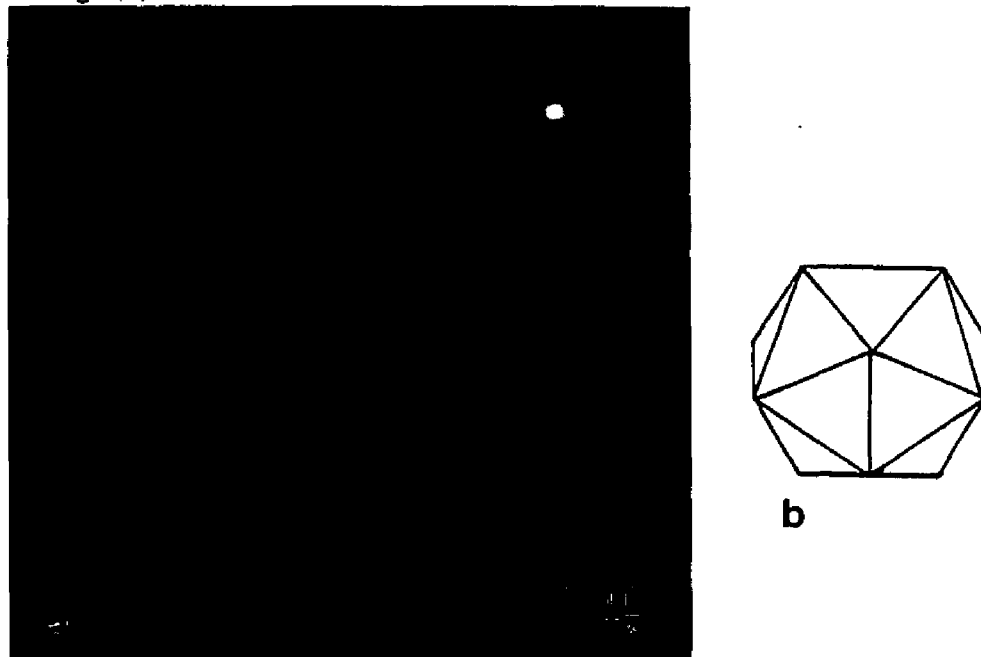


Figure 2.3.14: (a) HREM image of a fivefold symmetric (misoriented) icosahedral MTP in an amorphous background.

easily recognized by the presence of a ribbed structure along the central plane. The contrast, in terms of tetrahedra, arises mainly from eight tetrahedra, grouped in eight bitetrahedral domains. Only these tetrahedra are oriented to give atomic column contrasts (Figure 2.3.15).

The $\langle 111 \rangle$ orientation of the icosahedral MTP forms a three fold symmetric axis. In this orientation, six twin planes are parallel to the axis of observation leading to six $\{111\}$ sets, extending in both tetrahedra. The apparent atomic column contrast is actually a result of the superposition of the images of planes in overlapping tetrahedra. The lack of contrast at the common centre of the tetrahedral regions is due to a decrease in thickness of the tetrahedra contributing to the image towards the centre of the icosahedral MTP (Figure 2.3.16).

The images recorded in real time during morphological fluctuations are usually from asymmetric distorted structures and these variations maintain image contrasts similar to those in the basis set (as long as they are close to the orientation causing the characteristic contrast). Figure 2.3.17 illustrates the possible variations for the five fold orientation. Similar variations are also shown for the two fold symmetric [Figure 2.3.18] and three fold symmetric [Figure 2.3.19] icosahedral MTP. Sometimes, the orientations and crystal form could not be identified and these were included in the basis set as "unidentified" (for e.g: Figure 2.3.20).

An ideal situation would have allowed for computerization of the entire process through a pattern recognition routine, however, the large number of structures and small deviations from the basis set prevent fast analysis of the data. Therefore, the images were

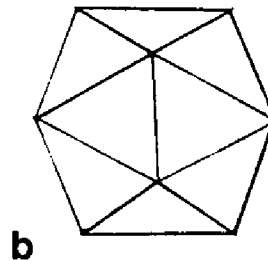
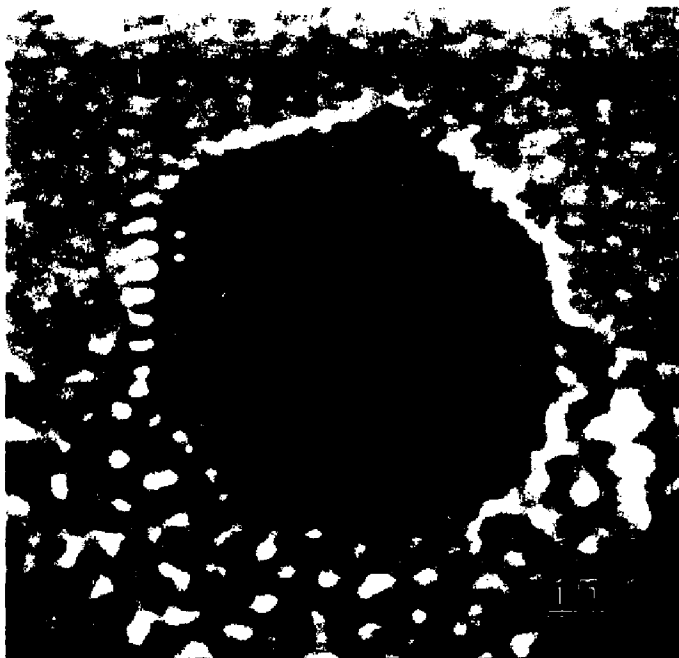


Figure 2.3.15: (a) HREM image of a two fold oriented icosahedral MTP. (b) Schematic of the two fold oriented icosahedral MTP.

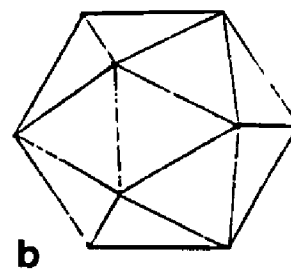


Figure 2.3.16: (a) HREM image of a three fold oriented icosahedral MTP. (b) Schematic of the three fold oriented icosahedral MTP.

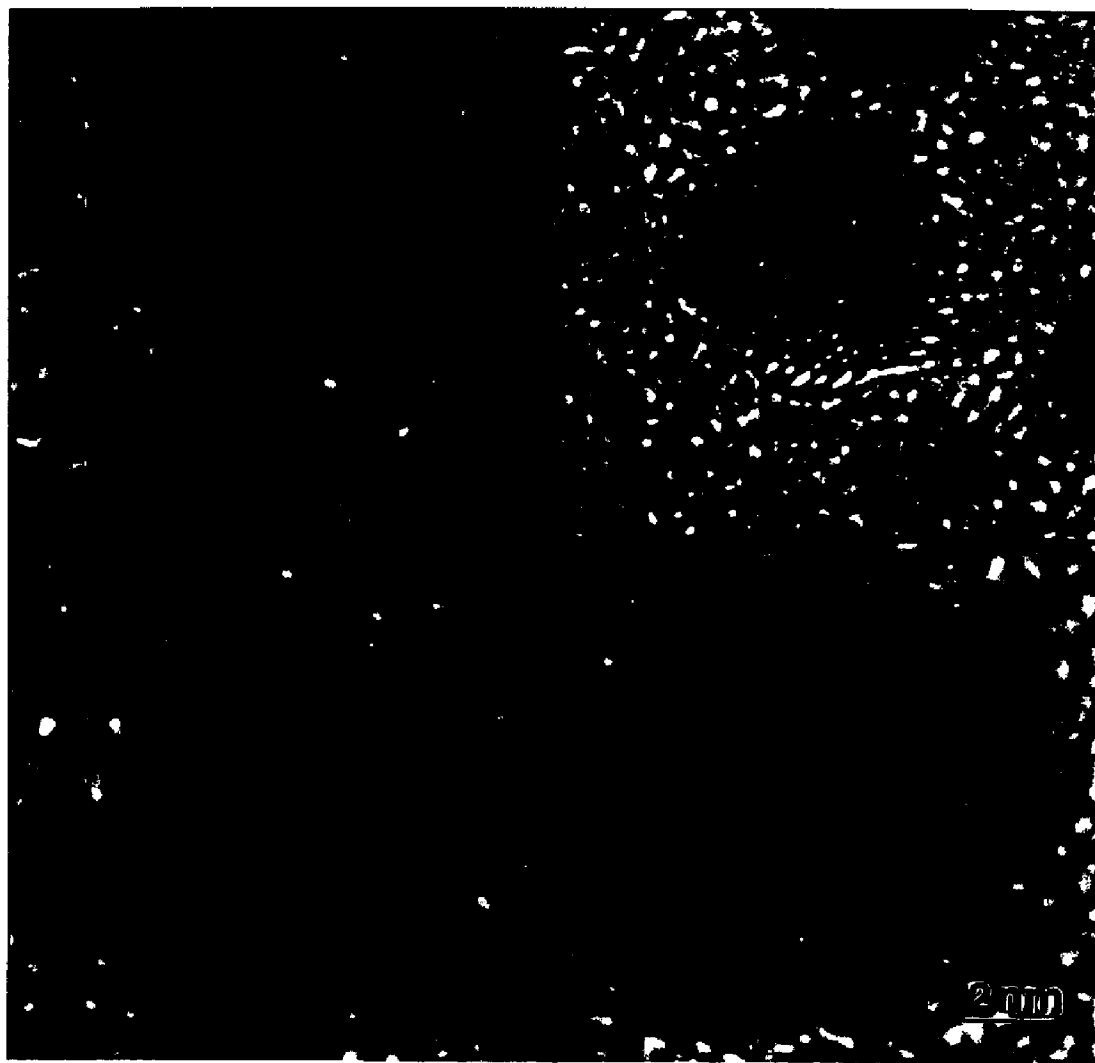


Figure 2.3.17: HREM images of decahedral MTPs which are misoriented from the fivefold axis.

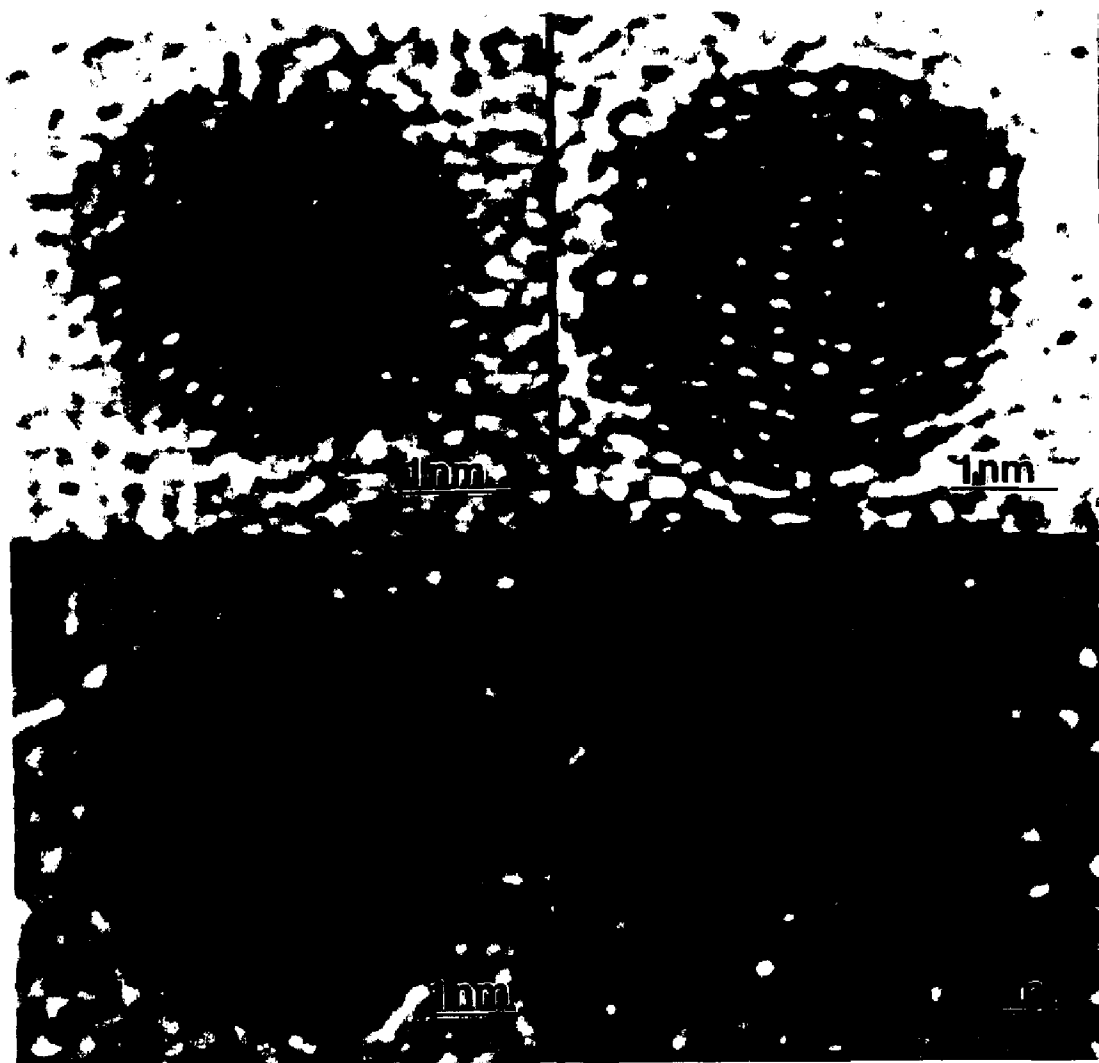


Figure 2.3.18: HREM images of icosahedral MTPs which are misoriented from the twofold axis.



Figure 2.3.19: HREM images of icosahedral MTPs which are misoriented from the threefold axis.

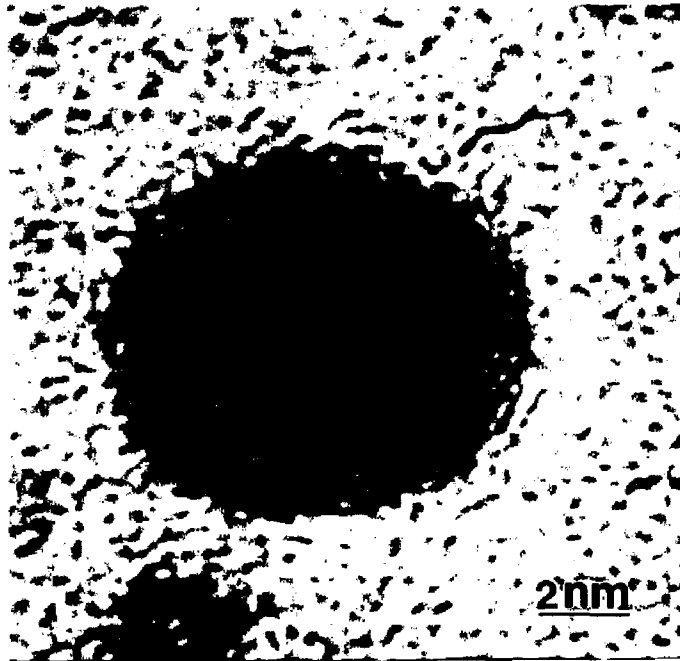


Figure 2.3.20: An unidentifiable HREM image.

processed by the time consuming process of visual comparison with the basis set using the computer as an aid to refine any structural details for easier identification.

2.4 RESULTS AND DISCUSSION

A typical set of time sequence series obtained by the data reduction scheme is shown in figure 2.4.1. The particle transformations does not show any order of preference, that is, any of the morphologies can form from any of the other morphologies in the basis set. The particles transformations encompass the entire basis set in a few seconds for even the lowest flux of observation. The sequences also show that increasing the beam flux increases the rate of transformation between morphologies. From these observations, it can be directly inferred that the electron beam provides an external driving energy for the particle to surmount the activation energy barriers between the different morphologies.

A better representation of the kinetics of morphology transformations can be extracted from the time sequence series in terms of the mean residence time (t_m) in a morphology which is directly related to the activation energy barrier as :

$$t_m = v \exp\left(\frac{-G}{kT}\right) \quad (2.4.1)$$

where v is the number of attempts made by the particle to overcome the activation barrier, G , at temperature T , k is the Boltzmann constant.

The mean residence times for all the morphologies show a very weak dependence on the beam flux (Figure 2.4.2). However, mean residence times extracted from time

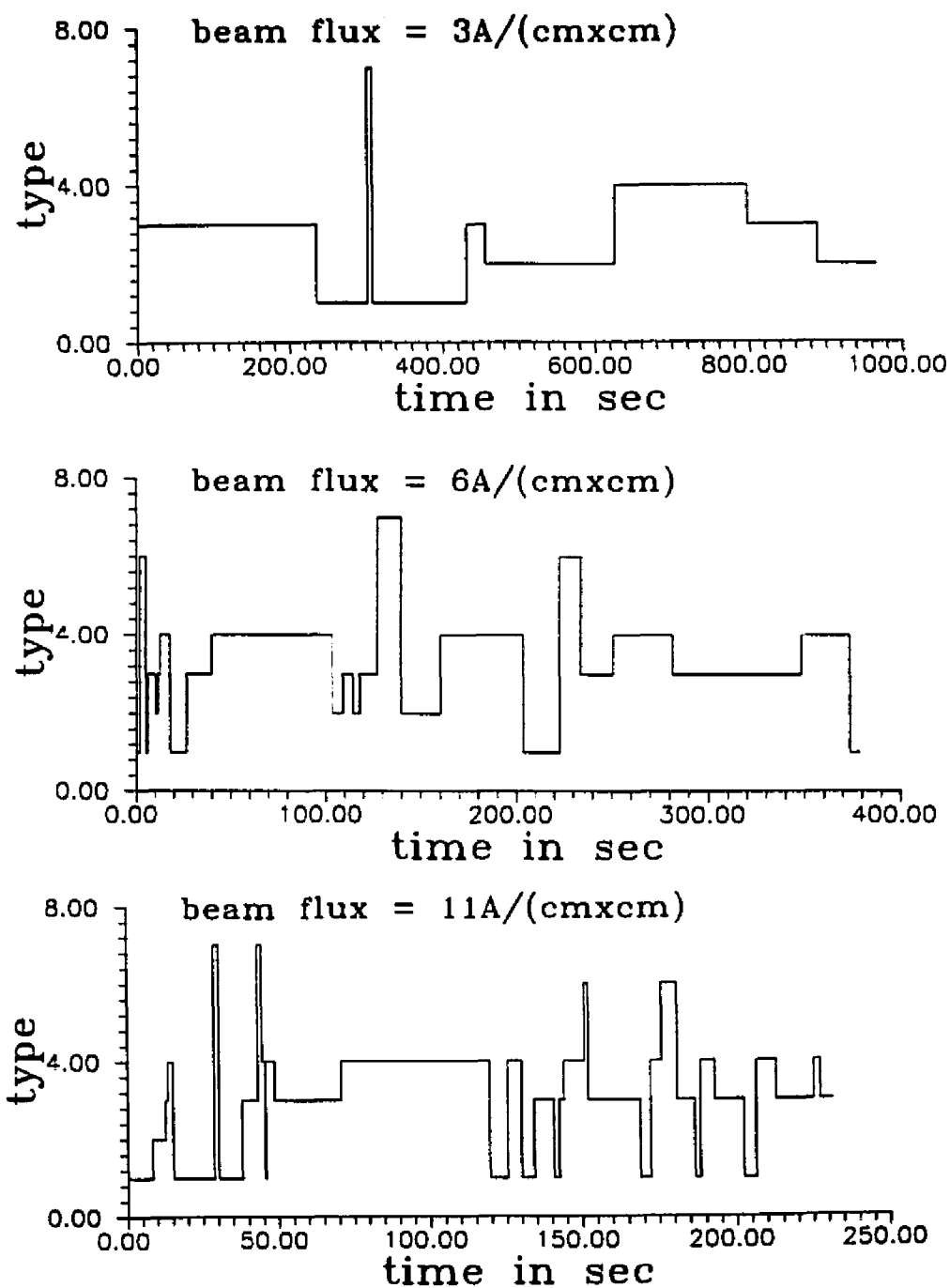


Figure 2.4.1: Plot of the time sequence evolution of the morphologies for a 6nm particle at a) $3\text{A}/\text{cm}^2$ b) $6\text{A}/\text{cm}^2$ c) $11\text{A}/\text{cm}^2$. Each type of morphology has been assigned an arbitrary value. 1 is for the decahedral MTP, 2 for Icosahedral MTP, 3 for Single Crystal, 4 for single twins, 6 for indistinguishable and 7 for unknowns. The x-axis represents the time in seconds spent in a morphology.

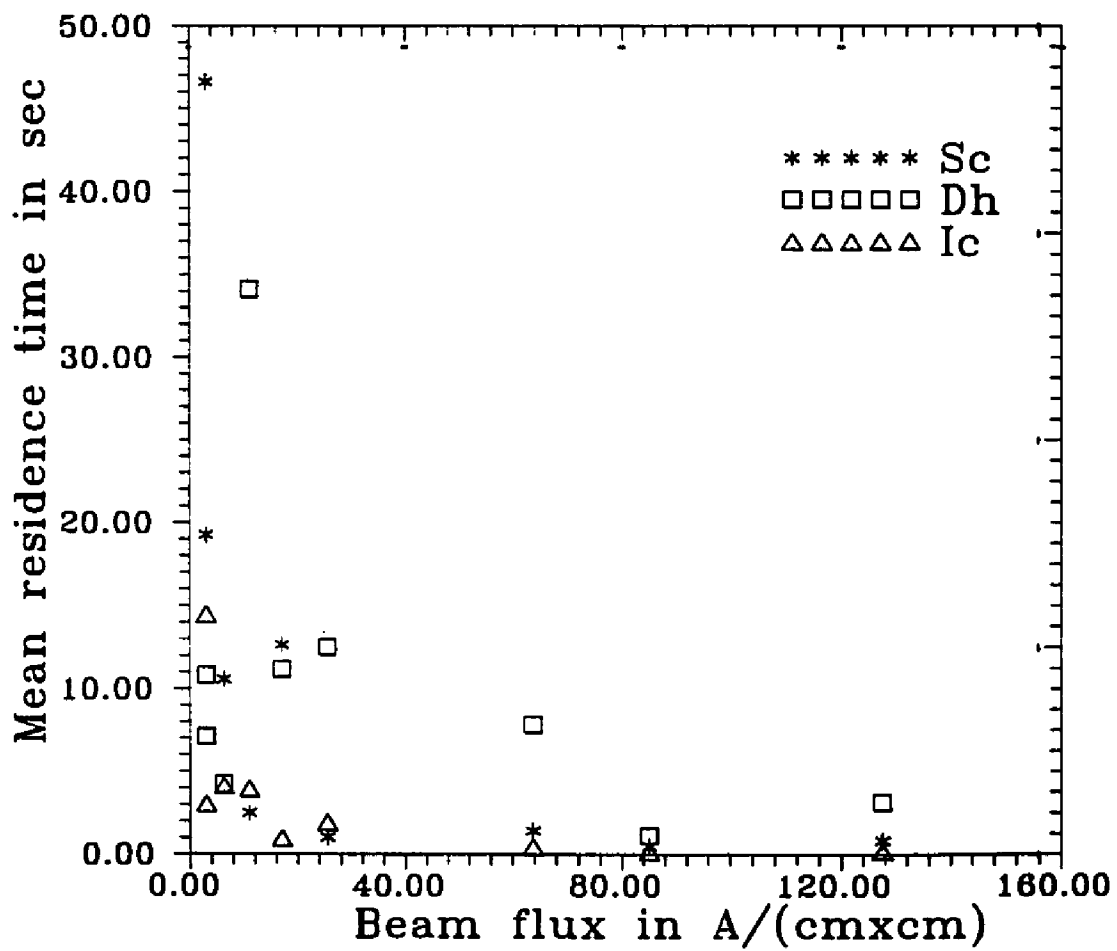


Figure 2.4.2: The mean residence time in seconds has been plotted as a function of the beam flux in $\text{\AA}/\text{cm}^2$ for various sizes in Angstroms.

sequence series (Figure 2.4.3) for constant fluxes show a size dependence. The Ic mean residence time shows a size invariance whereas the Sc and the Dh mean residence times increase with size.

The experimental occurrence probability of a morphology was measured as the fractional residence time which can be obtained as

$$F_{res} = \frac{T_{morph}}{\sum T_{morph}} \quad (2.4.2)$$

from the mean residence times. The summation is over all the morphologies characterized in the basis set.

This probability is plotted in figure 2.4.4 as a function of the particle size. The MTPs and the single crystals occur over the entire range of observations. Interestingly, the single crystal morphology shows a high abundance at all sizes and shows an increase with size. The decahedral MTP follows a similar trend, however, the relative abundance is much smaller. The icosahedral MTP shows a decrease in probability with size leading to a broad transition range between 5.5nm and 7.0nm in which the icosahedral MTP and the decahedral MTP have almost equal probabilities.

These experimental results show a predominance of Sc at all sizes and the Ics are not confined to very small sizes which are in direct contradiction to those expected from the phase map constructed by Ajayan and Marks (1988). The gradual increase of the decahedral phase with size over a large regime is also unexpected in terms of the phase

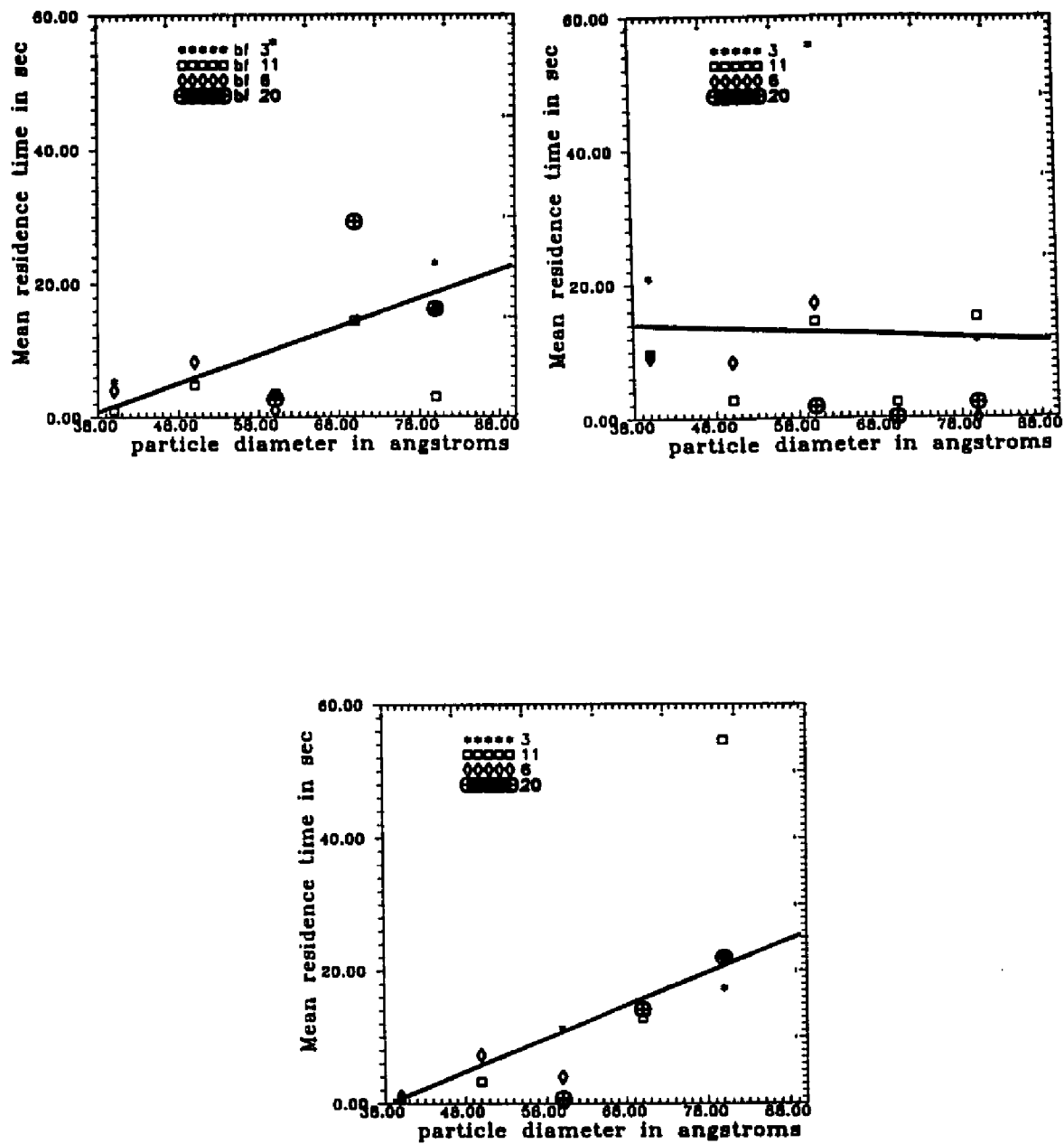


Figure 2.4.3: The mean residence time in seconds plotted as a function of particle diameter in angstroms at constant fluxes of 3, 6, 11, 20 A/cm² respectively for the three morphologies (a) Dc (b) Ic (c) Sc. The lines are drawn to guide the eye in observing the trend.

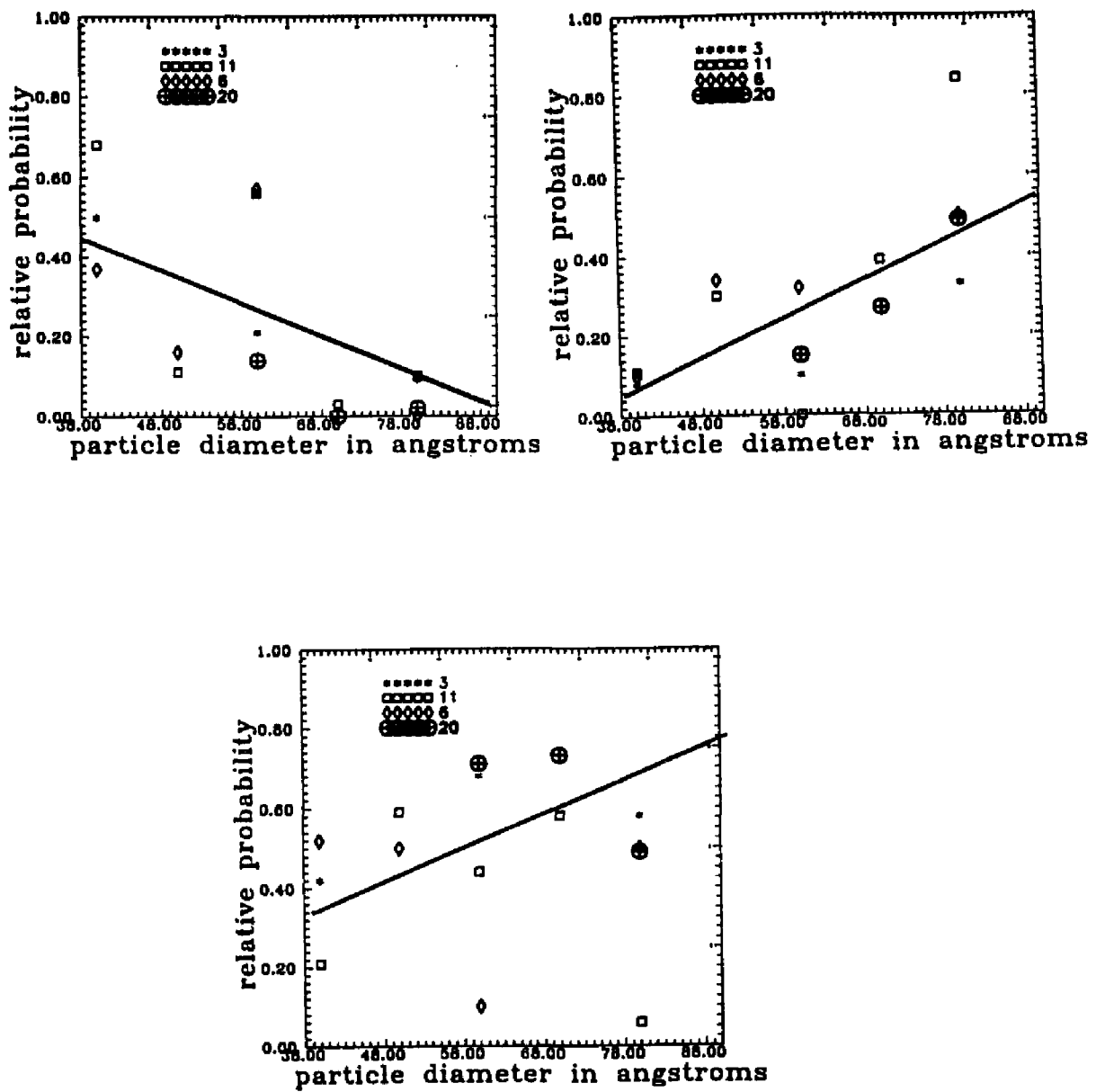


Figure 2.4.4: The experimental probability measured as fractional residence time in percent been plotted as a function of particle diameter in Angstroms for beam fluxes of 3, 6, 11, 20A/cm² respectively shows the downward trend in probability for the (a) Ic and the upward trends for (b)Dc and (c) Sc. The lines help guide the eye in observing the trend.

map. But the phase map does show a qualitative agreement with the electron diffraction studies on unsupported small particles of Ag [Hall et al. 1991] and Au [Patil et al. 1993] produced by inert gas aggregation. In these experiments the morphology is strongly affected by the temperature and saturation conditions at the evaporation source which was maintained at temperatures $>1200\text{K}$. Such high temperatures cannot be produced by the interaction of the electron beam with the small particles at the low fluxes used in our experimental analysis. The temperature at the particle due to the electron beam has been calculated by several workers [Gale and Hale 1961, Fisher 1970, Rez and Glaisher 1991] and it is now accepted that the beam heating is very small and the temperature rise is less than 100K . The experimental studies, therefore indicate that the phase map requires modification to be more quantitatively applicable. In addition, the time sequence analysis allows an average determination of the morphological fluctuation kinetics.

In conclusion, the dynamic experiments have shown that the small particles exhibit morphology changes with sizes which do not match completely with the earlier theoretical models. In the next chapter, a more refined model will be developed to predict the morphology changes in small particles.

CHAPTER 3: ANALYTICAL MORPHOLOGY MAP

3.1 INTRODUCTION

The experimental results obtained by real time HREM imaging do not agree with the phase map of Ajayan and Marks (1988): major deviations are seen in the occurrence of the decahedral MTPs at much smaller sizes and temperatures than those indicated in the phase map, also there is a dominance of single crystals at all particle sizes. While it does have qualitative agreement with electron diffraction data [Hall et al 1991], later studies on ultrafine silver particles [Reinhard et al 1993] show the existence of extremely large size icosahedra. Further, the phase map fails to provide an answer for the role of an external driving force on a system equilibrated at any given temperature. In the light of these results, it is clear that the "phase map" requires further refinement before being applicable as a predictive tool.

In this chapter, a morphology map will be developed using an approach similar to that of Howie and Marks (1984) and Ajayan and Marks (1988). The regimes of dominance of the various morphologies will be delineated in terms of the probabilities obtained from total energies of particle morphologies.

3.2 ANALYTICAL MODEL

The total energy of a particle can be determined as the gain in surface energy

compensated by the strain energies in the particle.

The surface free energy of single crystals can be evaluated by the use of the Wulff construction (Appendix A1.1) and that of MTPs from the modified Wulff construct (Appendix A1.2). But a direct evaluation at each size is rather cumbersome. A convenient method is to express the total energies in terms of a dimensionless parameter, ϵ_w , dependent only on the external shape of the unstrained particle and not the volume of the particle. It also includes the energy contributions from the external facets and the twin boundary energies. Using the modified Wulff construction [Marks 1983] the parameter can be determined as

$$\epsilon_w = \frac{1}{\gamma_{111}} \frac{\int \gamma_s dS}{(V)^{2/3}} \quad (3.2.1)$$

where γ_{111} is the surface energy per unit area of a (111) facet and γ the unstrained surface energy of the particle. V is the volume of the particle and S the surface area. Table 3.1 lists the expressions of ϵ_w for various morphologies [Marks 1983]. From ϵ_w and V the net surface energy for any particle can be written as

$$E_s = \epsilon_w \gamma_{111} V^{2/3} \quad (3.2.2)$$

The expressions for the surface energies in Table 3.1 include two terms β and η . β reflects the surface energy anisotropy between the {111} facets and the {100} facets and is given by

Table 3.1: Some common values of ϵ_w . The notation used is $\beta = 1 - \gamma_{100} / \sqrt{3}\gamma_{111}$, $\eta = \gamma_t / 2\gamma_{111}$ and $S = (1 + \eta^2 / 4\beta^2)^{1/2} - \eta/2\beta$, where γ_{111} , γ_{100} and γ_t are the energies per unit area of (111), (100) faces and a twin boundary respectively. The asymmetric twins are valid for $1/3 \leq \beta \leq 1/2$, all others are for $0 \leq \beta \leq 1/2$ (from Marks 1983).

Particle	ϵ_w^3	ϵ_w	
		$\beta = 1/3,$ $\eta = 0.005$	$\beta = 5/12,$ $\eta = 0.005$
Single crystal	$108\sqrt{3}(1 - 3\beta^3)$	5.499	5.271
LTP with m twin boundaries	$108\sqrt{3}\{1 - 3\beta^3 + \frac{1}{4}\eta m[5 + 2\eta(1 - \eta)]\}$	$m = 1$ 5.500 $m = 2$ 5.500 $m = 3$ 5.501 $m = 4$ 5.502	5.272 5.273 5.274 5.275
Decahedral MTP	$\frac{101}{4}\sqrt{3}[(1 + \eta)^3 - \frac{8}{3}(\beta^3 + \eta^3)]$	5.436	5.243
Icosahedral MTP	$\frac{67}{2}\sqrt{3}[(1 + 3\eta)^3 - 24\eta^3]$	4.899	4.899
Bi-icosahedral MTP	$\frac{67}{2}\sqrt{3}(\frac{216}{196}\eta(1 + 11\eta))$	5.051	5.051
Asymmetric twin	$108\sqrt{3}(1 - 3\beta^3 + \frac{1}{2}S\eta[\frac{1}{4}\beta\eta + (1 - 2\beta)(2 - 3\beta)])$	-	5.272
Asymmetric decahedral MTP	$108\sqrt{3}(1 - 3\beta^3 + \frac{1}{4}(\frac{1}{4} - \beta^2) - (1 - \beta)(3\beta - 1)^2 + \frac{1}{8}\eta[5 + \beta(1 + \beta)])$	-	5.256

$$\beta = 1 - \gamma_{100} / \sqrt{3} \gamma_{111} \quad (3.2.3)$$

while η is a measure of the contribution of the twin boundary energy, γ_t in comparison to γ_{111} . It is expressed as

$$\eta = \gamma_t / 2\gamma_{111} \quad (3.2.4)$$

The major contributions to the strain energy in MTPs are due to the angular misfit within the MTP. The angular misfit is equivalent to a wedge disclination. The strain energy contribution from the disclination is well studied and the resultant internal strain energy per unit volume of a decahedral MTP [Howie and Marks 1984] is

$$W_D = \frac{\mu \epsilon_d^2}{4(1-\nu)} \quad (3.2.5)$$

where ϵ_d is the angular deficit strain of a decahedral MTP (0.0205), μ the shear modulus and ν the Poisson's ratio, and that for an Ic as developed by Howie and Marks (1984) is

$$W_D = 2\mu \epsilon_d^2 (1+\nu) / (1-\nu) \quad (3.2.6)$$

In the above expressions, the surface energies are for unstrained surfaces. However, in reality, these surfaces undergo strain and an additional correction term, the surface strain energy, needs to be included. Although it is much smaller than the total surface energies of the particles, it is comparable to the differences between them. The

correction term can be determined by a Taylor's series expansion of the surface free energy per unit area as

$$\gamma = \gamma_s + \sum_{ij} e_{ij} \frac{\partial \gamma}{\partial e_{ij}} + \dots \quad (3.2.7)$$

where the strain variation is described by the "surface stress tensor" $g_{ij}(\theta, \phi)$ of the material, given as

$$g_{ij}(\theta, \phi) = \frac{\partial \gamma(\theta, \phi)}{\partial e_{ij}} \quad (3.2.8)$$

where i and j are taken over the directions in the surface plane. The corresponding term to be added to the total energy of the particle is

$$\Delta W = \sum_{ij} \int e_{ij} g_{ij} dS \quad (3.2.9)$$

where g_{ij} can be simplified as

$$g_{ij}(\theta, \phi) = g \delta_{ij} \gamma_s(\theta, \phi) \quad (3.2.10)$$

and the energy contribution becomes

$$g e_s \gamma_{111} e_w V^{2/3} \quad (3.2.11)$$

e_s , the mean strain at the surface, is

$$e_s = (2/9)e_d \quad (3.2.12)$$

for Icosahedral MTPs and

$$e_s = (2/3)e_d \quad (3.2.13)$$

for Decahedral MTPs.

The surface stress will also exert an expansive or compressive load on the surface, independent of any equilibrated stresses already existing in the particle due to internal distortions. Assuming a homogeneous strain, an additional energy change of

$$\epsilon_{gs} = \frac{-\epsilon_w^2 g^2 \gamma_{111} V^{1/3}}{3} \left(\frac{1-2\nu}{2} \right) \quad (3.2.14)$$

is incorporated in the evaluation of the surface energy contributions.

The total energy can thus be reduced as a function of the volume, shape and strain parameters as:

$$E_{tot} = (\epsilon_w + \epsilon_g) \gamma_{111} V^{2/3} + W_D V + \epsilon_{gs} V^{1/3} \quad (3.2.15)$$

where ϵ_w is a shape dependent parameter, W_D the strain dependent parameter, ϵ_{gs} the contribution to the surface energy due to the surface stress tensor (arising due to strain in the particle) and ϵ_g the strain energy arising due to surface stress.

3.3 POTENTIAL ENERGY SURFACE

In order to derive the Gibbs free energy change, G , from the potential energies

derived above, it is necessary to include the entropy of the energy terms. The entropy of the surface free energy change results from the entropy of the surface stresses and that due to the anisotropic nature of the surface. The entropic change in strain energy is a direct consequence of the temperature dependence of the elastic moduli. The Gibbs free energy can then be expressed by the standard thermodynamic expression as

$$G = E_{tot} - TS \quad (3.3.1)$$

From the Gibbs free energies, the relative probabilities of the morphologies are

$$P_{rel} = \frac{P_{morph}}{\sum P_{morph}} \quad (3.3.2)$$

where

$$P_{morph} = \exp\left(-\frac{G}{kT + \Delta E}\right) \quad (3.3.3)$$

where ΔE is the external driving energy [due to energy transfer from the electron beam] in addition to the temperature.

Small particles also show a depression in melting point with decreasing size. This effect was included in the model by using the values determined by Buffat and Borel (1976) as the upper limit of the solid phase of a small particle.

3.4 RESULTS AND DISCUSSION

From the relative probabilities and the depression in melting point one can construct a morphology map of the particles, namely the relative probabilities of

occurrence as functions of temperature and size.

A typical morphology map constructed from the above model for Au is shown in figure 3.4.1. The constants used in the evaluation of the relative probabilities are tabulated in table 3.4.1. A driving energy of 10eV was applied to the particles having a surface stress of 0.8N/m^2 and an anisotropy of 1.15 ($\gamma_{100} = 1.15\gamma_{111}$) to obtain figure 3.4.1. At all driving energies, anisotropy and surface stress, the Dh's appear only as secondary morphologies. The Ics dominate at lower sizes while the Scs are more dominant at larger sizes.

The variation of probabilities of the morphologies, at a particle temperature of 300K, is shown in figure 3.4.2 as a function of size and driving energy. On addition of an external driving energy of only 3eV, the Dh probability begins to rise and increases considerably at a driving energy of 10eV. Such energies can be provided by the electron beam. Rez and Glaisher (1991), assuming a linear dependence of the energy deposited per incident electron with particle radius, showed that a particle 4nm in diameter can acquire an energy of 4eV. It should be noted that these energies deposited in a particle are far less than that required to melt them. Increasing the beam flux, however, increases the rate of transformations between the morphologies (as shown in the time sequence) by decreasing the energy differences between the morphologies. But at these conditions, the beam energies rapidly increase the rotations and as a consequence, the particles tend to migrate randomly on the substrate.

Another factor that influences the regimes of dominance of morphologies is the surface stress. The variation of the relative probabilities with surface stress is shown in

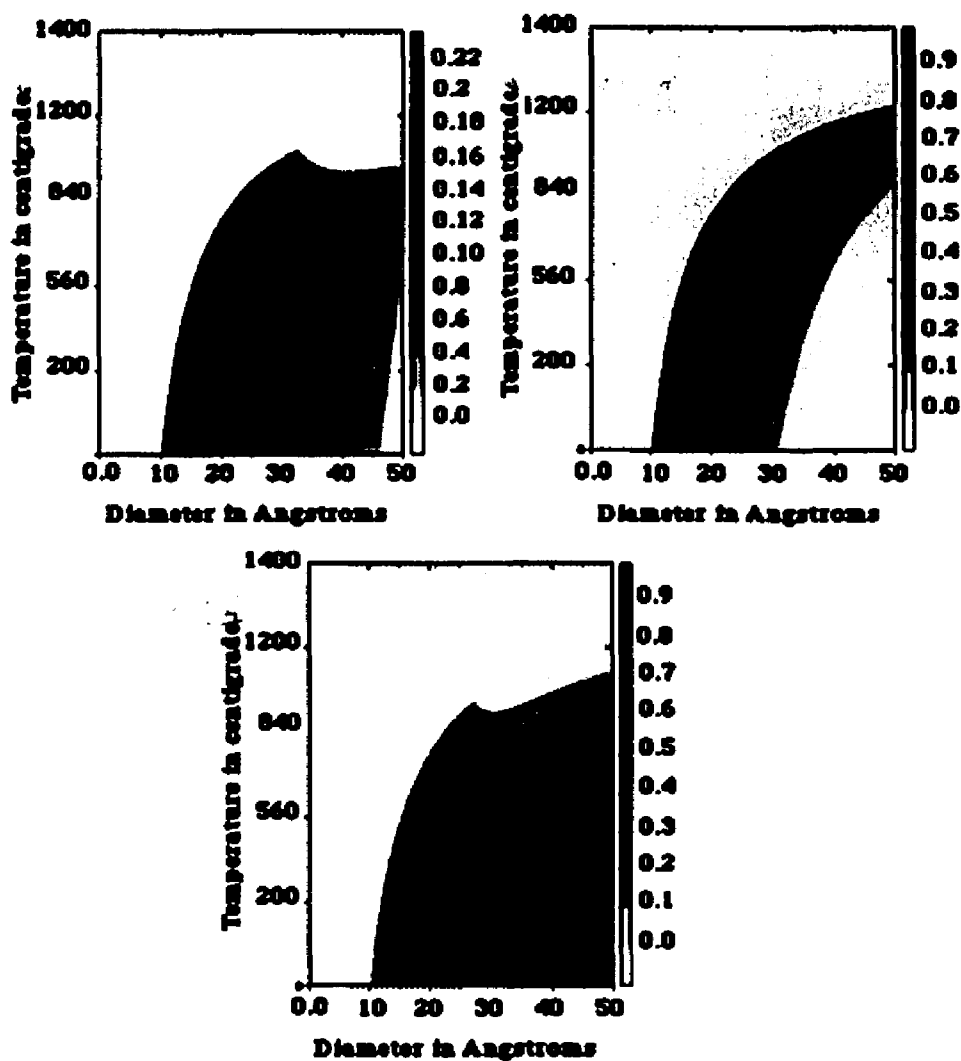


Figure 3.4.1: A typical set of relative probability maps of the morphologies at a driving energy of 10eV and the remaining constants determined from the standard values tabulated in Table 1. The contour lines define the probability as a function of the temperature and particle radius. The depression in melting point[Buffat and Borel 1976] curve separates the liquid and solid phases.(a) Dc relative probability map, (b) Dc relative probability map, (c) Sc relative probability map.

TABLE 3.4.1: Standard values of the various parameters used in the calculation of the morphology map of Au.

Bulk Melting Point [ref (Hultgren, Desai, Hawkins, Gleiser, Kelley and Wagman 1973)]	1336K
Bulk Enthalpy of Melting [ref (Kristyan and Olson 1991)]	12×10^3 J/mol
111 Surface energy [ref (Howie and Marks 1984)]	2.26 J/m²
100 Surface energy [ref (Howie and Marks 1984)]	2.71 J/m²
Liquid Surface energy [ref (Buffat and Borel 1976)]	1.135 J/m²
111 Surface entropy [ref (Linford 1973)]	1.2×10^{-3} J/(m²K⁻¹)
Surface stress [ref (Keene 1993)]	1.1 N/m
Surface stress entropy [ref (Keene 1993)]	-1×10^{-3} N/(mK)

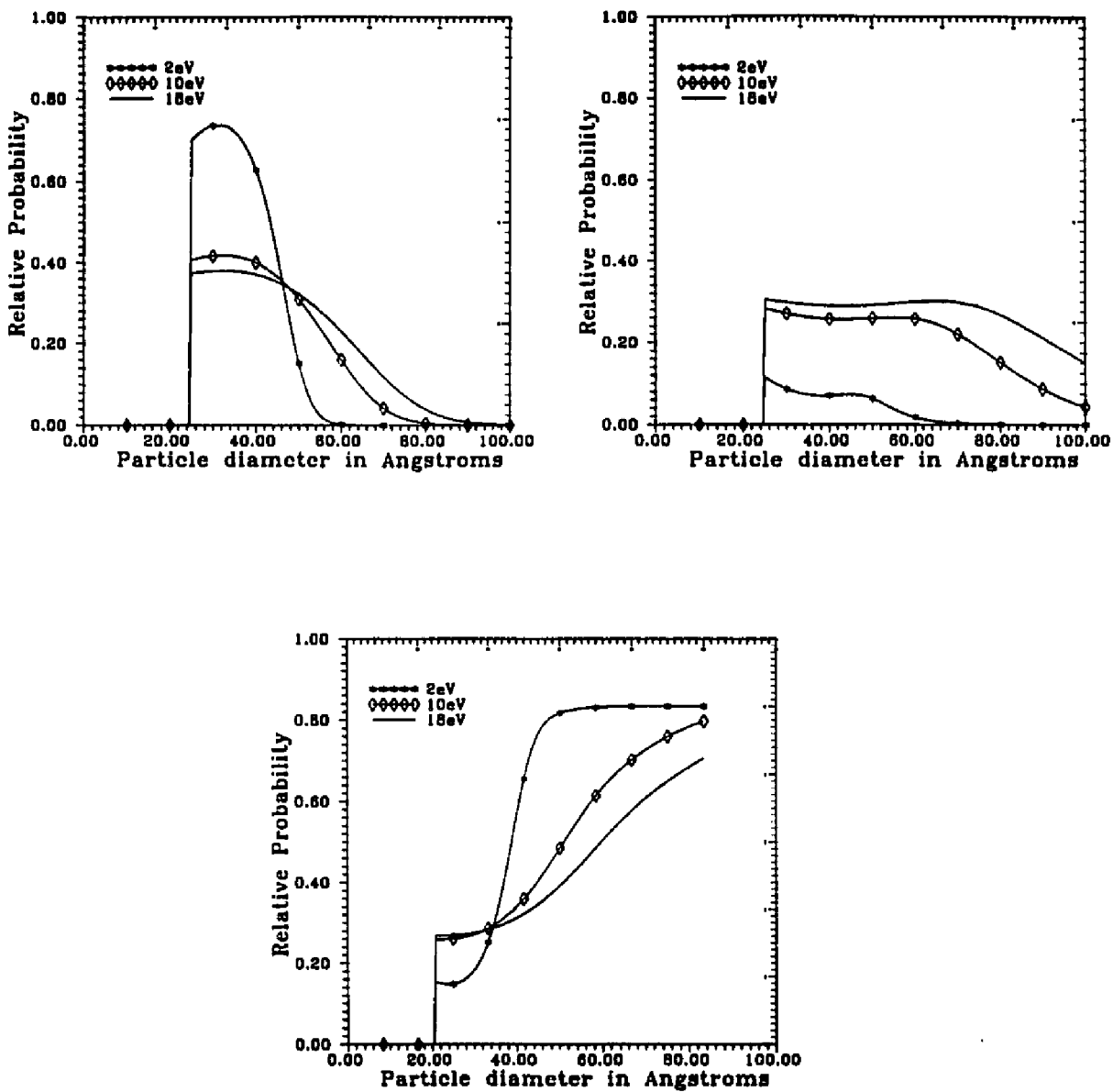


Figure 3.4.2: The variation of the relative probability of (a) Ic (b) Dc (c) Sc with driving energy is illustrated for driving energies of 2, 10, 18eV. The graphs are isothermal sections at 300K of a relative probability versus temperature, particle diameter in angstroms map.

figure 3.4.3 at a constant temperature of 300K and a driving energy of 10eV. There is a significant change in the relative probabilities of the morphologies with a change in the surface stress. Decreasing the surface stress to zero decreases the decahedral MTPs and the single crystals. At these conditions, the relative probability of finding a decahedral MTP also shifts more towards smaller sizes. On the other hand, the icosahedral MTP becomes more dominant with decreasing surface stress. Most metal clusters are known to have lattice contractions which are explained as an effect of the increase in pressure inside the particles arising due to their positive surface stress [Solliard and Flueli 1985]. Linford (1973) gives a detailed account of the dependence of the surface stress on various experimental conditions such as surface impurities, surface relaxations, lattice imperfections. Unfortunately, there is no accurate estimate of the surface stress due to its extreme sensitivity to experimental conditions and most tabulated values in the literature are derived from isotropic bulk surface tension values.

Finally, the effect of the surface energy anisotropy of the particle is illustrated in figure 3.4.4 at a constant temperature of 300K and a driving force of 10eV. Higher anisotropy leads to more favorable conditions for the stability of Ics. Dhs on the other hand have the maximum probability only at intermediate anisotropies.

3.5 COMPARISON WITH EXPERIMENTAL RESULTS

The data acquired from the experiment can be directly related to the relative probabilities. If t_{morph} is the time of residence in a morphology, P_{morph} , the probability of occurrence of a morphology, F_{res} , the fraction of the total residence time spent in a morphology and P_{rel} , the relative probability of a morphology then the relation between

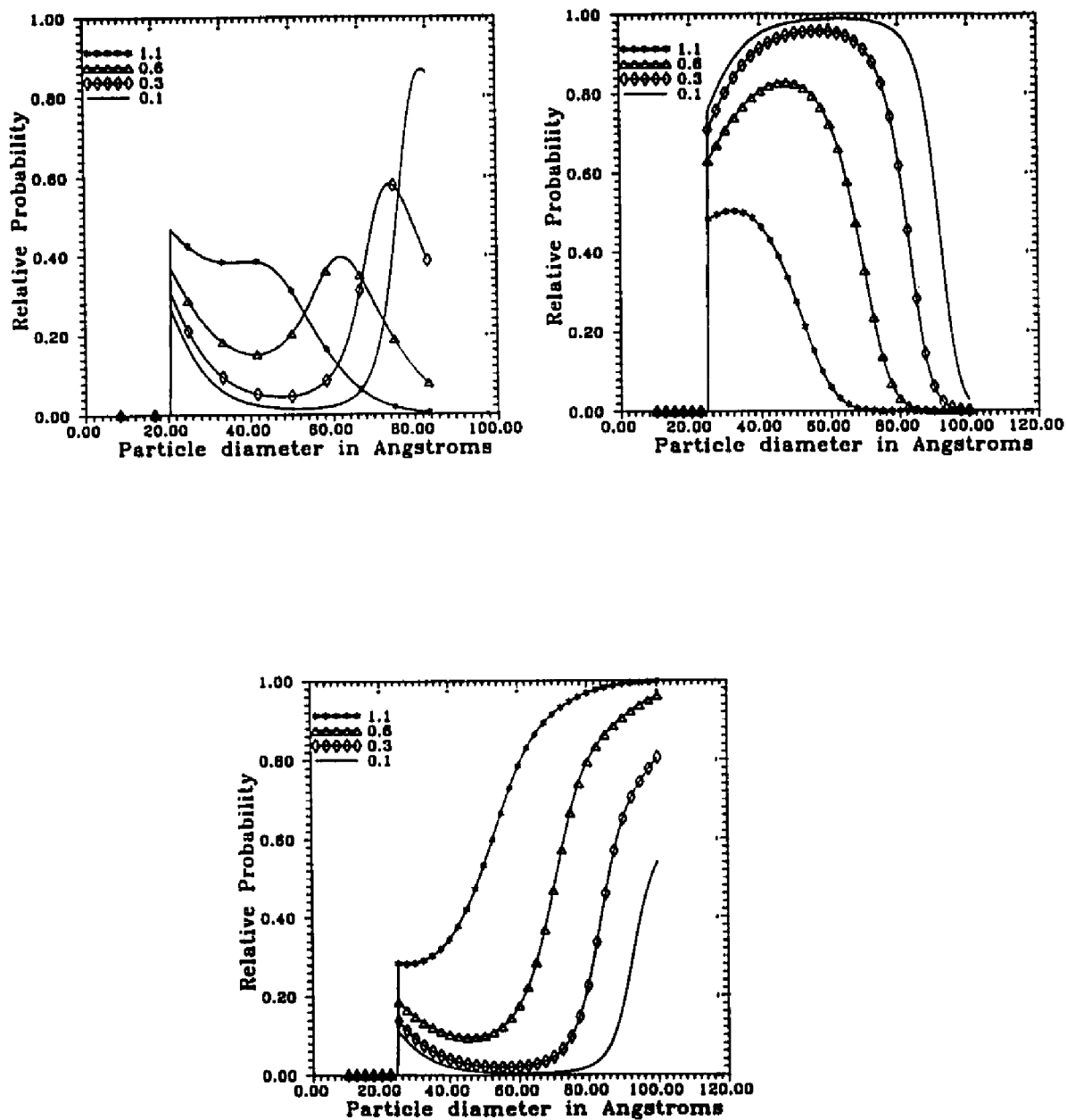


Figure 3.4.3: An isothermal section at 300K of a 3D morphology map of relative probability versus temperature, particle diameter in angstroms illustrating the variation of the relative probability with surface stress(in N/m^2) for (a) Dc (b) Ic (c) Sc at a driving energy of 10eV.

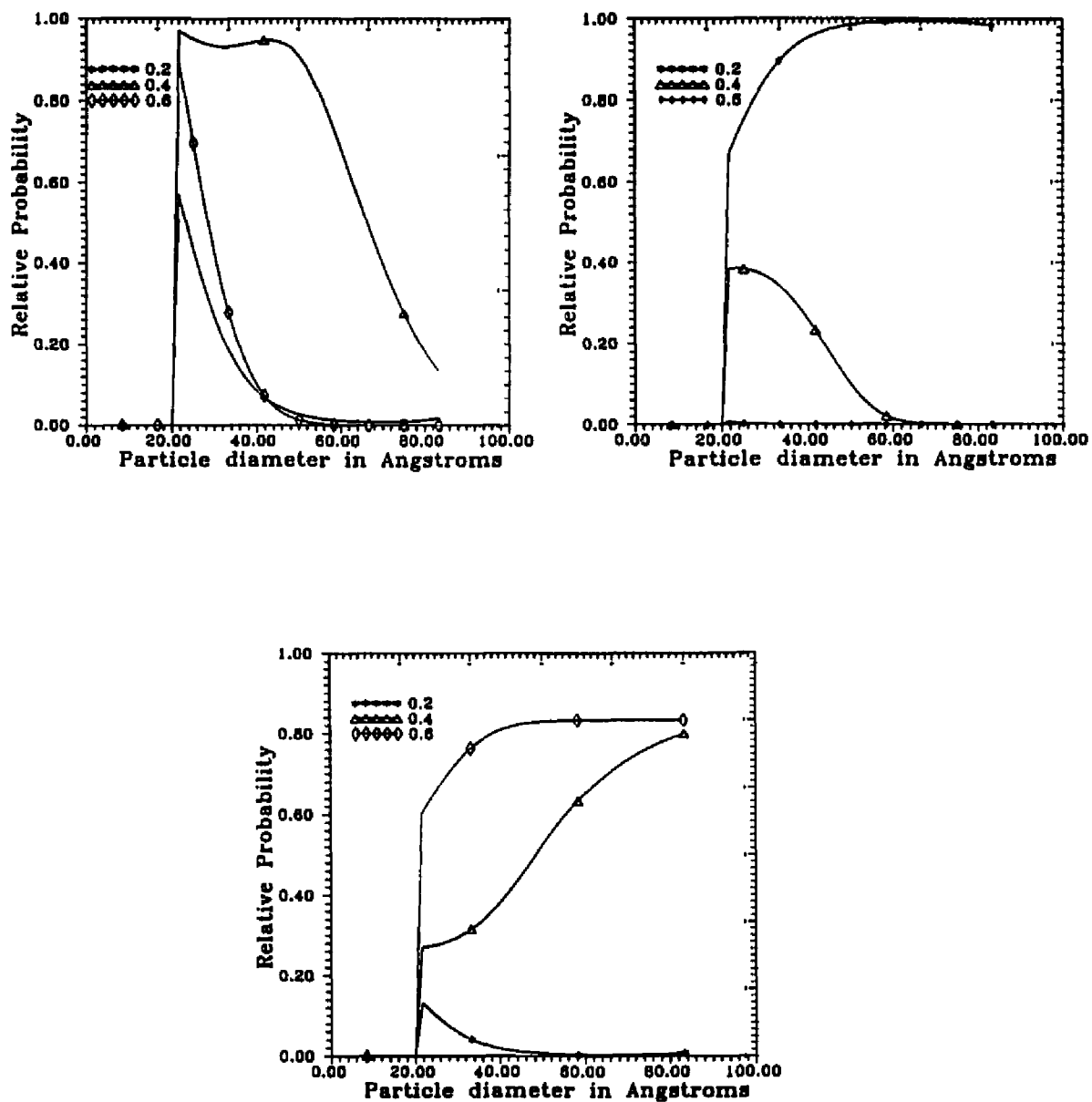


Figure 3.4.4: An isothermal section at 300K of a 3D morphology map of relative probability versus temperature, particle diameter in angstroms illustrating the variation of the relative probability with anisotropy [defined as $\beta = 1 - (\gamma_{100} / (\sqrt{3}\gamma_{111}))$] for (a) Dc (b) Ic (c) Sc at a driving energy of 10eV.

F_{res} and P_{rel} is given by the standard equation:

$$F_{res} = \frac{t_{morph}}{\sum t_{morph}} \propto \frac{P_{morph}}{\sum P_{morph}} = P_{rel} \quad (3.5.1)$$

The model shows a general agreement with the relative probabilities obtained from the experiment. The best fit is seen to occur at a driving energy of 10eV and a surface stress of 0.8N/m² at an anisotropy of $\gamma_{100}=1.15\gamma_{111}$ (Figure 3.5.1). The agreement is more in the reflection of a trend rather than in the fit with the data. A more accurate fit would require the collection of a much larger number of data points. However, the process is prohibitively time consuming. Each of the experimental data points presented in the results were averaged over a range of 1nm at each particle size and each data point is in fact the average of six different sequences of observations. The averaging was necessary due to the small amount of variability in the particle diameter and deviation from a spherical shape during the process of morphology transformations. The particle transformation rate is also affected by the height and width of the substrate pillars which varied by small amounts during each observation. While an amorphous substrate having a minimal area of contact with the particle does reduce the effect of the substrate, it does not eliminate the interaction. The effect of the interface is more dramatically observed by differences between our experimental observations and a similar time analysis conducted by Kizuka et al (1993) for Au particles on MgO crystallites. They restricted their observations to only one particle size of 2nm at a beam flux of 3A/cm² and found that the time of residence was split as 36%, 18%, 11% and 1% for the Dh, Sc, single twin

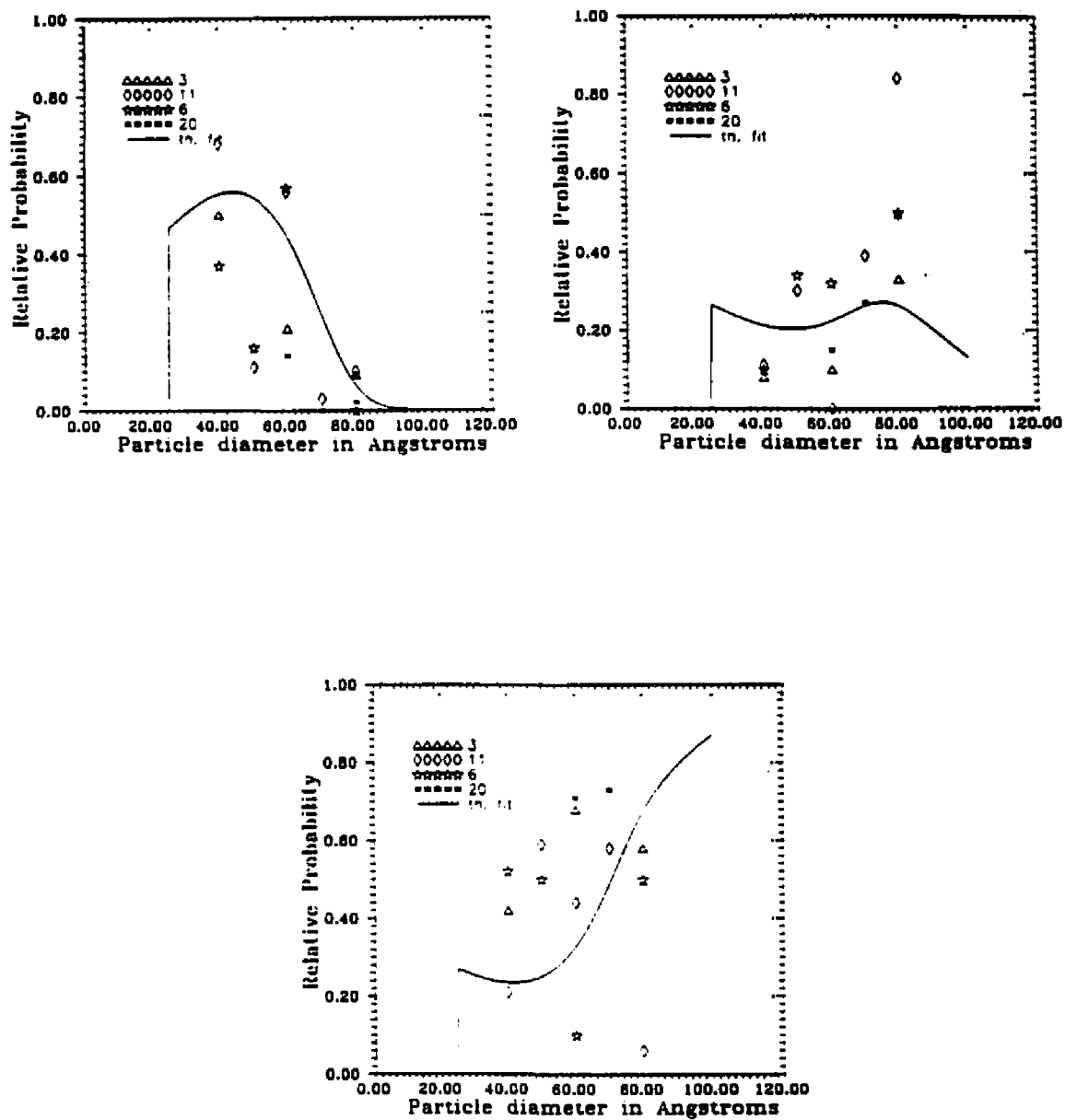


Figure 3.5.1: The best fit morphology sections, of (a) Ic, (b) Dc, (c) Sc at 300K of the probability model compared with the experimental data reveals the crossover regime centered at 6.5nm. The surface stress is 0.8N/m^2 and the anisotropy is such that $\gamma_{100} = 1.15\gamma_{111}$ at a driving energy of 10eV.

and Ic respectively. In our observations, a similar particle at the same beam flux showed an Ic dominance followed by the Sc and then the Dh. The difference in the observations can be accounted for by a shift in the stability of Ic arising as a result of the additional strain introduced by the interfacial relationship with a crystalline substrate. Another piece of evidence which supports this hypothesis is the relatively few number of icosahedral MTPs found in Ag islands deposited onto Si(100)-2x1 (see Chapter 5). However, when exposed to air the silicon surface oxidized into an amorphous interface and was accompanied by an increase in the number of Ics. Other investigations [Ajayan and Marks 1989, Giorgio et al 1991, Giorgio et al 1993] have also shown the effect of adhesion of the particle to the substrate on the particle morphology.

The driving energy plays a major role in influencing the behavior of small particles. Larger energies while increasing the rates of transformations increases the relative probability of Dhs. The increase in energy also causes the Ic probability to broaden over to larger sizes and decreases the Sc relative probability. The morphology maps have been calculated assuming the MTPs to be perfect in shape. Experimental observations show a number of MTP structures in which the disclination is much closer to the edge. Such structures have a much lower activation barrier [Dundurs et al 1988] and the Dhs would have higher occurrence than those calculated here. As a consequence small energy fluctuations cause larger changes in the morphology populations at low temperatures than at higher temperatures. This could be relevant for the conflicting reports of the number of MTPs observed in static morphology analyses which vary from a few [Avery and Sanders 1970] to 95% [Solliard et al 1976, Renou and Gillet 1981,

Renou and Rudra 1985] of the total number of observed particles. These experiments were also carried out under different condition of growth using different materials. A discussion of the various possible conditions resulting from the variations in the driving energy can be found in the review article by Marks (1994).

The particle morphologies are also strongly affected by the surface stress and anisotropy. Both of these parameters are very sensitive to the environment and the production of a large number of a type of morphology can be achieved by a simple change of these two parameters. While the role of the surface stress has not been experimentally confirmed, there is substantial evidence [eg: (Stephanopoulos et al 1977)] for the role of the gaseous environment in changing the faceting conditions in a particle. However, further examination of the role of these parameters in controlled environments is required to quantify the effects.

The morphology maps also show that MTPs decrease in number at large sizes only at very high temperatures which is consistent with experimental observations [eg:(Patil et al 1993)]. Therefore the formation of MTPs is a low temperature phenomenon and the fluctuations in small particles can occur at low temperatures. The model and the experimental results thus reaffirm the hypothesis that structural fluctuations of a small particle in the presence of an electron beam are due to the intrinsic instability of the particles rather than due to violent processes such as rapid melting and recrystallization. An interesting point observed in the morphology model is that it is not the overall temperature, but the small random energy fluctuations around the overall energy that affects the morphology fluctuations. The overall energy plays a role only in the softening

of the activation energy barriers but the random energy fluctuations carry the particles over the activation barriers. The model, thus, offers an explanation of the role of the electron beam in the fluctuations observed by Yoshida et al (1992) at high temperatures. They also noted that the electron beam did not affect the particles at low temperatures at which the activation energy barrier would be higher than the random energy fluctuation produced by the electron beam.

CHAPTER 4: MORPHOLOGY TRANSFORMATION KINETICS

4.1 INTRODUCTION

The potential energy surface of a small particle calculated within the framework of a continuum model and free energies gives the thermodynamics, but no real insight into the kinetics of the process of morphological transformations. The relative probabilities measured (Chapter 2) and calculated (Chapter 3) provide a means of estimating the occurrence of a morphology with respect to the others without any reference to the path or the mechanism of the transformation process. To illustrate this, consider the potential energy surface. With a large number of particles, the relative populations of the different configurations will map this surface. Similarly, a single small particle observed for "long enough" will also map out the surface. How long is "long enough"? The electron microscope experiments indicate that this can be several minutes under certain circumstances. Thermodynamics alone cannot determine this time scale. In many cases, the particles might be kinetically frozen into a metastable state and the growth mode would not reflect a true equilibrium situation.

4.2 LIQUID DROPLET MODEL

In order to estimate the rate of the fluctuations, it is necessary to find values for an effective frequency of attempts and an activation energy barrier, so that the rate can

be written in the standard form of:

$$K = \nu \exp(-\Delta E/kT) \quad (4.2.1)$$

where K is the transition frequency.

The prefactor term can be calculated as a vibrational frequency if the long wavelength oscillations of a small cluster can be evaluated. These oscillations can be obtained by modelling such a cluster within a continuum model as a vibrating, non-viscous droplet; this is similar to calculations of surface capillary wave modes [Weeks et al. 1989]. The solution for small amplitude vibrations (see appendix 4.1 for a simple derivation) is a standard problem [Lamb 1932, Reid 1960, Chandrashekhhar 1961], and the so-called Lamb frequencies are given by:

$$\nu^2 = \ell(\ell + 1)(\ell + 2)\gamma/\rho R^3 \quad (4.2.2)$$

where ℓ is the mode of the oscillation (normally taken as the first mode i.e. $\ell = 1$), γ the surface free energy per unit area, R the particle radius and ρ the density. This shows that there is a $R^{-2/3}$ dependence of the Lamb frequencies. For reference, the form of the equations governing the radial component of the velocity of the droplet is given by:

$$u = \{\epsilon_0 \prod / \nu\} \ell(\ell + 1) R^{\ell-1} Y_\ell^m e^{-i\omega t} \quad (4.2.3)$$

where t is the time, R the radius, ϵ_0 is a function of time, Y_ℓ^m is the spherical harmonic governing the departure from the equilibrium shape (spherical) of the liquid droplet, ν the frequency of oscillations of the droplet, the constant \prod is given by

$$\Pi = (\gamma/\rho R^3)(l - 1)(l + 2)/(l + 1)R^{l-1} \quad (4.2.4)$$

Although, it might be reasonable to include some form of viscous damping, for the size scales of relevance there are no oscillatory solutions for any realistic viscous term so viscous damping has been ignored in the approximation. The solution, strictly, is only valid for very small oscillations, but experimental [Trinh et al. 1982] and numerical [Miller 1968] analyses indicate that it can be carried over to large oscillations with only a minor correction. Typical values, shown in figure 4.2.1, give quite reasonable values for vibration frequencies when extrapolated down to small sizes where they can be directly compared with phonon values.

4.3 ACTIVATION ENERGY

The second part of the calculation, the activation energy barrier, is not so easy to estimate. One possibility is to use the values of ΔG calculated by Ajayan and Marks (1988). This leads to unreasonably large rates. This can be understood quite readily since these values do not fully describe the potential energy surface - they are instead positions where all the atoms (both inside and at the surface) have been allowed to equilibrate for a given value of the disclination in the center of a decahedral MTP. In between these points the cluster must go into some sort of transition state whereby the central disclination moves from one position to another, as illustrated in figure 4.3.1.

There are two possible models for the transition state. Following the idea of DeWit 1971),(1972), Harris and Scriven (1971), the disclination can move through one atomic plane by the motion of a partial edge dislocation through the crystal [Figure 4.3.2].

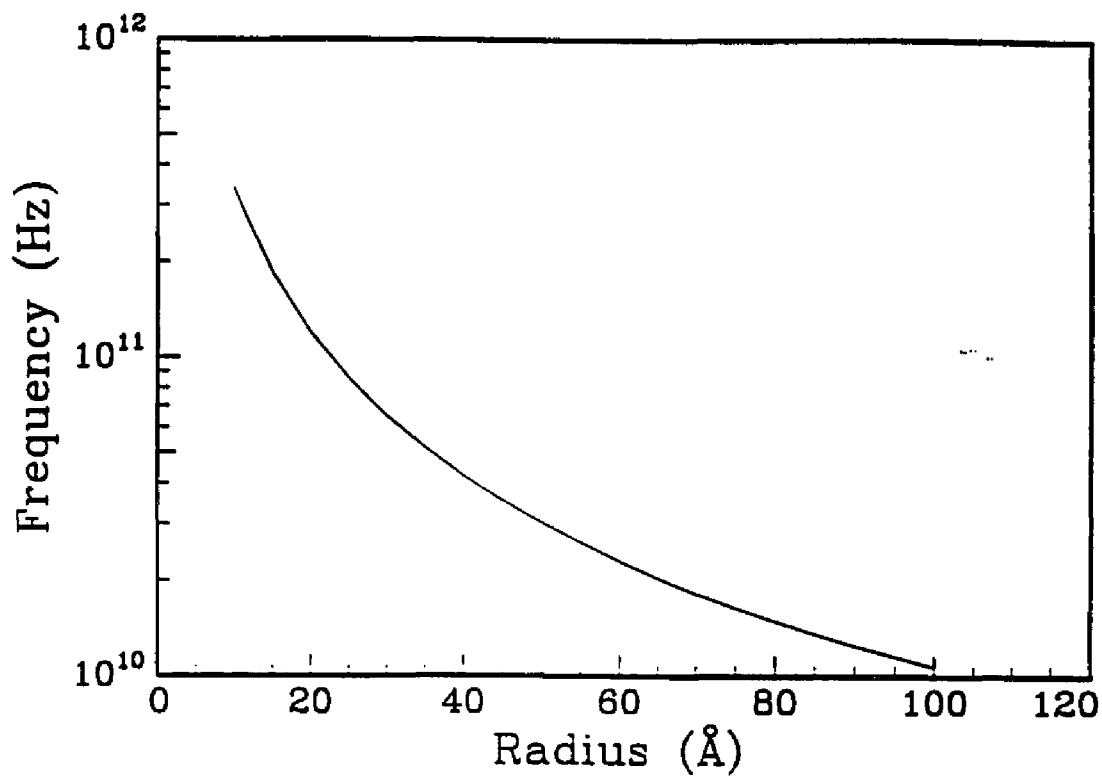


Figure 4.2.1: Values of the vibration frequency as a function of the particle size of gold.

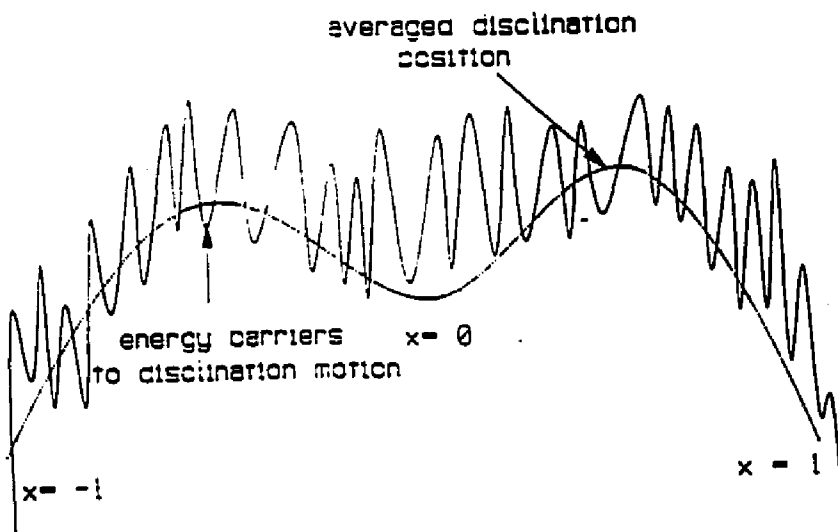


Figure 4.3.1: Schematic of the energy barrier to a disclination as it moves from a single crystal structure ($x=-1$) to a symmetrical decahedral MTP ($x=0$) to a single twin structure ($x=1$).

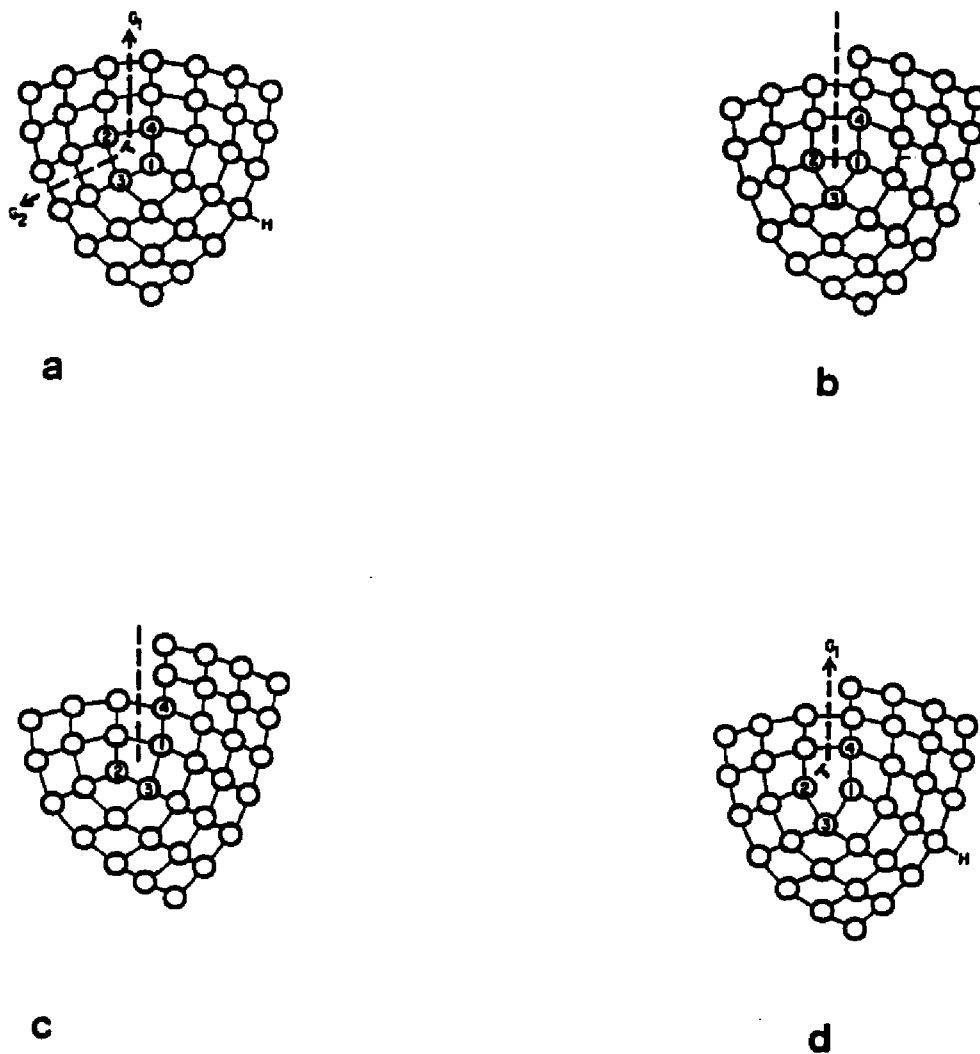


Figure 4.3.2: Movement of a disclination by the generation of an edge dislocation. The figure illustrates an intrinsic disclination of rotation $\pi/2$ acting as the source of two dislocations. The first dislocation leaves along glide line G_1 , resulting in the displacement of the disclination from 1 in (a) to the center of the triangle formed by 1, 2 and 3 in (b). A second dislocation, shown in (c), glides along the same glide line, the disclination is displaced to 2 in (d). G_2 in (a) is a second possible glide line for the dislocations. (Reproduced from Harris and Scriven 1971).

A typical estimate of the energy involved in the process is [Hirth and Lothe 1982, Hull and Bacon 1984]:

$$\Delta E = Gb^2R \quad (4.3.1)$$

where G is the shear modulus and b the Burger's vector ($1/6[112]$). A second model is a direct, torsional vibration coupling the different structures [Marks 1980]. As an illustration, Figure 4.3.3 shows how one can transform an icosahedral structure into a form of a decahedral MTP by a torsional vibration. Estimates of the magnitude of this term are very difficult. An approximate form will be to use the theoretical shear strength of a material, typically estimated as $G/30$ [Hirth and Lothe 1982, Hull and Bacon 1984], and then use the work done to move an atomic layer from its original site to a twin related site under the action of such a shear.

Using a simple form for the potential energy of

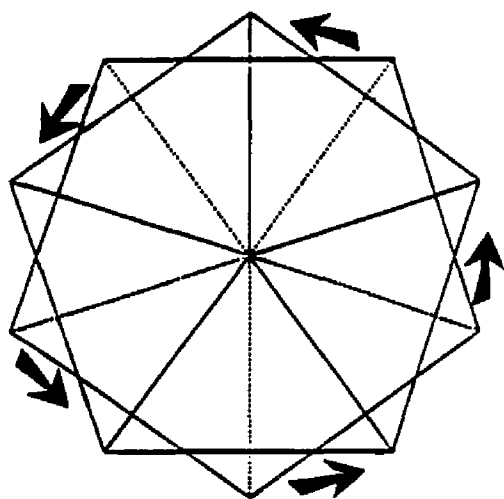
$$U(r) = U_0 \cos(2\pi r/b) \quad (4.3.2)$$

where b is the separation between the appropriate sites and is the same as that given above for a dislocation. The derivative with respect to r is

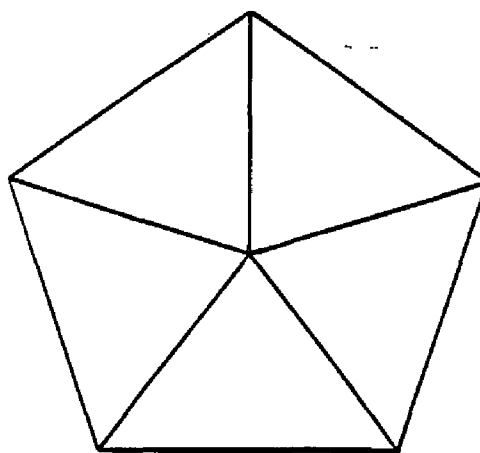
$$U'(r) = -U_0 2\pi \sin(2\pi r/b)/b \quad (4.3.3)$$

Equating this maximum force with the theoretical shear strength given above the activation energy can be estimated as:

$$\Delta E = GbR^2/60\pi \quad (4.3.4)$$



ICOSAHEDRAL MTP



STRAINED DECAHEDRAL MTP

Figure 4.3.3: Torsional rotation between two pentagonal faces of an icosahedral particle resulting in the formation of a strained decahedral MTP.

4.4 DISCUSSION

The values that were obtained for the activation energy, from both these later models are high by roughly a factor of 10, whereas the first model was too low. Matching the transition frequencies to the values calculated by Sawada and Sugano (1991), i.e. reducing the second two activation energies by 0.1 the values are quite consistent with the molecular dynamics cluster calculations and the initial experimental electron microscopy data, see figure 4.4.1. It is very difficult if not impossible to raise the values for the first model enough; this continuum analysis should overestimate the magnitude of the free energy variations. The only parameter that can be questioned is the shear modulus G .

In fact, there is every reason to question whether the large values of G for a bulk crystal are relevant here. To show this, it is easier to turn the problem on its head and consider a small particle near to its melting temperature. Independent of whether melting is a first order or a second order phase transition in the bulk, finite size effects [Challa et al. 1990] indicate that it should be second order in a small particle. Standard analyses of phase transitions in terms of fluctuations can be applied to melting, for instance the Kosterlitz-Thouless model [Kosterlitz and Thouless 1973] with fluctuations in dislocation pair creation and destruction. Independent of how one handles these fluctuations, they must be energetically of the same order as the thermal energy available to the system, i.e. the effective shear modulus must be small. Indeed, severe softening of the shear modulus is associated with melting, since a liquid cannot sustain a shear. If a dislocation appears

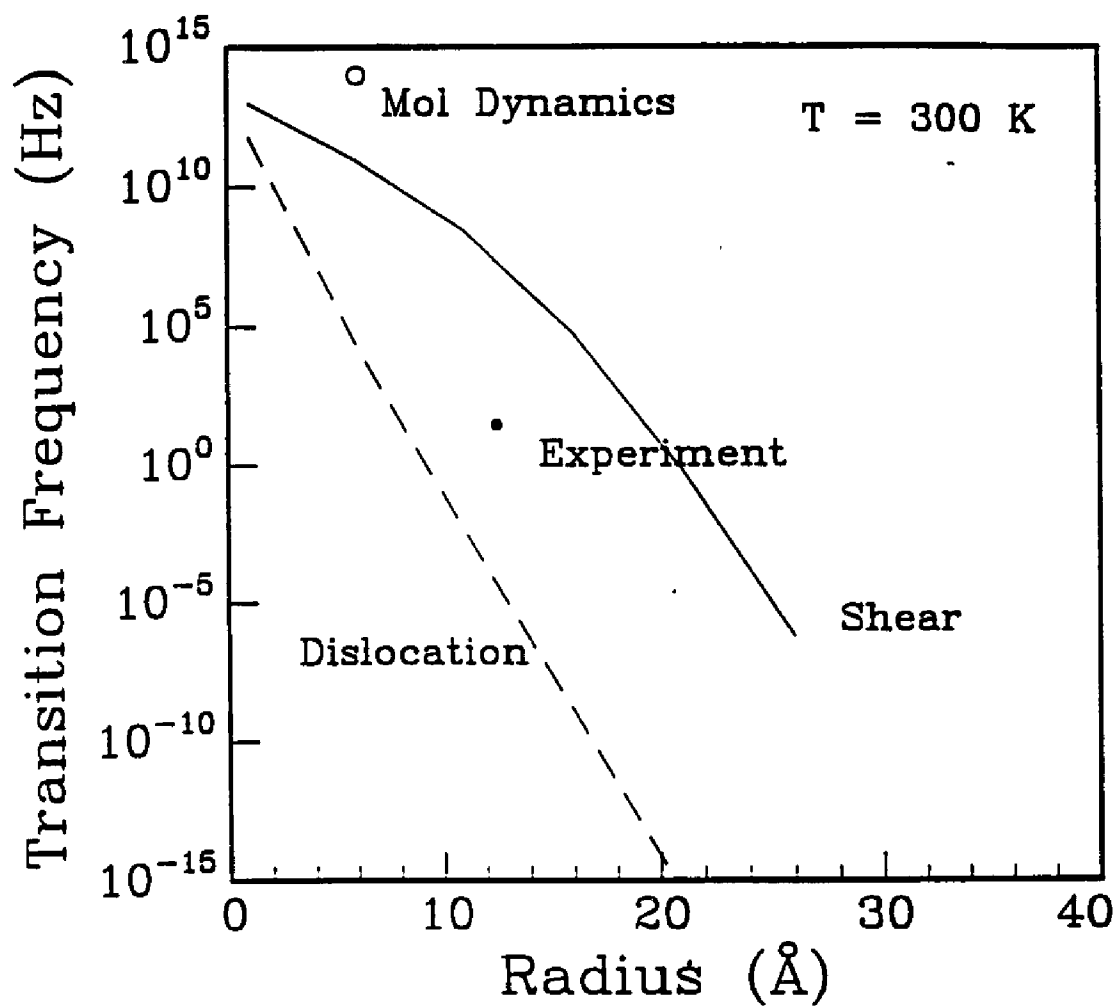


Figure 4.4.1: Rate of fluctuations for a) Dislocation model. b) Shear model assuming a shear modulus softening by a factor of 10.

in a small particle by a fluctuation phenomenon there is no reason why after it has vanished that the structure should be the same, it is very unlikely to be the same due to the softness of the potential energy surface. Therefore combining well accepted ideas of fluctuations and softening of the shear modulus with the potential energy surface appears to yield an explanation of the kinetics of the structural fluctuations. In fact, if structural fluctuations did not occur this would *disprove* standard models. Since only the occasional fluctuations are needed to explain the electron microscopy data, the particles could easily be sitting on the low temperature tail of the fluctuations, and do not need invocation of high temperature conditions very near to the melting point.

However, while the mechanisms of shear and dislocation induced disclination motion are both feasible, later experimental data (figure 4.4.2) do not match any of the models. The particle fluctuation rates are all of the same order of magnitude and do not decrease rapidly, by orders of magnitude, with size. As shown earlier (see figure 2.4.1) the rates of fluctuation increase with beam flux for a given size. This increase of the fluctuation rate indicate that the deviation from the model are probably due to the damping from (a) the particle substrate interaction and (b) inherent viscosity of the particle.

It is a common experimental observation that the small particle must be only weakly coupled to the support before it can start changing its shape and structure. It is a standard result with vibrating droplets that interfacial friction acts as a strong damper of the vibrations [Trinh et al. 1982, Miller and Scriven 1968, Tsampoulos and Brown 1983]. Thus the requirement for weak coupling to a substrate can be directly correlated

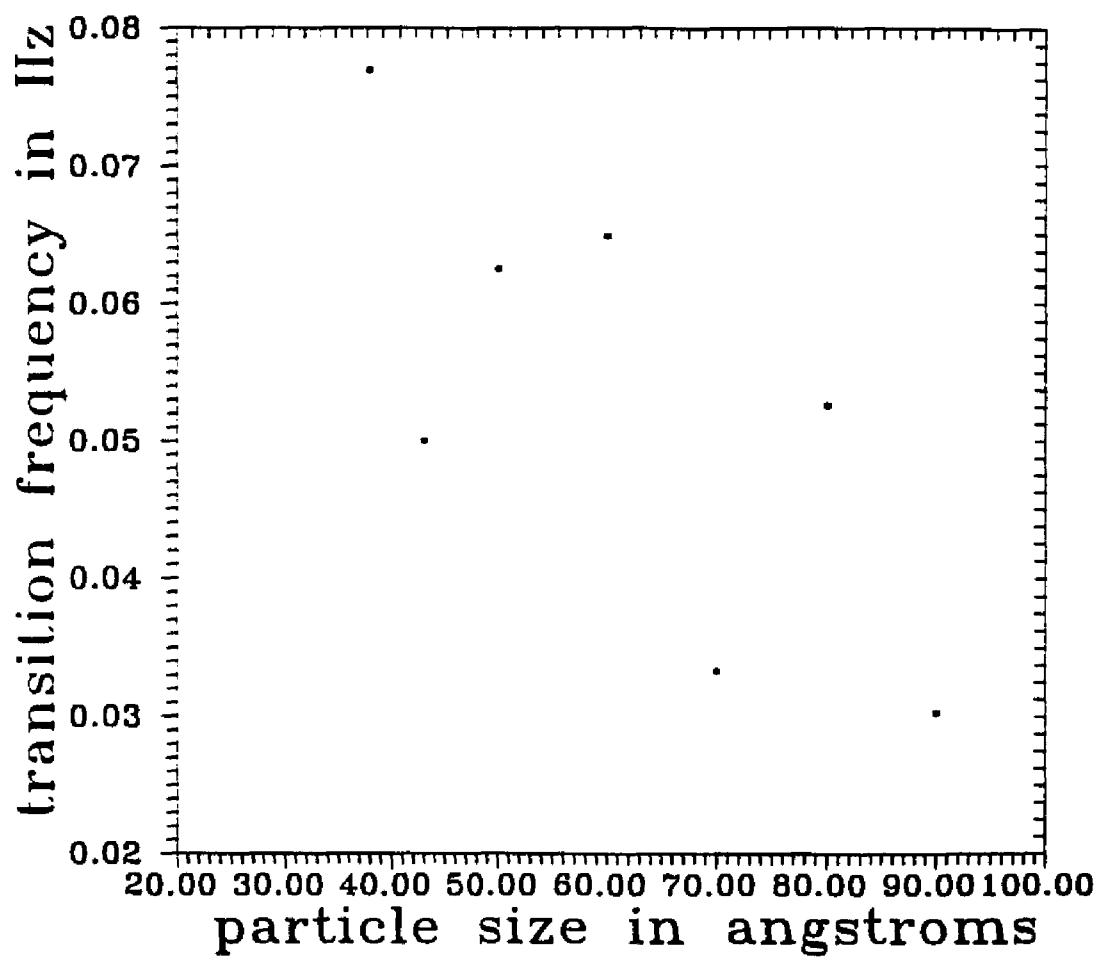


Figure 4.4.2: The experimental average transition frequency plotted against particle diameter.

with frictional damping of the oscillations by the substrate.

The inherent viscous damping has also been ignored in the models. A simple estimation of the viscosity can be obtained on the lines of the work by Lamb (1932) as

$$\tau = \frac{1}{(n-1)(2n+1)} \frac{R^2}{\nu} \quad (4.4.1)$$

where τ is the viscous decay, ν the viscosity, R the radius of the particle and n the order of the spherical harmonic. This viscous damping term can be included in the calculation of the vibrational frequency as an exponential decay term given as

$$A = \exp(1/\tau) \quad (4.4.2)$$

The influence of the damping is vanishingly small and is relatively insensitive to small size changes.

The above discussion indicates that while the models discussed in this chapter are the only mechanisms which even come close to explaining the nature of the transformation kinetics, they remain rather inadequate. The insight gained by the modelling and experimental analysis does show that weak coupling to the substrate aids transformations. Further development of the models to include damping effects would be essential to make them more applicable. The model described in this chapter, while giving an intuitive idea of the process of the kinetic transformations is far from the real situation. However, there does not seem to be any other feasible model and the problem remains unsolved.

CHAPTER 5: APPLICATION TO Ag/Si(100)

5.1 INTRODUCTION

The early stages of nucleation and growth play a crucial role in determining the final structure and therefore the properties of epitaxial deposits. It is well known that nucleation during crystal growth typically proceeds via one of the following three routes [Figure 5.1.1]: layer by layer (Frank-van der Merwe), three dimensional islands (Volmer-Weber) or layer plus island (Stranski-Krastanov). In the latter two cases, further growth of the 3D islands occurs by enlargement of pre-existing nuclei and/or coalescence of neighboring islands. During these processes, the islands can either retain their original structures or undergo recrystallization to form new structures. The final morphology and orientation are thus complex processes decided not only by the thermodynamic stability of the morphologies but also by the kinetics of the transformations. In many instances, the formation of multiply twinned particles does not favor the formation of quality thin films. The role of the island structure is thus critical in controlling the properties of many heteroepitaxial systems and an understanding of their initial structure is therefore highly desirable. One such example is the Ag/Si(100) system.

The Si(100) substrate, under clean conditions, exhibits a 2x1 reconstruction. The current knowledge of the surface structure favors a buckled asymmetric dimer model

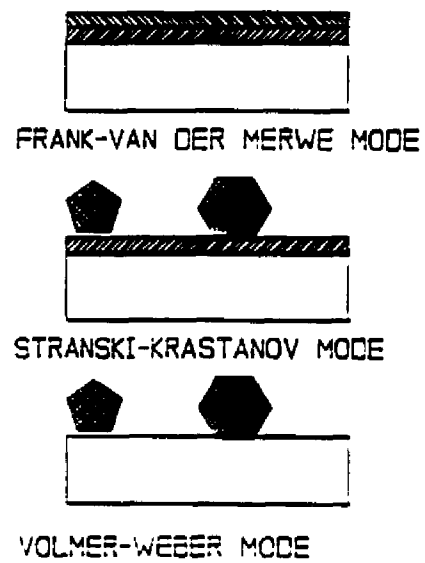


Figure 5.1.1: Three modes of epitaxial growth.

[Jayaram et al. 1993] as illustrated in figure 5.1.2. The other possible configuration, a symmetric structure, is also shown in figure 5.1.3. The energy differences between the two structures are very small. Both the structures show a ridge-valley arrangement of Si atoms. The 2x1 structure is extremely sensitive to vacuum conditions and its presence is a clear indication of not only a clean surface but also very good vacuum conditions.

The nature of the Ag deposit on this (2x1) surface is governed by island nucleation and growth and is of interest primarily from a technological standpoint: the Ag/Si interface is atomically abrupt and is therefore used as a model system to study Schottky barrier heights as a function of interfacial microstructure. However, despite its importance, the Ag particles on Si(100) system has received relatively little attention. The nucleation and growth mode of Ag both at the initial stages and for thicker films has been characterized as being Stranski-Krastanov (SK) from STM [Samsavar et al. 1988, Samsavar et al. 1989, Hashizume et al. 1990, Brodde et al. 1990, Lin et al. 1993, Lin et al. 1993, Winau et al. 1994], LEED-AES [Hanawa and Oura 1977, Hanbucken et al. 1982, Hanbucken et al. 1984, Hanbucken and LeLay 1986] and RHEED [Nishimori et al. 1991, Kimura and Takayanagi 1992] investigations (although a recent STM study reports a pseudo-SK [Winau et al. 1994] growth mode i.e. 3D island nucleation commencing before completion of the 2D layer). Further, the Ag layer is reported to grow with different epitaxies i.e. $\langle 100 \rangle$, $\langle 110 \rangle$ and $\langle 111 \rangle$ of Ag normal to the Si(100) surface. Surprisingly, little is actually known about the structure of the 3D islands: while the external morphology is assumed to be flat with mostly $\{111\}$ and $\{100\}$ facets [Hanbucken and Lelay 1986, Brodde et al. 1990, Kimura and Takayanagi 1992,

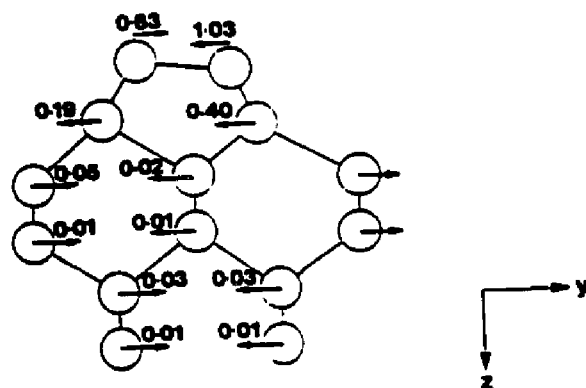


Figure 5.1.2: A schematic of the Si(100)-2x1 structure for a six layer relaxation model; the dimer bond lies in the plane of the paper. Arrows show the direction of dimerization while the numbers denote the magnitude (in Å) of atom displacements (along the "2" direction of the reconstruction, i.e., the y axis in the calculations) from the bulk positions (from Jayaram et al. 1993).

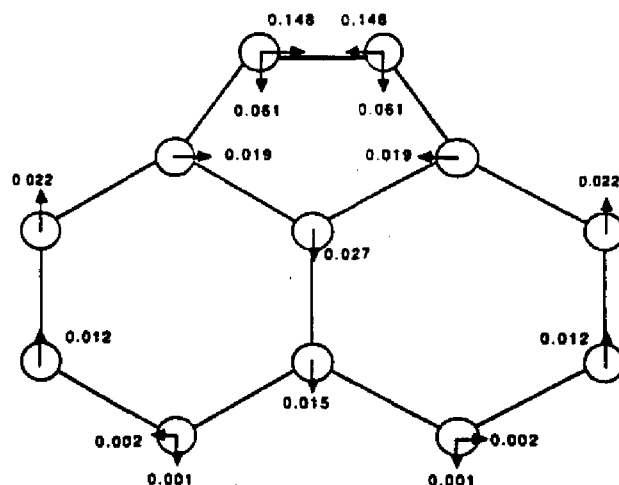


Figure 5.1.3: Section through the symmetric (2x1) dimer surface. The dimer bond is in the plane of the paper, the dimer rows run perpendicular to the plane of the paper. The arrows indicate the directions of displacements of the atoms away from their bulk positions and the numbers give the magnitude of these displacements as a fraction of the lattice constant (5.29 Å) (from Roberts and Needs 1990).

Borenzstein and Alameh 1993], only two investigations [Shirokoff and Erb 1988, Luo et al. 1991] have even alluded to the internal structure within the islands; most studies assume a simple single crystal structure.

This chapter is an account of the first detailed study of the structure of 3D islands that nucleate during the early stages of growth of Ag on Si(100)-2x1 surfaces at room temperature using a combination of UHV-high resolution transmission electron microscopy imaging (HREM) and diffraction (TED) techniques. Contrary to earlier suppositions, the Ag islands are seen to be a mix of single crystal and multiply twinned particle [Ino 1966] morphologies. While the observation of mixed morphologies is in good agreement with similar studies on carbon and SiO substrates, the dominance of the decahedral type (Dh) over the icosahedral type (Ic) MTPs contradicts all earlier experimental and theoretical studies.

5.2 SAMPLE PREPARATION

Thin samples of n-type Si(100) (B doped at 1 ohm-cm) were polished, dimpled and chemically thinned in a 10% HF + 90% HNO₃ solution before being transferred into a UHV surface science chamber (UHV-SSC) attached to a Hitachi UHV-H9000 electron microscope [Bonevich and Marks 1992] (which was operated at 300 kV and 250 kV, the latter to minimize radiation damage) with a working vacuum of 7×10^{-11} torr [Figure 5.2.1]. *In situ* sample preparation involved a cyclic combination of 2.5 kV Ar⁺ sputtering and electron-beam annealing cycles. Clean surfaces were characterized by the appearance of the 2x1 type surface spots. The Ag evaporator filaments were carefully outgassed and several monolayers of Ag were then deposited onto clean Si(100) surfaces at room

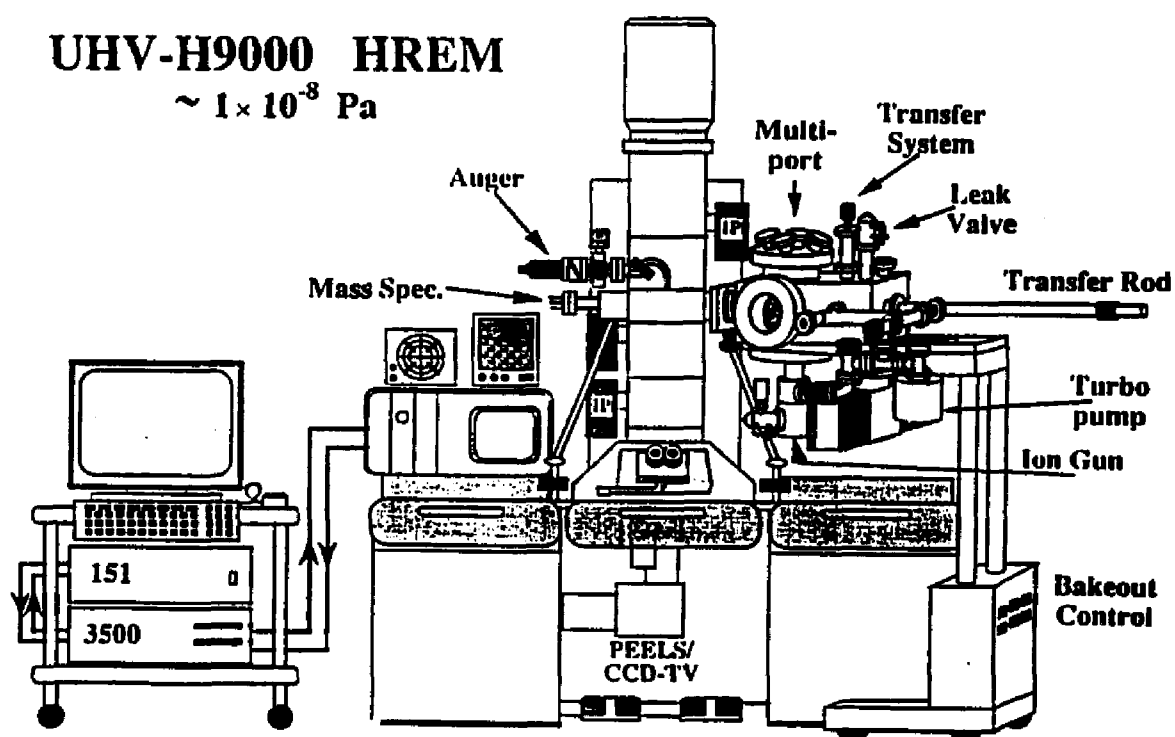


Figure 5.2.1: The UHV-HREM facility (courtesy Dr. J. E. Bonevich).

temperature inside the UHV-SSC. Following each observation, the sample was ion milled and annealed to establish the clean Si surface reconstruction before further deposition (sample cleanliness was carefully monitored after each deposition cycle using parallel electron energy loss spectroscopy). Figure 5.2.2 illustrates the sharp 2x1 surface spots in a diffraction pattern obtained after a cleaning cycle. The results reported below are from numerous such observations.

5.3 RESULTS AND DISCUSSION

Consistent with earlier diffraction studies [Hanawa and Oura 1977, Hanbucken et al. 1982, Nishimori et al. 1991], TED patterns showed a decrease in the intensity of the Si surface reconstruction spots with increasing Ag coverage. Faint arcs whose spacings correspond to those of bulk Ag were also observed from the very initial stages suggestive of an abrupt Ag/Si interface. A typical TED pattern in Figure 5.3.1 shows the coexistence of the 2x1 spots of the clean substrate and (111), (220) arcs of Ag. These can be indexed in terms of a primary $\langle 110 \rangle$ epitaxy with some rotational disorder and strain, moiré fringes between the particles and substrate and moiré fringes internal to the particles themselves [Ino 1966, Marks and Smith 1981]; this will be clarified later but for the moment it should be noted that these diffraction patterns are actually highly misleading. With increasing coverages an increase in the intensities of these arcs was accompanied by the disappearance of the Si reconstruction spots (leaving behind the 1x1 Si lattice); at somewhat higher coverages a true polycrystalline ring pattern developed.

HREM images were acquired in both the on- and off-zone axis modes; the former reveals the presence of islands as darker contrast features with extensive moiré fringes

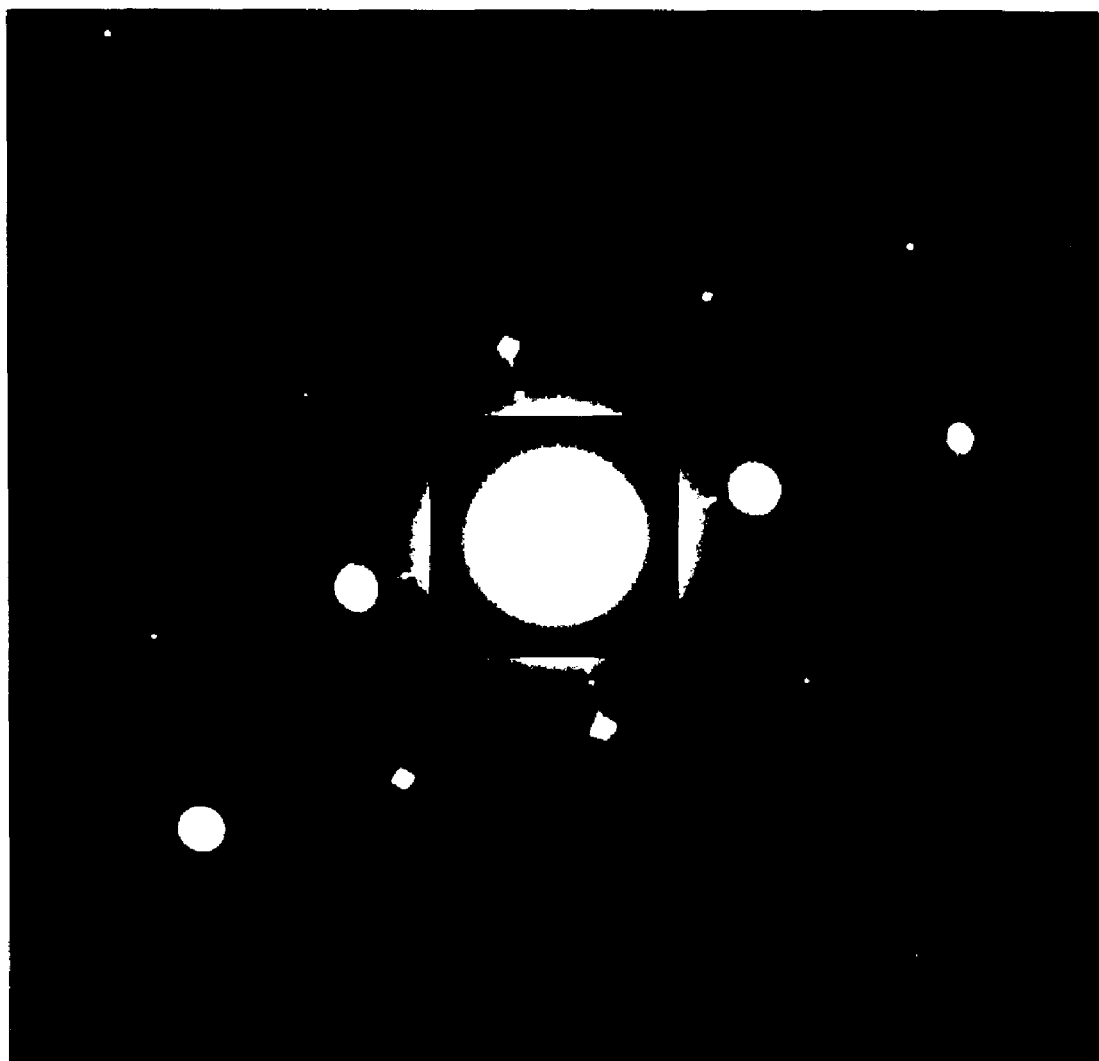


Figure 5.2.2: A TED of a clean 2x1 Si(100) surface. Arrows indicate the surface spots.

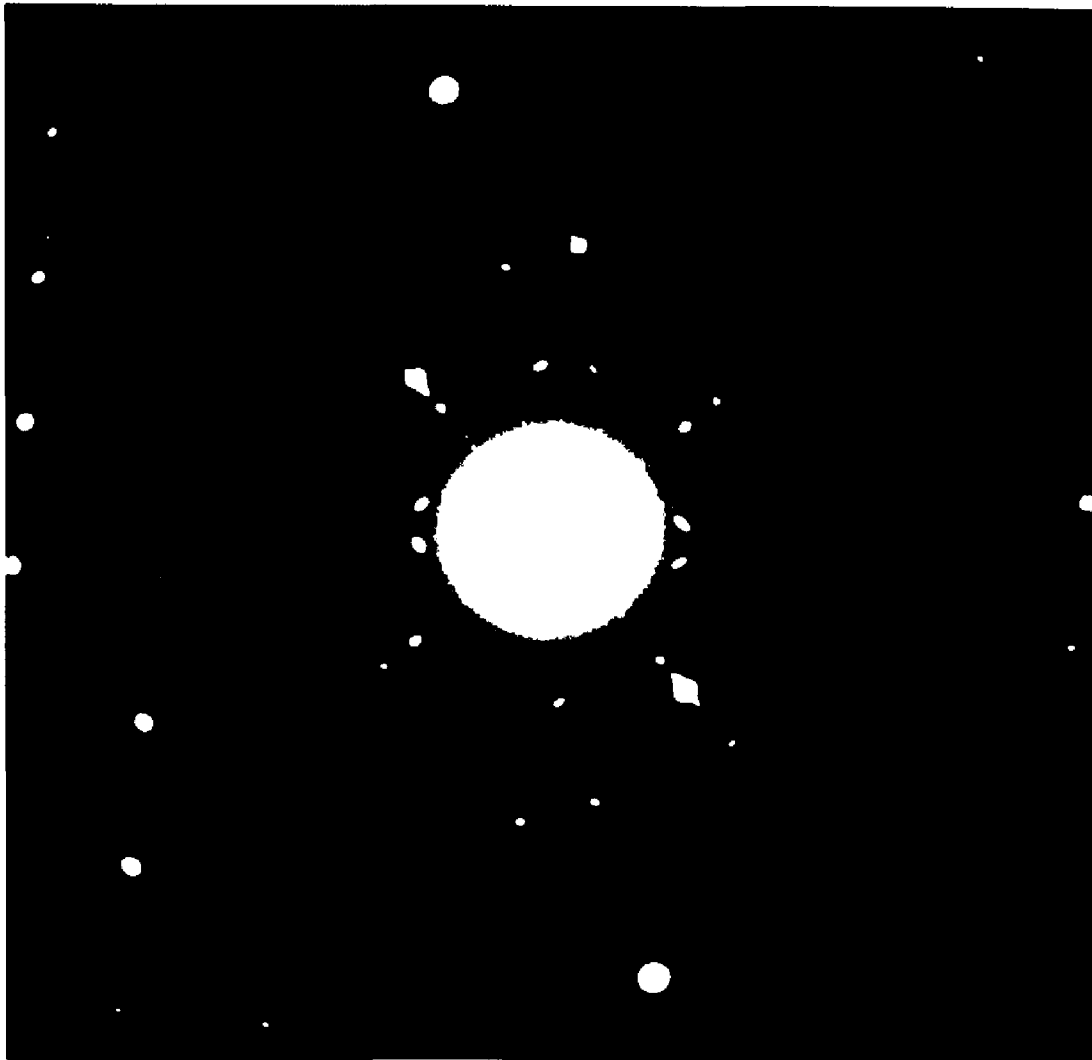


Figure 5.3.1: A typical TED pattern following Ag deposition on a Si(100)-2x1 surface; arrowed surface reconstruction spots coexist with the (111) and (220) ring of Ag, denoted by the letters A and B. All the features can be interpreted by a combination of silicon, silver and moiré spacings.

(origin explained in the earlier paragraph) (Figure 5.3.2). However, these images do not provide much information about the nature (i.e. 2D or 3D) or the structure of the islands, due to the strong bulk signal. In order to reduce the latter, off-axis (2-3° tilt off the (100) zone) images were obtained; this technique is very sensitive to the substrate surface [Xu et al. 1993] or deposit overlayers i.e. Ag islands in the present case, and reveals information about their structure and nature. In order to further enhance the image contrast a modified Wien filter [Marks 1994] was applied to all the HREM images (to reduce the shot noise in the image without introducing any artifacts). Although most of the Ag islands were 3D in nature, isolated regions exhibited incomplete 2D Ag layers indicating that the growth mode is actually pseudo-SK (Figure 5.3.3). The 3D Ag islands have a more complicated structure and were analyzed using an image processing software, SEMPER and a data reduction scheme established in Chapter 2.

Most of the particles were around 3-4nm in size. Analysis of the internal particle morphologies revealed that about half of them were single crystals (Sc) with a primary $\langle 110 \rangle$ epitaxy (Figure 5.3.4) and a smaller number in a $\langle 100 \rangle$ epitaxy. All the single crystals had a rectangular shape and were aligned along the $\{110\}$ planes of the Si substrate. All the single crystals showed increasing aspect ratios with increase in size. This trend can be clearly observed by measuring the variation of the aspect ratio as a function of one of the sides of the single crystals. Figure 5.3.5 clearly indicates this trend even within the narrow size regime of this study. Figure 5.3.6 is a better representation of the trend as a function of the area occupied by the single crystal. Figure 5.3.7 is an example of one such single crystal with a large aspect ratio.



Figure 5.3.2: An on-zone filtered image showing the moiré contrast arising from the interference between the bulk Si and the small particles.

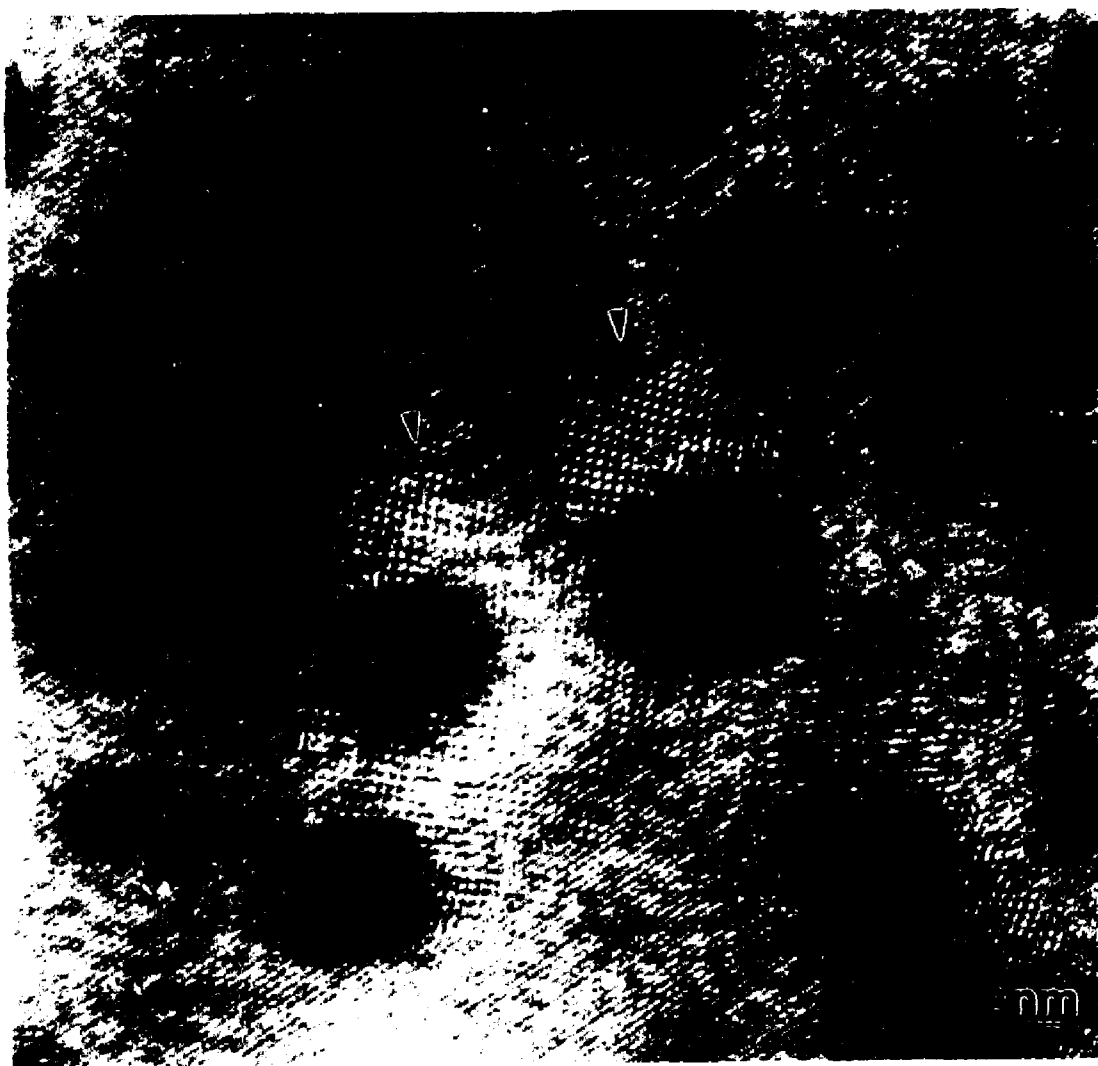


Figure 5.3.3: HREM micrograph illustrating the occurrence of a structure that appears to be an incomplete layer of Ag (indicated by arrows).

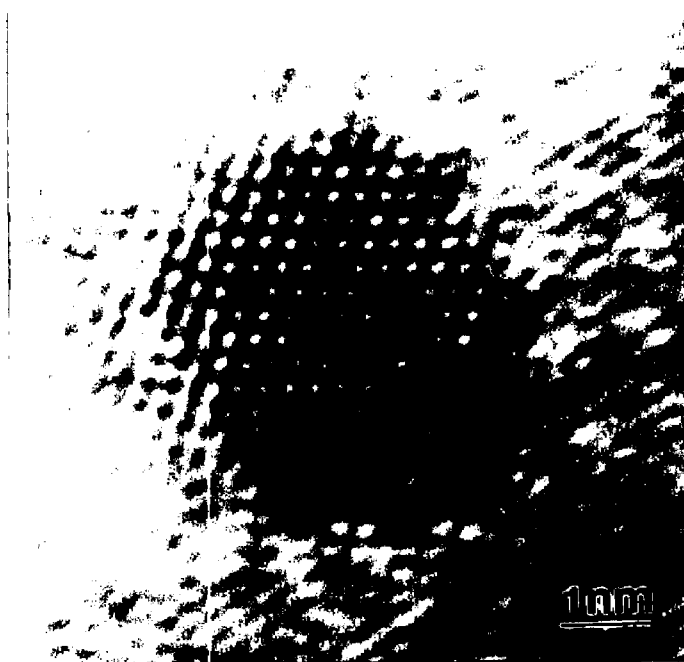


Figure 5.3.4: UHV-HREM micrograph of a $\langle 110 \rangle$ oriented single crystal; the cross fringes in the single crystal image are due to the (111) planes.

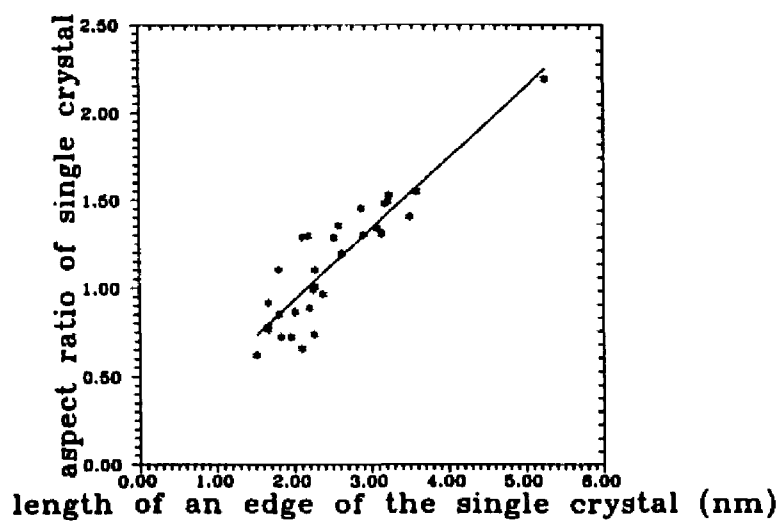


Figure 5.3.5: The aspect ratios of Ag single crystals plotted as functions of the length of one edge of the crystals.

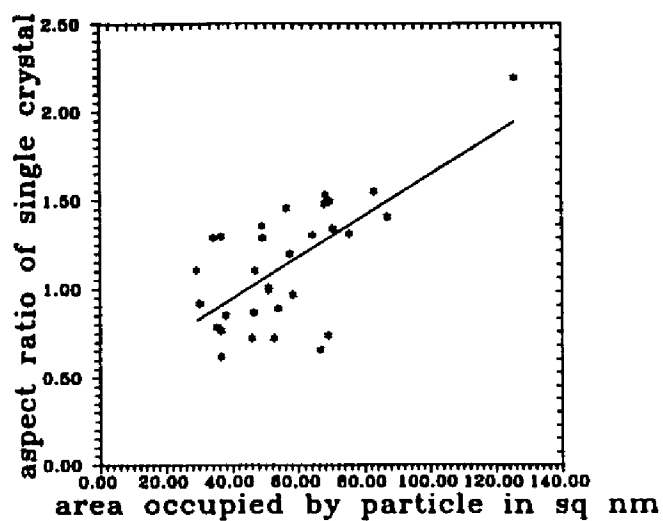


Figure 5.3.6: The aspect ratios of Ag single crystals plotted as functions of the area of the crystals.

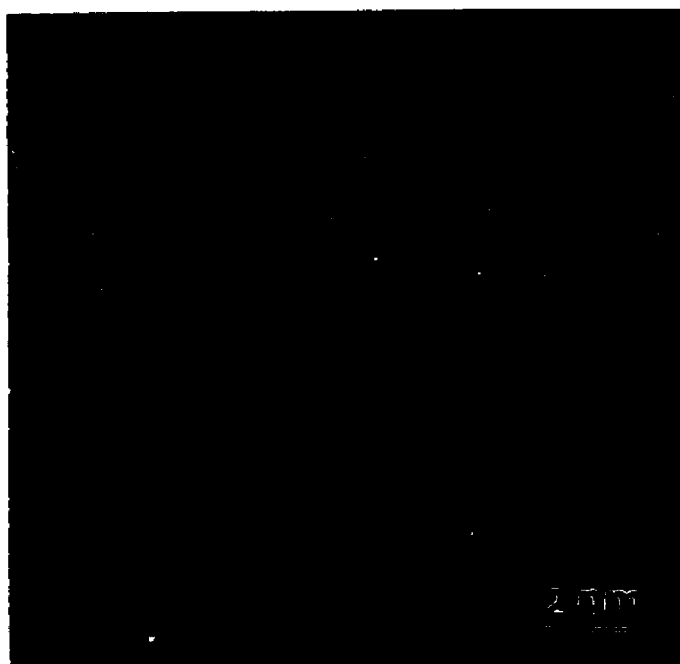


Figure 5.3.7: A single crystal with a long aspect ratio.

The rest of the particles had internal twins (between the adjoining (111) faces) i.e. multiply twinned particles (MTPs) [Ino 1966]. The highest fraction of these particles were of the decahedral (Dh) type that had nucleated with a $\langle 110 \rangle$ epitaxy, see Figure 5.3.8 while a very small population (about 2% of the total) were seen to be of the icosahedral (Ic) type with a $\langle 112 \rangle$ orientation, as shown in Figure 5.3.9 (for more details on the structure of these MTPs as observed by HREM, see Chapter 2). It is the presence of these more complicated particles that cause both the arcs and the other additional spots in the diffraction patterns.

Such mixed morphology growth is known to exist in fcc metal islands deposited on oxide and alkali halide substrates [Ino 1966, Gillet 1977, Marks and Smith 1981, Renou and Rudra 1985, Altenhein et al. 1991, Hofmeister 1991] and was first observed only under very clean conditions [Ino 1966, Allpress and Sanders 1967]. Theoretical studies, e.g [Ino 1969, Marks 1984, Howie and marks 1984, Ajayan and Marks 1990, Cleveland and Landman 1991] have also clearly demonstrated that MTPs are the thermodynamically stable entities at the small sizes seen in this investigation; similar results in terms of relative probabilities of occurrence of Ics, Dhs and Scs have been reported in a recent experimental study [Doraiswamy and Marks 1994].

In contrast to these studies, the Ag/Si(100) system behaves uniquely i.e. although it is a mixed morphology system, there was an unusual lack of Ic particles. Without exception, Ic particles are considered to be energetically preferred over the Dh particles [Ino 1969, Marks 1984, Howie and Marks 1984, Ajayan and Marks 1990, Cleveland and

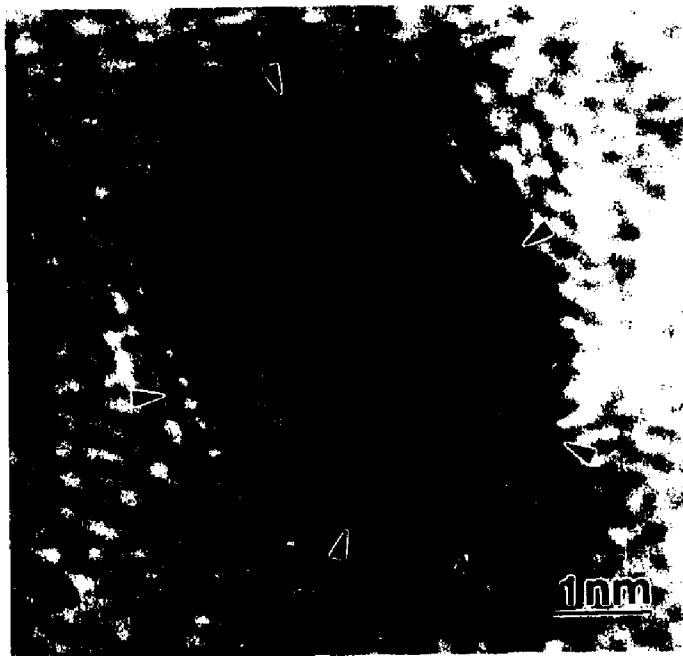


Figure 5.3.8: UHV-HREM micrograph of a $\langle 110 \rangle$ oriented decahedral MTP with arrows indicating the five twins separating $\{111\}$ facets.



Figure 5.3.9: UHV-HREM micrograph of a $\langle 112 \rangle$ oriented icosahedral MTP.

Landman 1991, Hall et al. 1991] at these small size ranges. All theoretical analyses to date (except the early work of Ino (1969)) have ignored the substrate interaction effect. Since there is no simple way for an Ic particle to adopt an $\langle 110 \rangle$ epitaxy, it can be hypothesized that the deposit/substrate interaction effect inhibits their formation. Influence of the substrate on the particle morphologies was supported by the following observation: on exposure to air, although the Ag particles continued to exhibit a mixed morphology of single crystals and MTPs, the fraction of Ic particles increased. This can be attributed to the effect of the gas environment on both the interface between Ag and Si and on the Ag surface free energy [Marks 1984, Howie and Marks 1984] (both its absolute value and anisotropy).

The distribution of decahedral MTPs and single crystals showed an increase in single crystal morphology with increasing size (Figure 5.3.10). The decahedral MTP, however, showed a decrease in population with an increase in size (Figure 5.3.11). These results coupled with that of the absence of icosahedral MTP imply extensive reconfiguration of the particles and a strong effect of the substrate in modifying the potential energy surface. In fact, the origin of the rectangular shape of the single crystal islands can be traced back to the nature of Ag adsorption on the underlying 2×1 Si substrate. STM works [Samasavar et al. (1988),(1989), Brodde et al. (1990), Nogami et al. (1993) and Winau et al. (1994)] all show that the Ag adatoms are preferentially adsorbed on the cave sites between two Si dimer rows (see Figure 5.3.12). Higher coverages were observed to lead to long Ag adatoms chains, aligned along these two fold bridge sites. Further, a cluster model study [Ru-Hong Zhou et al. (1993)] of Ag bonding

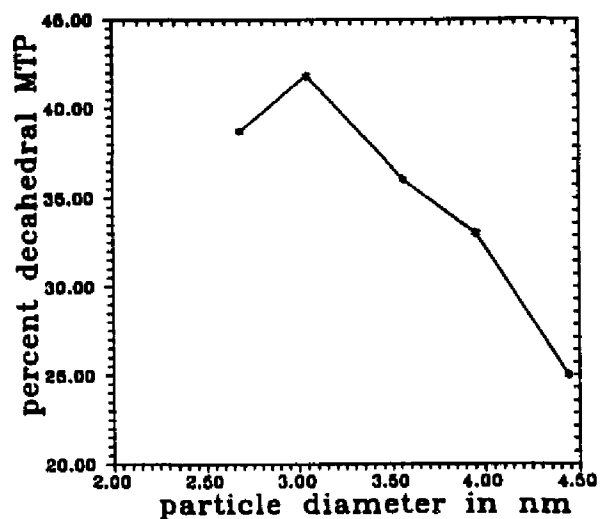


Figure 5.3.10: The plot of the percent yield of decahedral MTPs as a function of the average size of the Ag particles.

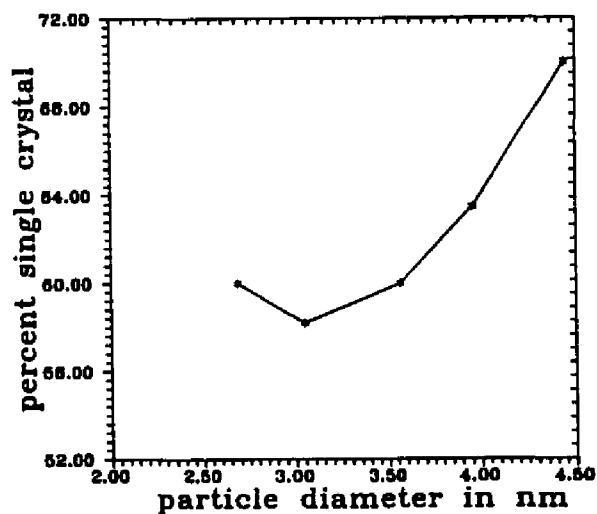


Figure 5.3.11: The plot of the percent yield of single crystal as a function of the average size of the Ag particles.

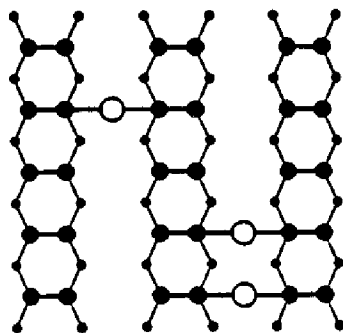


Figure 5.3.12: Plan view of a structural model illustrating the adsorption site for Ag atoms on Si(100)-2x1 (from Samsavar et al. 1989). The circles, large filled circles and small filled circles represent Ag adatoms, Si dimer atoms and the Si atoms just below the dimer layer.

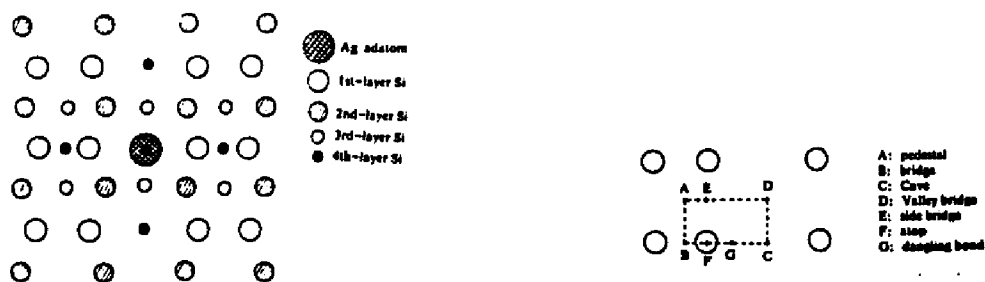


Figure 5.3.13: A cluster model for Ag adsorption and migration on Si(100)2x1, as well as the possible adsorption sites (from Ru-Hong Zhou et al. 1993).

and migration on Si(2x1) compared the different adsorption sites on Si(2x1) (see Figure 5.3.13) and found that the Ag adatoms strongly favor migration between Si dimer rows and perpendicular to them. The single crystals, in this study, were all aligned in mutually perpendicular directions and in parallel epitaxy to the Si(100). The presence of raft-like features in the incomplete Ag intermediate layer (also aligned along the same direction) [Figure 5.3.14] leads one to relate the anisotropic growth to the 2x1 substrate. Clearly, this self alignment and growth of Ag islands is a very interesting phenomenon by itself and would definitely respond to heat treatment (leading to diffusion along favored directions) to give a better yield of high aspect ratio single crystals of Ag. It opens up several interesting possibilities for the growth of nanowires. But complete analysis requires a much more careful temperature controlled set of experiments and is beyond the scope of this thesis.

Although the morphologies reported in this study are of the static type (no fluctuations were observed under the beam fluxes used), there was evidence for interconversion during growth. One particularly striking example is the pentagonal shaped single crystal shown in Figure. 5.3.15 (which was observed in UHV prior to the air transfer). A pentagonal shape is not close to any equilibrium shape for a Sc indicating that a Dh particle has transformed by grain-boundary migration [Bonevich and Marks 1992] to a single crystal. Interconversion of particles is relatively well documented [Yagi et al. 1975, Iijima and Ichihashi 1985, Marks 1994] since the initial observations by Yagi et al [Yagi et al. 1975] during growth in UHV conditions.

The small fraction of Ic particles raises some fundamental scientific questions on

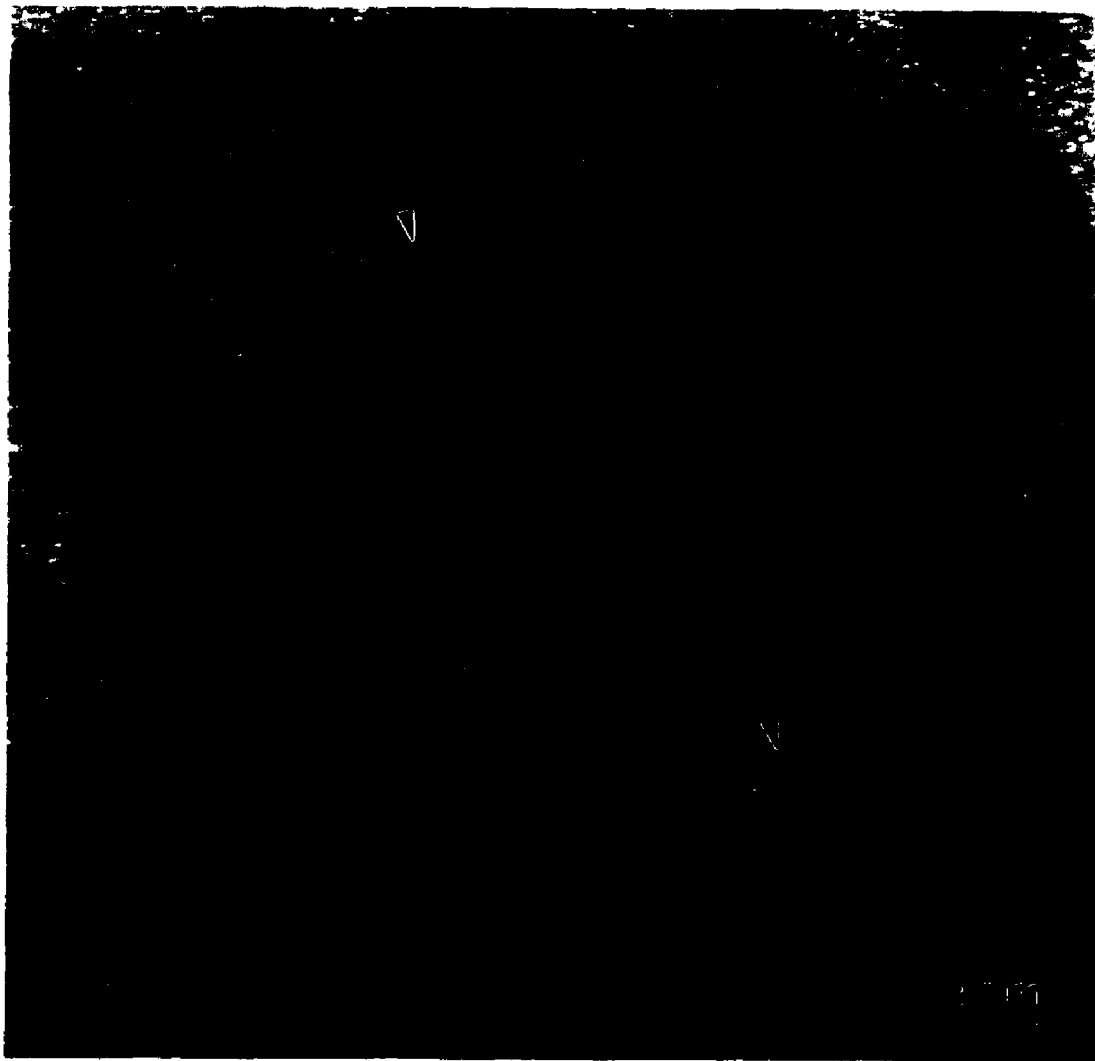


Figure 5.3.14: UHV-HREM (off-zone image) showing chain like adsorption sites (indicated by arrows).

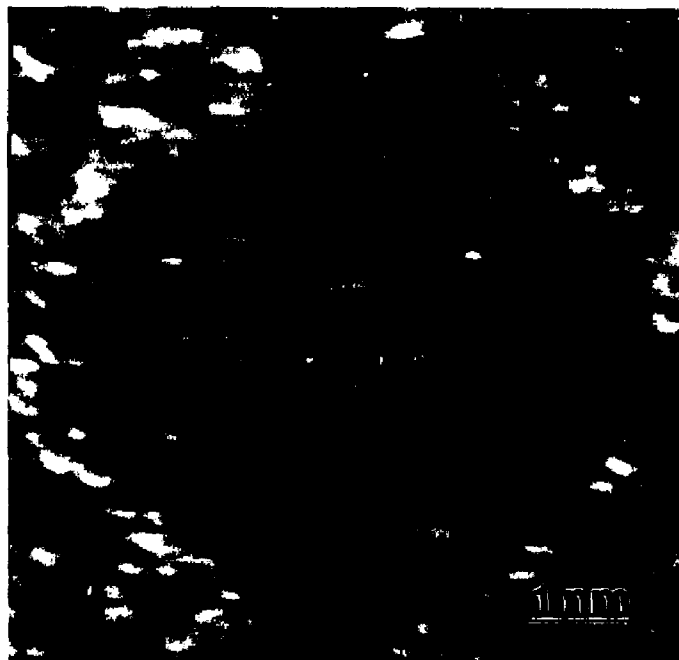


Figure 5.3.15: An atypical pentagonal Ag single crystal on a Si(100)-2x1 surface indicating inter-morphology conversion via grain boundary migration.

the variation in types of island morphologies with environment conditions and merits further investigation. Further, the changes in the fraction of Ic particles on exposure to air underlines the importance of observation under UHV conditions. A subtle point that also arises is the advantage of UHV-HREM over STM as an imaging technique in resolving the local structure within these small 3D islands; the pitfall of erroneous interpretation of nucleation and growth mechanism based solely on diffraction data is also revealed.

The observations conclusively show that, rather than being simple flat single crystals (as suggested without proof in earlier studies), the 3D Ag islands show a classic mixed morphology MTP growth [Ino 1966] i.e. a combination of single crystals and multiply twinned particles with different orientations relative to the substrate (this is possibly the reason for the different epitaxies reported for this system by earlier studies). This could also be the case for the Ag/Si(111) system; MTPs have also been observed in the Au/Si(111) system [Plass 1994]. The investigation thus demonstrates that one of the most fundamental questions about the growth mode of Ag on clean Si(100), i.e. the particle structure, has escaped more than a decade of study.

The formation of MTPs in the initial stages has profound implications on the later stages of growth. Earlier studies [Honjo et al. 1979] have shown that these MTPs on coalescence can either form single particles (with either the MTP/Sc structure) or polyparticles (partially coalesced MTPs) or polycrystals (single crystals separated by a grain boundary); recrystallization is also seen to occur in these particles as a means of relieving the strain. The final film is a result of these processes; its structure will

therefore be strongly dependent on the processing conditions (temperature, deposition rate, vacuum etc). A time-temperature-transformation morphology map similar to that suggested by Marks (1994) would be essential in controlling the final structure and therefore the properties in such mixed morphology systems (e.g. the resulting film [Weitering 1993] would have a variation in Schottky barrier height ranges depending on the inhomogeneity and polycrystallinity developed during the process of growth).

CHAPTER 6: SUMMARY AND SUGGESTIONS

6.1 SUMMARY

The primary focus of this work was on elucidating the dynamic behavior of small particles and extracting a form of map which would help determine the morphology of small particles in an environment.

In the first phase of the work, a data reduction scheme was developed for the breakdown of the morphologies of small particles into categories classified by a well characterized basis set. The scheme was then applied to the analysis of the dynamic fluctuations of Au particles supported on SiO substrates. The analysis revealed that under the conditions of the environment:

- a) The morphology transformation rates of the particles were much slower than the rotation rates about their centers of mass.
- b) A threshold beam flux was required to loosen the particles from the substrate and later fluctuations required very small beam fluxes.
- c) The rate of fluctuations dropped rapidly with size at low beam fluxes and for a given size the rates of fluctuations had a weak dependence on the beam flux. High beam fluxes lead to very rapid fluctuations accompanied by rapid rotations and translations of the particles. In many cases the particles detached from the substrate.

d) In the size regimes studied the particles resided most often in the Sc morphology followed by the decahedral morphologies at larger sizes (more than 5nm). The icosahedral morphology was assumed by the particles only for very small sizes (less than 5nm). A broad transition regime was observed in which the particles showed almost equal relative probabilities of occurrence for all the three morphologies studied, i.e Sc, Dh and Ic.

In order to determine morphology maps, the energetics of the small particles were obtained from earlier works and converted to free energies. A driving energy term, apart from the effects of surface stress and anisotropy was added as a better representation of the influence of these parameters in the morphology. The morphology map calculated in this manner showed moderate agreement with the experimental data.

Morphology maps only consider the thermodynamic feasibility of a transformation. In many instances, the kinetics of the transformations become more important. These were analytically modelled by considering particles as liquid droplets and the transformations were assumed to occur either by the movement of disclinations or by shear transformations. While both models neglected the viscous damping due to the substrate as well as that occurring within the particle, they show the necessity of a weak substrate-particle coupling for increased rates of fluctuations. In addition, the models demonstrate that the particles change configuration without the need to undergo violent changes such as charge imbalances.

The morphological fluctuations observed for small particles by microscopy has often been hypothesized to be a beam induced heating effect. Two simple experiments were conducted to understand the nature of the electron beam interaction. Ag and Pb

were separately deposited onto holey carbon and SiO grids, under UHV conditions. When subjected to intense electron beam fluxes, neither Ag sublimed nor did Pb melt. Instead, Ag and Pb quasimelted on SiO. But Ag did not quasimelt on carbon. These experiments clearly put an upper limit (less than 200K) on the temperature rise due to the electron beam.

More interestingly, Pb showed clear MTP structures and quasimelted between morphologies. These are in direct contradiction to the often assumed isotropic surface energy properties of Pb. These "anomalies" from the often assumed simple single crystal behavior are not just restricted to such fcc materials on oxides. They occur in very important technological systems too. In this work, one such system (Ag/Si(100)) was investigated and revealed large fractions of MTP structures. Further these fractions were found to be sensitive to the surrounding conditions. Current static morphology analyzes also indicate a process dependent morphology distribution. These results indicate several promising directions for future work.

6.2 SUGGESTIONS FOR FUTURE WORK

The tools already developed in this thesis can be applied to various other epitaxial systems. The morphology map for the Au/SiO is currently being analyzed by static morphology methods to confirm the results obtained by dynamic studies. There is no reason to limit the study to the Au/SiO system. As shown in the earlier chapter, the Ag/SiO system has several interesting features with changes in conditions. The current configuration of the UHV-microscope system at Northwestern allows for in situ heating and better chemical analysis than before. Ag on Si(100) 2x1 undergoes several different

transformations and the shape of the single crystal changes with increasing deposition to elongated rod-like shapes. A mapping of the behavior of this system would bring the ideas of a morphology map to fruition and also help in the development of reproducible nanostructures.

The morphology maps would also refine the theoretical framework for the construction of morphology maps which include a larger number of structures than that used in the current study.

The construction of an environmental cell would greatly aid in these studies. The roles of chemisorption, surface energy anisotropy and surface stress continue to remain black boxes. The quantification of these data would probably be the next most important step in the research of small particles.

A question that remains unanswered in small particle research is the usefulness of the Ic and Dh MTP. The determination of the conditions for maximizing their yield would help shed light on their individual properties and in the engineering of materials formed by the compaction of only these MTPs.

Finally, the pillar formed by the small particles (or fine tipped filaments) could be used to nanospin rods of various materials. This has been tapped to form bucky tubes. It could also be used for the formation of rods of band gap engineered materials. An experimental trial by YeongCheol Kim, Richard Plass and myself showed that micron sized Si rods could be grown by this method. However, a lack of time and the need to complete other projects prevented us from continuing this work to form nanosized pillars. The process has been applied to the formation of atom probe samples for several years

and initial studies were also conducted on InP [Bootsma and Gassen 1971].

APPENDIX 1: WULFF CONSTRUCTS

1.1 The Wulff Construct

The equilibrium shape of a given amount of matter is that which minimizes the surface energy over the entire volume of matter. Mathematically, it can be stated as

$$\int \gamma dS \quad (\text{A1.1.1})$$

where, γ is the surface energy and S the surface over which the shape is determined. In general, the specific surface free energy γ is a function of the orientation of the unit outward normal \mathbf{n} at each surface point. The first formulation of the problem was proposed by Gibbs (1878) and the solution without proof is credited to Wulff (1901).

The Wulff equilibrium polyhedron can be geometrically constructed by the following procedure:

1. Construct the γ -plot by drawing a surface whose radius vector in the direction of any unit vector \mathbf{n} has a length proportional to the surface energy $\gamma\mathbf{n}$ of a plane normal to \mathbf{n} .

This is equivalent to the proposition :

$$\frac{\gamma_1}{h_1} = \frac{\gamma_2}{h_2} = \frac{\gamma_3}{h_3} = \dots = \text{constant} \quad (\text{A1.1.2})$$

where the γ s are the surface free energies and the h values represent the lengths of the radius vectors in a given direction.

2. Draw a plane through the end of each radius vector of the γ -plot and perpendicular to the radius vector.
3. The body enclosed by all points connected to the origin without crossing any of the planes constructed in step 2 is the Wulff equilibrium shape.

Figure A1.1 is an arbitrarily drawn Wulff construct.

Several different proofs [Hilton 1903, Liebmann 1914, Laue 1943] exist for the construct, but these proofs are not completely general and do not establish that the Wulff construct is an absolute minimum. Using the Brunn-Minkowski inequality, Dinghas (1944) generalized the proof of the Wulff construct to include any surface. The proof discussed below follows Herring's interpretation of the Dinghas proof [Herring 1953].

Consider any two bodies P_1 , P_2 . Choose an arbitrary point in the interior of P_2 and call it the center of P_2 . If P_2p is the set of points covered by P_2 when its center is at p and if P_n is the set of all points included in any P_2 when p is allowed to range over P_1 then the Brunn-Minkowski inequality states that the volumes V_1 , V_2 and V_n of P_1 , P_2 and P_n , respectively, satisfy

$$V_n \geq (V_1^{1/3} + V_2^{1/3})^3 \quad (\text{A1.1.3})$$

and that the inequality hold if and only if P_1 and P_2 are geometrically similar and in indistinguishable orientations.

To prove the Wulff construct, let P_1 be a hypothetical shape. Let P_λ be the body generated from P_1 by displacing each point of the surface outward along its normal \mathbf{n} by

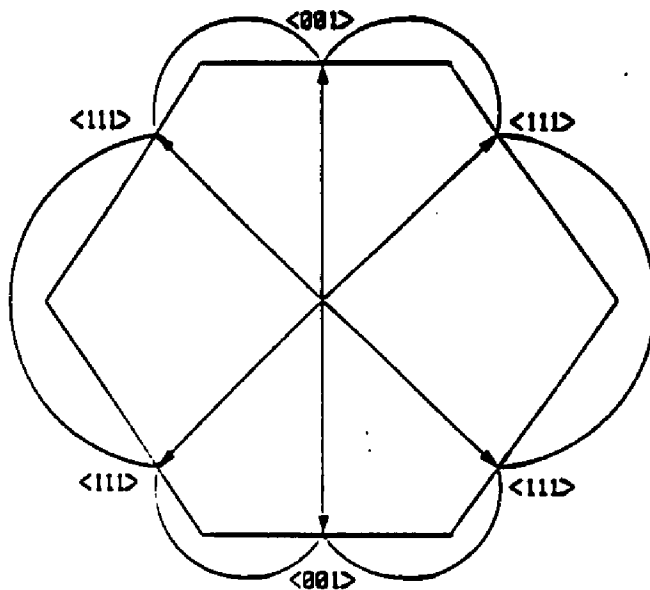


Figure A1.1: A $\langle 110 \rangle$ section of the Wulff construct for a particle with only $\{111\}$ and $\{100\}$ facets.

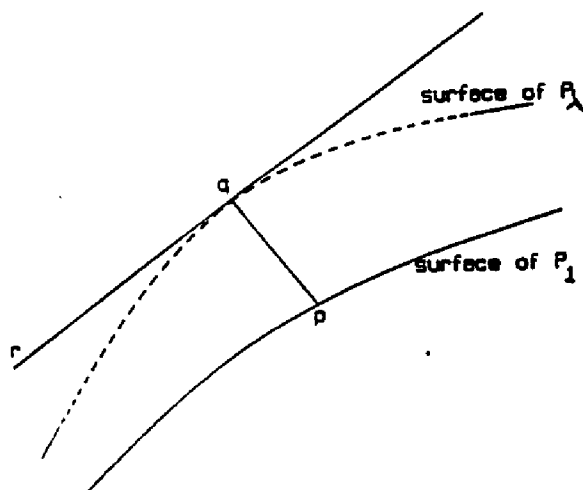


Figure A1.2: Schematic of the geometrical construction used to prove the Wulff construct using the Brunn-Minkowski inequality (Reproduced from Herring 1953).

a distance λn . Then, if V_0 is the volume of P_0 ,

$$\int \gamma dS = \lim_{\lambda \rightarrow 0} \frac{V_\lambda - V_1}{\lambda} \quad (\text{A1.1.4})$$

Now consider Figure A1.2, any point p of the surface of P_1 and the corresponding point q of the surface of P_λ , so that the vector pq is λn . The Wulff construct with scale factor λ centered on p will not contain any points outside the plane rq normal to n through q . Let $V_{\lambda n}$ be the volume of P_λ formed as described for V_0 and let equivalent of P_2 in the Brunn-Minkowski relation be the Wulff construct with volume V_w . Then if γ is a continuous function over the surface, except at edges and corners:

$$\lim_{\lambda \rightarrow 0} \frac{V_{\lambda n} - V_1}{\lambda} \leq \lim_{\lambda \rightarrow 0} \frac{V_\lambda - V_1}{\lambda} \quad (\text{A1.1.6})$$

Combining the above two equations and the Brunn-Minkowski relation:

$$\int \lambda dS \geq \lim_{\lambda \rightarrow 0} \frac{(V_1^{1/3} + \lambda V_w^{1/3})^3 - V_1}{\lambda} = 3V_1^{2/3} V_w^{1/3} \quad (\text{A1.1.7})$$

Again, as mentioned earlier, the equality in the above relation can hold only if P_1 and the Wulff construct are similar. This completes the proof.

1.2 The Modified Wulff Construct

The equilibrium shape of single crystals are well understood in terms of the Wulff construct. However, it does not address the problem of surface morphologies of twinned particles. In order to include the effect of twins Marks (1983) introduced the modified Wulff construct. In the modified Wulff construct, the energy per unit area associated with

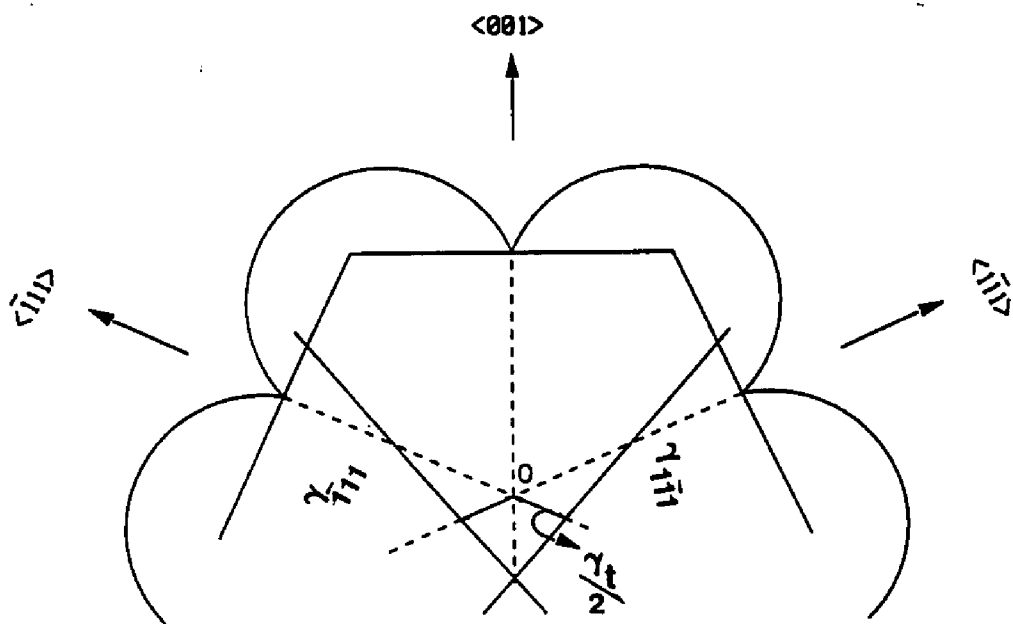


Figure A1.3: The shape of the $\langle 110 \rangle$ sectioned single crystal segment derived from the modified Wulff construct for a perfectly symmetrical decahedral MTP (from Marks 1980).

a twin boundary separating two single crystal elements, A and B, is partitioned between them as $\alpha\gamma_i$ and $1-\alpha\gamma_i$ and then each section is separately treated as a single crystal unit with the twin faces as external facets. The solution of the minimal surface energy configurations of A and B taken independently includes all the local minima of the complete particle and the problem is reduced to constraining the minimization to ensure that the two twin facets remain identical. The construction involves the following steps:

1. Construct a Wulff polyhedron using the standard Wulff construct.
2. Extract the appropriate area by including the twin boundaries in the equivalent form of external facets of energy per unit area $\alpha\gamma_i$ and $1-\alpha\gamma_i$.
3. Find any discrete values of α and the relative volumes of the segmented single crystals for which the twin facets can be matched.

A common solution uses $\alpha=1/2$ and equal volumes of all the segments leading to symmetric structures. Figure A1.3 shows the modified Wulff construct for a symmetrical Dh. The modified Wulff construction has been used to model the structure of several different types of complicated particles including MTPs, lamellar twinned particles and polyparticles. While there is no direct proof of the modified Wulff construct, atomistic calculations [Raoult et al 1989, Cleveland and Landman 1991] support its validity. Its application to map the "phases" of small particles [Dundurs et al 1988, Ajayan and Marks 1988] shows qualitative agreement with experiments. A recent observation by Haluska et al (1993) shows millimeter size MTPs of buckyballs which follow the model predicted by the modified Wulff construct.

APPENDIX 2: LIQUID DROPLET

2.1.1 Vibrational Modes of a Liquid Droplet

The vibrational modes of a dense sphere can be categorized into three modes (Figure A2.1.1), namely: a) repeated contraction and expansion mode b) spheroidal mode and c) torsional mode. Among the three modes the spheroidal mode is very much analogous to the behavior of a fluctuating small particle. There have been many extensive proofs of the vibrations of a dense sphere, specially with regard to the vibrations of a liquid droplet [Lamb 1932, Reid 1960, Chandrashekhar 1962]. The following proof is based on the work of Lamb (1932).

Consider a liquid drop which, in the undisturbed state, will be spherical under the influence of surface tension. If the external pressure is zero, then the internal pressure will have a constant value of

$$p = 2T_1/R \quad (A2.1.1)$$

where T_1 is the surface tension per unit length and R is the radius of the sphere. To study the oscillations of this configuration. Consider figure A2.2 , take the origin to be the center of the drop. Let the shape of the perturbed surface at any instant be given by:

$$r = R + \zeta = R + \epsilon Y^m(\theta, \phi). \sin(\sigma t + \eta) \quad (A2.1.2)$$

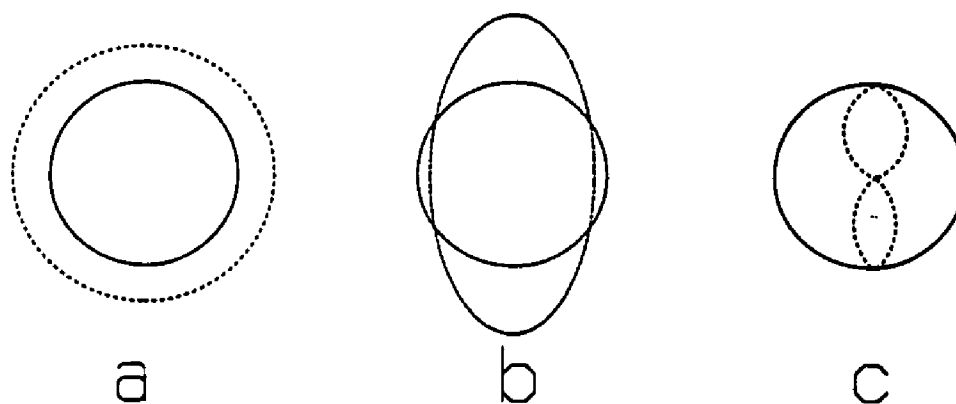


Figure A2.1: The vibrational modes of a dense sphere (a) the repeated contraction and expansion mode (b) the spheroidal mode and (c) the torsional mode.

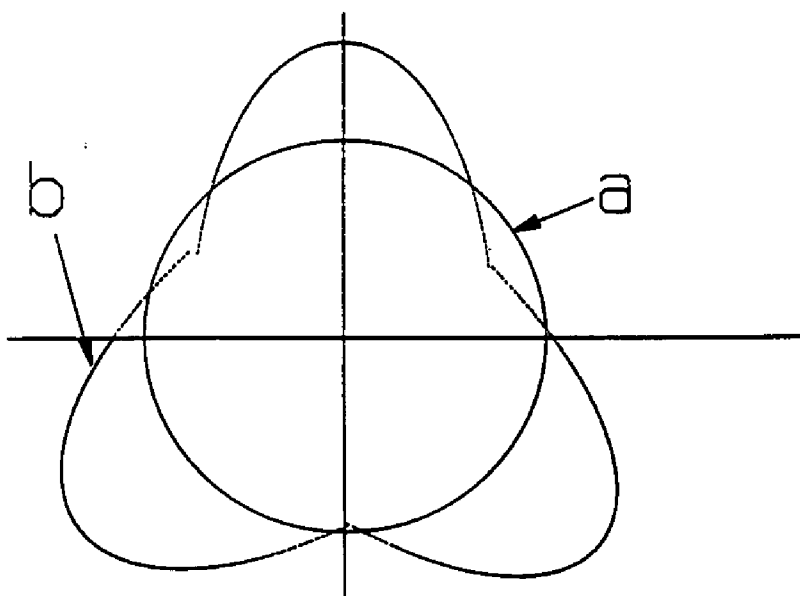


Figure A2.2: An Oscillating droplet. (a) spherical equilibrium shape, (b) departure from equilibrium described by Legendre polynomials.

where R is the mean radius, σ the frequency of oscillations and

$$Y(\theta, \phi)_l^m = P_l^m(\theta)e^{im\phi} \quad (\text{A2.1.3})$$

is a surface spherical harmonic of the first kind and $\epsilon \ll 1$. The internal pressure of the drop then would have a variable component :

$$p = \dots + \frac{\rho \sigma^2 R}{n} Y_l^m(\theta, \phi) \cdot \sin(\sigma t + \eta) \quad (\text{A2.1.4})$$

But the fluid pressure, due to capillarity, is also given as

$$p = T_1 \left(\frac{1}{R_1} + \frac{1}{R_2} \right) \quad (\text{A2.1.5})$$

where R_1, R_2 are the principle radii of curvature and T_1 the surface tension per unit area.

To find the sum of the curvatures introduced by the capillarity, it can be seen that if $\lambda,$

μ, ν are the direction cosines of a normal at (x, y, z) to the surface of the family

$$F(x, y, z) = \text{constant} \quad (\text{A2.1.6})$$

which passes through the point (x, y, z) then

$$\lambda, \mu, \nu = \frac{F_x, F_y, F_z}{\sqrt{(F_x^2 + F_y^2 + F_z^2)}} \quad (\text{A2.1.7})$$

and therefore

$$\frac{1}{R_1} + \frac{1}{R_2} = \frac{\partial \lambda}{\partial x} + \frac{\partial \mu}{\partial y} + \frac{\partial \nu}{\partial z} \quad (\text{A2.1.8})$$

Now the equation for the perturbation can also be written as

$$r = R + \Lambda \quad (\text{A2.1.9})$$

where

$$\Lambda = \frac{r^n}{R^n} Y_l^m(\theta, \phi) \cdot \sin(\sigma t + \eta) \quad (\text{A2.1.10})$$

by neglecting the square of the spherical harmonic. From the above equation the direction cosines can be determined as

$$\lambda = \frac{x}{r} - \frac{\partial \Lambda}{\partial x} + n \frac{x}{r^2} \Lambda \quad (\text{A2.1.11})$$

$$\mu = \frac{y}{r} - \frac{\partial \Lambda}{\partial y} + n \frac{y}{r^2} \Lambda \quad (\text{A2.1.12})$$

$$v = \frac{z}{r} - \frac{\partial \Lambda}{\partial z} + n \frac{z}{r^2} \Lambda \quad (\text{A2.1.13})$$

This finally gives

$$\frac{1}{R_1} - \frac{1}{R_2} = \frac{2}{r} + \frac{n(n+1)}{r^2} \Lambda \quad (\text{A2.1.14})$$

therefore

$$\sigma^2 = n(n-1)(n+2) \frac{T_1}{\rho R^3} \quad (\text{A2.1.15})$$

which completes the proof.

REFERENCES

- Agarwal G. S., Jha S. S., Tsang J. C., "Surface plasmon polariton resonance factors in a classical calculation of surface-enhanced Raman scattering," *Physical Review B* **25**, 2089-2093 (1982).
- Ajayan P. M., Marks L. D., "Quasimelting and phases of small particles," *Physical Review Letters* **60**, 585-587 (1988).
- Ajayan P. M., Marks L. D., "Experimental evidence for quasimelting in small particles," *Physical Review Letters* **63**, 279-282 (1989).
- Ajayan P. M., *Phase instabilities in small particles* PhD Thesis. (Northwestern University, Evanston, 1989).
- Ajayan P. M., Marks L. D., "Phase instabilities in small particles," *Phase Transitions* **24**, 229-258 (1990).
- Ajayan P. M. and Marks L. D., "Evidence for sinking of small particles and implications for heterogeneous catalysis," *Nature* **338**, 139-141 (1989).
- Akhter P., Baig A., "Comments on Stranski-Krastanov growth of Bi and Ag on Si(100)," *Japanese Journal of Applied Physics* **30**, 11203-11203 (1991).
- Allpress J. G., Sanders J. V., "Decoration of facets on silver," *Philosophical Magazine* **9**, 645-658 (1964).
- Allpress J. G., Sanders J. V., "The structure and orientation of crystals in deposits of metals on mica," *Surface Science* **7**, 1-25 (1967).
- Altenheim C., Giorgio S., Urban J., Weiss K., "Structure of supported palladium, silver and gold clusters," *Zeitschrift fur Physik D19*, 303-306 (1991).
- Amelinckx S., Zhang X. B., Bernaerts D., Zhang X. F., Ivanov V., Nagy J. B., "A formation mechanism for catalytically grown helix-shaped graphite nanotubes,"

- Science* **265**, 635-639 (1994).
- Apai G., Hamilton J. F., Stohr J., Thompson A., "Extended X-ray absorption fine structure of small Cu and Ni clusters: Binding energy and bond length changes with cluster size," *Physical Review Letters* **43**, 165-169 (1979).
- Avery N. R., Sanders J. V., "The structure of metallic particles in dispersed catalysts," *Journal of Catalysis* **18**, 129-132 (1970).
- Badzian A. R., Badzian T., Roy R., Messier R., Spear K. R., "Crystallization of diamond crystals and films by microwave assisted CVD-II," *Materials Research Bulletin* **23**, 531-549 (1988).
- Bagley B. G., "A dense packing of hard spheres with five fold symmetry," *Nature* **208**, 674-675 (1965).
- Balerna A., Bernieri E., Picozzi P., Reale A., Santucci S., Burattini E., Mobilio S., "Extended X-ray absorption fine structure and near edge structure studies on evaporated small clusters of Au," *Physical Review* **B31**, 5058-5065 (1985).
- Barry J. C., Bursill L. A., Sanders J. V., "Electron microscope images of icosahedral and cuboctahedral (f.c.c packing) clusters of atoms," *Australian Journal of Physics* **38**, 437-448 (1985).
- Beaglehole D., "Surface melting of small particles, and the effects of surface impurities," *Journal of Crystal Growth* **112**, 663-669 (1991).
- Beck T. L., Leitner D. M., Berry R. S., "Melting and phase space transitions in small clusters: Spectral characteristics, dimensions and K entropy," *Journal of Chemical Physics* **89**, 1681-1694 (1988).
- Benson G. C., Shuttleworth R., "The surface energy of small nuclei," *Journal of Chemical Physics* **19**, 130-131 (1951).
- Bernal J. D., "The structure of liquids," *Proceedings of the Royal Society* **A280**, 299-321 (1964).
- Bernholc J., Yi J. L., Sullivan D. J., "Structural transitions in metal clusters," *Faraday Discussions of the Chemical Society* **92**, 1-12 (1991).
- Berry R. S., Jellinek J., Natanson G., "Melting of clusters and melting," *Physical Review* **A30**, 919-931 (1984).

- Blackman M., Sambles J. R., "Melting of very small particles during evaporation at constant temperature," *Nature* **226**, 38-38 (1970).
- Bond G. C., "Supported Metal Catalysts: Some unsolved problems," *Chemical Society Review* **20**, 441-475 (1991).
- Bonevich J. E., *Atomic structure and sintering behavior of ultrafine ceramic particles*. PhD Thesis. (Northwestern University, 1991).
- Bonevich, J. E., Marks, L. D., "The sintering behavior of ultrafine alumina particles" *Journal of Materials Research* **7**, 1489-1500 (1992).
- Bonevich, J. E., Marks, L. D., "The sintering behavior of ultrafine alumina particles" *Microscopy: The key research tool* **22**, 95-102 (1992).
- Bootsma G. A., Gassen H. J., "A quantitative study on the growth of silicon whiskers from silane and germane whiskers from germane," *Journal of Crystal Growth* **10**, 223-234 (1971).
- Borel J. P., "Thermodynamic size effect and the structure of metallic clusters," *Surface Science* **106**, 1-9 (1981).
- Borenztein Yves, Alameh Rakia. "The growth of Ag on Si(100)-2x1," *Applied Surface Science* **65/66**, 735-741 (1993).
- Bovin J. O., Malm J. O., "Atomic resolution electron microscopy of small metal clusters," *Zeitschrift Fur Physik* **D19**, 293-298 (1991).
- Briant C. L., Burton J. J., "Molecular dynamic study of the structure and thermodynamics of argon microclusters," *Journal of Chemical Physics* **63**, 2045-2058 (1975).
- Brodde A., Badt D., Tosch St., Neddermeyer H., "The growth of Ag films on Si(100)," *Journal of Vacuum Science and Technology* **A8**, 251-254 (1990).
- Buckett M. I., *Electron irradiation damage in transition metal oxides* PhD Thesis(Northwestern University, Evanston, 1991).
- Buffat P. A., Flueli M., Spycher R., Stadelmann P., Borel J. P., "Crystallographic structure of small gold particles studied by high resolution electron microscopy," *Faraday Discussions* **92**, 173-187 (1991).

- Buffat Ph., Borel J-P., "Size effect on the melting temperature of gold particles," *Physical Review* **B13**, 2287-2298 (1976).
- Burbank R. D., Heidenreich R. D., "Microtwinning in epitaxial nickel iron films," *Philosophical Magazine* **5**, 373-382 (1960).
- Burton J. J., "Configuration, energy, and heat capacity of small spherical clusters of atoms," *Journal of Chemical Physics* **52**, 345-352 (1970).
- Challa M. S. S., Landau D. P., Binder K., "Monte-Carlo studies of finite size effects at first order transitions," *Phase Transitions* **24-26**, 343-369 (1990).
- Chandrashekar. S, *Hydrodynamics and Hydrodynamic stability* (Oxford University press, 1961).
- Chaudhri M. M., Yoffe E. H., "The area of contact between a small sphere and a flat surface," *Philosophical Magazine* **A44**, 667-675 (1981).
- Cleveland C. L., Landman U., "The energetics and structure of nickel clusters: Size dependence," *Journal of Chemical Physics* **94**, 7376-7396 (1991).
- Couchman P. R., Karasz F. E., "The effect of particle size on Debye temperature," *Physics Letters* **A62**, 59-61 (1977).
- Couchman P. R., Jesser W. A., "Thermodynamic theory of size dependence of melting temperature in metals," *Nature* **269**, 481-483 (1977).
- Couchman P. R., Ryan C. L., "The Lindemann hypothesis and the size dependence of melting temperature," *Philosophical Magazine* **37**, 369-373 (1978).
- Cowley J. M., *Diffraction Physics* (North-Holland, New York, 1981).
- Cowley J. M., "The use of scanning transmission electron microscopes to study surfaces and small particles," in *Catalytic Materials: Relationship between structure and reactivity*, edited by T. E. Whyte, R. A. D. Betta, E. G. Derouane, R. T. K. Baker, ACS Symposium Series No. 248 (American Chemical Society, New York, 1984), pp. 353-366.
- Crescenzi M. De., Diociaiuti Lozzi, L., Picozzi P., Santucci S., "Surface electron energy loss fine structure investigation on the local structure of copper clusters on graphite." *Physical Review* **B35**, 5997-6003 (1987).

- Dahmen U., Westmacott K. H., "Observations of pentagonally twinned precipitate needles of germanium in aluminum," *Science* **233**, 875-876 (1986).
- Davis H. L., Wales D. J., Berry R. S., "Exploring potential energy surfaces with transition state calculations," *Journal of Chemical Physics* **92**, 4308-4319 (1990).
- Daw M. S., Baskes M. I., "Embedded atom method: Derivation and application to impurities, surfaces, and other defects in metals," *Physical Review* **B29**, 6443-6448 (1984).
- deWit R., "Relation between dislocations and disclinations," *Journal of Applied Physics* **42**, 3304-3308 (1971).
- de Wit R., "Partial disclinations," *Journal of Physics C. Solid State Physics* **5**, 529-534 (1972).
- Dickey J. M., Paskin A., "Phonon spectrum changes in small particles and their implications for superconductivity," *Physical Review Letters* **21**, 1441-1443 (1968).
- Dinghas A. V., "Uber einen geometrischen satz von Wulff fur die gleichgewichtsform von kristallen," *Zeitschrift fur Kristallographica* **105**, 304-314 (1944).
- Dundurs J., Marks L. D., Ajayan P. M., "Structural fluctuations in small particles," *Philosophical Magazine* **A57** (4), 605-620.
- Eaglesham D. J., Unterwald F. C., Jacobson D. C., "Growth morphology and the equilibrium shape: The role of "surfactants" in Ge/Si island formation," *Physical Review Letters* **70**, 966-969 (1993).
- Eaglesham D. J., Cerullo M., "Low temperature growth of Ge on Si(100)," *Applied Physics Letters* **58**, 2276-2278 (1991).
- Ercolessi F., Andreoni W., Tosatti E., "Melting of small gold particles - Mechanism and size effects," *Physical Review Letters* **66**, 911-914 (1991).
- Ertner W., "Laser cooling and storage of free atoms," *Physica Scripta* **36**, 306-311 (1987).
- Etters R. D., Kaelberer J., "Thermodynamic properties of small aggregates of rare gas atoms," *Physical Review* **A11**, 1068-1079 (1975).

- Etters R. D., Kaelberer J., "On the character of melting transitions in small atomic aggregates," *Journal of Chemical Physics* **66**, 5112-5116 (1977).
- Farges J., de Feraudy M. F., Raoult B., Torchet G., "Non-crystalline structure of argon clusters-I: Polyicosahedral structure of Ar_N clusters," *Journal of Chemical Physics* **78**, 5067-5080 (1983).
- Farges J., de Feraudy M. F., Raoult B., Torchet G., "Surface arrangements on multilayer icosahedra," in *Dynamics of Surfaces*, edited by B. Pullman et al (1984), pp. 425-430.
- Fisher S. B., "On the temperature rise in electron irradiated foils.," *Radiation effects* **5**, 239-243 (1970).
- Fleischmann M., Handra P. J., McQuillan A. J., "Raman spectra of pyridine adsorbed at a silver electrode," *Chemical Physics Letters* **26**, 163-166 (1974).
- Flueli M., Borel J. P., "Surface energy anisotropy measurements on a small cuboctahedron of gold observed by high resolution electron microscopy (HREM)," *Journal of Crystal Growth* **91**, 67-70 (1988).
- Flueli M., Buffat P. A., Borel J. P., "Real time observation by high resolution electron microscopy (HREM) of the coalescence of small gold particles in the electron beam," *Surface Science* **202**, 343-353 (1988).
- Flueli M., Spycher R., Stadelmann P., Buffat P. A., Borel J. P., "Determination par microscopie électronique a haute résolution de la structure de petites particules d'or: Observations et simulation d'images," *Journal of Microscopy, Spectroscopy and Electronics* **14**, 351-364 (1989).
- Frank J., "The role of correlation techniques in computer image processing," in *Computer techniques for image processing*, edited by W. O. Saxton (Springer-Verlag, New York, 1978), pp. 187-222.
- Fukano Y., Wayman C. M., "Shapes of nuclei of evaporated fcc metals," *Journal of Applied Physics* **40**, 1656-1664 (1969).
- Gai P. L., Goringe M. J., Barry J. C., "HREM image contrast from supported small metal particles," *Journal of Microscopy* **142**, 9-24 (1986).
- Gale B. and Hale K. F., "Heating of metallic foils in an electron microscope," *British journal of applied physics* **12**, 115-117 (1961).

- Garrigos R., Kofman R., Cheyssac P., Peerin M. Y., "Optically monitored melting supercooling and solidification of lead aggregates embedded in a dielectric matrix," *Europhysics Letters* **1**, 355-360 (1986).
- Gedwill M. A., Altstelter C. J., Wayman C. Y., "External symmetry of Cobalt particles produced by hydrogen reduction of CoBr_3 ," *Journal of Applied Physics* **35**, 2266-2267 (1964).
- Gibbs J. W., "On the equilibrium of heterogeneous substances," in *The scientific papers of J. W. Gibbs*, edited by H. A. Bumstead, R. G. Van Name (Longmans Green, New York, 1906), pp. 55-349.
- Gillet E., Gillet M., "Croissance continue, a partir de germes a symetrie quinaire des cristallites "multiples" formes lors de la nucleation heterogene," *Journal of Crystal growth* **13/14**, 212-216 (1972).
- Gillet M., "Structure of small metallic particles," *Surface Science* **67**, 139-157 (1977).
- Giorgio S., Chapon C., Henry C. R., Nihoul G., Penisson J. M., *Philosophical Magazine* **A64**, 87 (1991).
- Giorgio S., Nihoul G., Urban J., Sack-Kongehl H., "Structures and defects of Au particles (1-3nm) by HREM," *Zeitschrift fur Physik* **D24**, 395-400 (1992).
- Giorgio S., Chapon C., Henry C. R., Nihoul G., "High-resolution transmission electron microscopy studies of structural deformations at the interface between Pd particles and MgO surfaces," *Philosophical Magazine* **B67**, 773-785 (1993).
- Givargizov F. I., "Fundamental aspects of VLS growth," *Journal of Crystal Growth* **31**, 20-30 (1975).
- Gordon M. B., Cyrot-Lackmann F., Desjonqueres M. C., "Relaxation and stability of small transition metal particles," *Surface Science* **80**, 159-164 (1979).
- Green A. K., Dancy J., Bauer E., "Insignificance of lattice misfit for epitaxy," *The Journal of Vacuum Science and Technology* **7**, 159-163 (1969).
- Griffin G. L., Andres R. p., "Microscopic capillary approximation: free energies of small clusters," *Journal of Chemical Physics* **71**, 2522-2530 (1979).
- Gryaznov V. G., Kaprelov A. M., Belov Yu. A., "Real temperature of nanoparticles in electron microscope beams," *Philosophical Magazine Letters* **63** (5), 275-279

(1991).

- Gryaznov V. G., Trusov L. I., "Size effects in micromechanics of nanocrystals," *Progress in Materials Science* **37**, 289-401 (1993).
- Halicioglu T., White P. J., "Structures of microclusters: an atomistic approach with three body interactions," *Surface Science* **106**, 45-50 (1981).
- Hall M. J., Thompson M. W., "Epitaxy and twinning in foils of some noble metals condensed upon lithium fluoride and mica," *British Journal of Applied Physics* **12**, 495 (1961).
- Hall C. R., Fawzi S. A. H., "On the occurrence of multiply twinned particles in electrodeposited nickel films," *Philosophical Magazine* **A54**, 805-820 (1986).
- Hall B. D., Flueli M., Monot R., Borel J. P., "Multiply twinned structures in unsupported ultrafine silver particles observed by electron diffraction," *Physical Review* **B43**, 3906-3917 (1991).
- Haluska M., Kuzmany H., Vybornov M., Rogi P., Fejdi P., "A double temperature gradient technique for the growth of single crystal fullerites from the vapor phase," *Applied Physics* **A56**, 161-167 (1993).
- Hanawa T., Oura K., "Deposition of Ag on Si(100) surfaces as studied by LEED-AES," *Japan Journal of Applied Physics* **16**, 519-520 (1977).
- Hanbucken M., Neddermeyer H., Rupieper P., "Low energy electron diffraction, auger electron spectroscopy and angle resolved photoemission from silver films on Si(100) and Si(111)," *Thin Solid Films* **90**, 37-42 (1982).
- Hanbucken M., Futamoto M., Venables J. A., "Nucleation, growth and the intermediate layer in Ag/Si(100) and Ag/Si(111)," *Surface Science* **147**, 433-450 (1984).
- Hanbucken M., Lay Le G., "Formation of noble-metal-Si(100)interfaces," *Surface Science* **168**, 122-132 (1986).
- Hardeveld R. V., Montfoort A. V., "The influence of crystallite size on the adsorption of molecular nitrogen on nickel, palladium and platinum: an infrared and electron-microscopic study," *Surface Science* **4**, 396-430 (1966).
- van Hardeveld R., Hartog F., "The statistics of surface atoms and surface sites on metal crystals," *Surface Science* **15**, 189-230 (1969).

- Hasegawa M., Hoshino K., Watabe M., "A theory of melting in metallic small particles," *Journal of Physics. F: Metal Physics* **10**, 619-635 (1980).
- Hashizume T., Hamers R. J., Demuth J. E., Markert K., "Initial stage deposition of Ag on the Si(100)2x1 surface studied by scanning tunneling microscopy," *Journal of Vacuum science and technology A* **8**, 249-250 (1990).
- Hayashi M., Tamura I., Fukano Y., and Kanemaki S., "Mossbauer effect in small iron particles," *Surface Science* **106**, 453-458 (1981).
- Heinemann K., Yacaman M. J., Yang C. Y., and Poppa H., "The structure of small vapor deposited particles, I. experimental study of single crystals and particles with pentagonal profiles," *Journal of Crystal Growth* **47**, 177-186 (1979).
- Heinemann K., Osaka T., Poppa H., Avalos-Borja M., "In-situ TEM studies of Pd on MgO," *Journal of Catalysis* **83**, 61-78 (1983).
- Herring C., "Some theorems on the free energies of crystal surfaces," *Physical Review* **82**, 87-93 (1951).
- Herring C., "Surface tension as a motivation for sintering," in *The physics of powder metallurgy*, edited by W. E. Kingston (Mcgraw-Hill, 1951), pp. 143-164.
- Herring C., "The use of classical macroscopic concepts in surface free energy problems," in *Structure and properties of solid surfaces*, edited by R. Gomer, C. S. Smith (University of Chicago press, 1953), pp. 5-72.
- Heyraud J. C., Metois J. J., "Establishment of the equilibrium shape of metal crystallites on a foreign substrate: Gold on graphite," *Journal of Crystal Growth* **50**, 571-574 (1980).
- Heyraud J. C., Metois J. J., Bermond J. M., "Equilibrium shapes of microcrystals," *Journal of Crystal Growth* **98**, 355-362 (1989).
- Heyraud J. C., Metois J. J., "Equilibrium shape of gold crystallites on a graphite cleavage surface: Surface energies and interfacial energy," *Acta Metallurgica* **28**, 1789-1797 (1980).
- Hilton H., *Mathematical Crystallography* (Oxford, Oxford, 1903).
- Hirth J. P., Lothe J., *Theory of Dislocations* (John Wiley, New York, 1982).

- Hoare M. R., Pal P., "Physical cluster mechanics: statics and energy surfaces for monoatomic systems," *Advances in Physics* **20**, 161-196 (1971).
- Hoare M. R., Pal P., "Statistics and stability of small assemblies of atoms," *Journal of Crystal Growth* **17**, 77-96 (1972).
- Hoare M. R., "Structure and dynamics of simple microclusters," *Advances in Chemical Physics* **40**, 48-135 (1979).
- Hofmeister H., Bardamid A. F., Junghanns T., Nepijko S. A., "Crystalline particles with multiply twinned structure in amorphous films of germanium," *Thin Solid Films* **205**, 20-24 (1991).
- Honeycutt J. D., Anderson H. C., "Molecular dynamic study of melting and freezing of small Lennard-Jones clusters," *Journal of Chemical Physics* **91**, 4950-4963 (1987).
- Honjo G., Takayanagi K., Kobayashi K., Yagi K., "On cluster mobilities in nucleation and growth processes of epitaxial thin films," *Physica Status Solidi* **55**, 353-367 (1979).
- Howie A., Marks L. D., "Elastic strains and the energy balance for multiply twinned particles.," *Philosophical Magazine* **A49**, 95-109 (1984).
- Howie A., "Coulomb explosions in metals?," *Nature* **320**, 684-684 (1986).
- Hull D., Bacon D. J., *Introduction to dislocations* (Pergamon press, New York, 1984).
- Hultgren R., Desai P. R., Hawkins D. T., Gleiser M., Kelley K. K., Wagman D. D., *Selected values of the thermodynamic properties of the elements* (American Society for Metals, Metals Park, Ohio, 1973).
- Iijima S., "Observations of single and clusters of atoms in bright field microscopy," *Optik* **48**, 193-214 (1977).
- Iijima S., Ichihashi T., "Structural instability of ultrafine particles of metals," *Physical Review Letters* **56**, 616-619 (1986).
- Iijima S., "Fine particles of silicon. II. Decahedral multiply twinned particles," *Japanese Journal of Applied Physics* **26**, 365-372 (1987).
- Iijima S., "Helical microtubules of graphitic carbon," *Nature* **354**, 56-58 (1991).

- Iijima S., "Fine particles of silicon. I. Crystal growth of spherical particles of Si," *Japanese Journal of Applied Physics* **26**, 357-364 (1987).
- Ino S., "Epitaxial growth of metals on rocksalt faces cleaved in vacuum II - Orientation and structure of gold particles formed in ultrahigh vacuum," *Journal of the Physical Society of Japan* **21**, 346-362 (1966).
- Ino S., "Stability of multiply twinned particles," *Journal of the Physical Society of Japan* **27**, 941-953 (1969).
- Itoh N., Tanimura K., "Radiation effects in ionic solids," *Radiation effects* **98**, 269-287 (1986).
- Jayaram G., Xu P., Marks L. D., "Structure of Si(100)-(2x1) surface using UHV transmission electron diffraction," *Physical Review Letters* **71**, 3489 - 3492 (1993).
- Johnson K. L., Kendall K., Roberts A. D., "Surface energy and the contact of elastic solids," *Proceedings of the royal society of London* **A324**, 301-313 (1971).
- Kamino T., Tomita M., Ohtsuka I., Saka H., "High resolution transmission electron microscopy observation of the motion of a surface dislocation on a gold particle," *Physica Status Solidi* **122**, K105-K108 (1990).
- Karlan A., Tholen A. R., "On the motion of ultrafine particles in the electron microscope," in *Institute of Physics Conference. No 93* (1988), Vol. 2, pp. 373-374.
- Keene B. J., "Review of data for the surface tension of pure metals," *International Metals Review* **38**, 157-192 (1993).
- Khlyustikov I. N., Buzdin A. I., "Twinning-plane superconductivity," *Advances in Physics* **36**, 271-329 (1987).
- Kimura K., "The effect of shape and size on the electronic properties of ultrafine metallic particles," *Phase Transitions* **24-26**, 493-527 (1990).
- Kimura Y., Takayanagi K., "Freezing of the 2x1 structure at commensurate Ag(100)-Si(100) interface," *Surface Science* **276**, 166-173 (1992).
- Kirkland A. I., Jefferson D. A., Tang D., Edwards P. P., "High resolution image simulations of small metal particles," *Proceedings of the Royal Society of London* **A434**, 279-296 (1991).

- Kizuka T., Kachi T., Tanaka N., "Effect of interface on structural fluctuation in gold clusters fixed on MgO rods," *Zeitschrift fur Physik D26*, S58-60 (1993).
- Knight W. D., Clemenger K., de Heer W. A., Saunders W. A., Chou M. Y., Cohen M. L., "Electronic shell structure and abundance of sodium clusters," *Physical Review Letters* **52**, 2141-2143 (1984).
- Komoda T., "Electron microscopic observation of crystal lattices on the level with atomic dimension," *Japanese Journal of Applied Physics* **5**, 603-607 (1966).
- Komoda T., "Study on the structure of evaporated gold particles by means of a high resolution electron microscope," *Japanese Journal of Applied Physics* **7**, 27-30 (1968).
- Kosterlitz J. M., Thouless D. J., "Ordering, metastability and phase transitions in two dimensional systems," *Journal of Physics C: Solid State Physics* **6**, 1181-1203 (1973).
- Kristyan Sandor, Olson John A., "A possible role of the surface free enthalpy excess of solid chemical elements in their melting and critical temperatures," *Surface science letters* **255**, L562-L570 (5 June, 1991).
- Kroto H. W., Heath J. R., O'Brian S. C., Curl R. F., Smalley R. E., " C_{60} : Buckminsterfullerene," *Nature* **318**, 162-163 (1985).
- Kubo R., "Electronic properties of metallic fine particles," *Journal of the Physical Society of Japan* **17**, 975-986 (1962).
- Lamb. H., "Hydrodynamics," (Cambridge, 1932).
- Laue M. V., "Der Wulffsche satz fur die gleichgewichtsform von kristallen," *Zeitschrift fur Kristallographica* **105**, 124-133 (1943).
- Legoues F. K., Liehr M., Renier M., Krakow W., "Microstructure of epitaxial Ag/Si(111) and Ag/Si(100) interfaces," *Philosophical Magazine* **B57**, 179-189 (1988).
- Lewis J., Smith D. J., "Structural rearrangements in small gold particles," *Proceedings of the 47th Annual Meeting of EMSA*, 640-641 (1989).
- Liebmann H., "Der Curie-Wulff'sche satz uber combinations-formen von krystallen," *Zeitschrift fur Kristallographica* **53**, 171-177 (1914).

- Lin X. F., Wan K. J., Nogami J., "Ag on Si(001): Growth behavior of the annealed surface," *Physical Review* **B47**, 10947-10950 (1993).
- Lin X. F., Wan K. J., Nogami J., "Ag on the Si(001) surface: Growth of the first monolayer at room temperature," *Physical Review* **B47** (20), 13491-13497 (1993).
- Linford R. G., *Solid State Surface Science II* (Marcel Dekker, 1973), pp. 1.
- Luo Frank C. H., Hembree Gary G., Venables John A., "Initial growth of Ag/Si(100) studied with high spatial resolution AES and SEM," *Materials Research Society symposium proceedings* **202**, 49-54 (1991).
- Mackay A. L., "A dense non-crystallographic packing of equal spheres," *Acta Crystallographica* **15**, 916-918 (1962).
- Malm J. O., Bovin J. O., Petford-Long A. K., Smith D. J., "Real time atomic-resolution imaging of polymorphic changes in ruthenium clusters," *Angewandte Chemie* **27**, 555-558 (1988).
- Marcus M. A., Andrews M. P., Zegenhagen J., Bommanavar A. S., Montano P., "Structure and vibrations of chemically produced Au₅₅ clusters," *Physical Review* **B42**, 3312-3316 (1990).
- Marks L. D., "Imaging small particles," *Ultramicroscopy* **18**, 445-452 (1985).
- Marks L. D., Howie A., "Multiply twinned particles in silver catalysts," *Nature* **282**, 196 (1979).
- Marks L. D., *The structure of small silver particles*. PhD Thesis (Cambridge, England, 1980).
- Marks L. D., Smith D. J., "High resolution studies of small particles of gold and silver. I. Multiply twinned particles," *Journal of Crystal Growth* **54**, 425-438 (1981).
- Marks L. D., "Modified Wulff constructions for twinned particles," *Surface Science* **61**, 556-565 (1983).
- Marks L. D., Smith D. J., "Direct surface imaging in small metal particles," *Nature* **303**, 316-317 (1983).
- Marks L. D., Smith D. J., "HREM and STEM defects in multiply twinned particles," *Journal of Microscopy* **130**, 249-261 (1983).

- Marks L. D., "Surface structure and energetics of multiply twinned particles," *Philosophical Magazine A* **49**, 81-93 (1984).
- Marks L. D., "Particle size effects on Wulff constructions," *Surface Science* **150**, 358-366 (1985).
- Marks L. D., "Inhomogeneous strains in small particles," *Surface Science* **150**, 302-318 (1985).
- Marks L. D., "High resolution electron microscopy of surfaces," in *Structure and Dynamics of surfaces: Topics in current physics*, edited by W. Schommers, P. V. Blackenbagen (Springer-Verlag, New York, 1986), Vol. 41, pp. 71-109.
- Marks L. D., "Solid-like growth," *Thin Solid Films* **136**, 309-315 (1986).
- Marks L. D., *Lecture Notes on HREM* (Northwestern University, Chicago, 1990).
- Marks L. D., Zhang J. P., "Is there an electron wind?," *Ultramicroscopy* **41**, 419-422 (1992).
- Marks L. D., "Experimental studies of small particle structures," *Reports of progress in physics* **57**, 603-649 (1994).
- Marks L. D., Doraiswamy N., "Structural fluctuations in small particles," in *Phase transitions and adsorbate restructuring at metal surfaces*, edited by D. A. King, D. P. Woodruff, The Chemical Physics of Solid Surfaces, vol. 7 (Elsevier, New York, 1994), Vol. 7, pp. 443-464.
- Marks L. D., 1995 (in preparation).
- Martins J. L., Car R., Buttet J., "Variational spherical model of small metallic particles," *Surface science* **106**, 265-271 (1981).
- Matsubara T., Iwase Y., Momikita A., "Theory of anharmonic lattice vibration in metallic fine particles," *Progress in Theoretical Physics* **58**, 1102-1113 (1977).
- Matsuoka H., Hirokawa T., Matsui M., Doyama M., "Solid-Liquid transitions in Argon clusters," *Physical Review Letters* **69**, 297-300 (1992).
- Matthews J. W., Allinson D. L., "A mechanism for the formation of twins in evaporated fcc metal films," *Philosophical Magazine* **8**, 1283-1303 (1963).

- McGinty D. J., "Vapor phase homogeneous nucleation and the thermodynamic properties of small clusters of Argon atoms," *Journal of Chemical Physics* **55**, 580-588 (1971).
- Melmed A. J., Hayward D. O., "On the occurrence of five fold rotational symmetry in metal whiskers," *Journal of Chemical Physics* **31**, 545-546 (1959).
- Metois J. J., Spiller G. D. T., Venables J. A., "Lead on Graphite: Equilibrium shape, crystal growth, melting and the early stages of oxidation," *Philosophical Magazine A* **46**, 1015-1022 (1982).
- Miller C. A. and Scriven L. E., "The oscillations of a fluid droplet immersed in another fluid," *Journal of Fluid Mechanics* **32**, 417-435 (1968).
- Mitome M., Tanishiro Y., Takayanagi K., "On the structure and stability of small metal particles: high resolution UHV electron microscope study," *Zeitschrift Fur Physik* **D12**, 45-51 (1989).
- Mitome M., Takayanagi K., "Commensurate reconstruction on a (001) facet of a gold particle," *Physical Review* **B42**, 7238-7241 (1990).
- Mizushima S., "Dislocation model of liquid structure," *Journal of the Physical Society of Japan* **15**, 71-77 (1960).
- Montano P. A., Shenoy G. K., Alp E. E., Schulze W., Urban J., "Structure of Copper microclusters isolated in solid Argon," *Physical Review Letters* **56**, 2076-2079 (1986).
- Murphy S. M., "Kinetic theory of diffusion in the presence of irradiation," *Philosophical Magazine* **59**, 1163-1179 (1989).
- Narayanaswamy D., Marks L. D., "Transformations in quasimelting," *Zeitschrift fur Physik* **D26**, S70-72 (1993).
- Natanson G., Amar F., Berry R. S., "Melting and surface tension in microclusters," *Journal of Chemical Physics* **78**, 399-408 (1983).
- Hanbucken M., Neddermeyer H., "A LEED-AES study of the growth of Ag films on Si(100)," *Surface Science* **114**, 563-573 (1982).
- Nepijko S. A., Styopkin V. I., Hofmeister H., Scholtz R., "Defects in multiply twinned particles," *Journal of Crystal Growth* **76**, 501-506 (1986).

- Nihoul G, "Theoretical image-processing of simulated supported particles (1-3nm)," *Microscopy Microanalysis Microstructures* **3**, 71-81 (1992).
- Nimtz G., Marquardt P., Weiss W., "Raoult's law and melting point depression in mesoscopic systems," *Science* **242**, 1671-1672 (1989).
- Nishimori K., Tokutaka H., Tamon T., Kishida S., Ishihara N., "A RHEED study of the initial growth of Ag on the Si(001) surface," *Surface Science* **242**, 157-161 (1991).
- Nishioka K., Sawyer R., Bienenstock A., Pound G. M., "Replacement partition function for small crystals in homogeneous nucleation theory," *Journal of Chemical Physics* **55**, 5082-5094 (1971).
- Ogawa S., Ino S., "Particular structures of thin epitaxial crystals," in *Advances in epitaxy and endotaxy: Physical problems of epitaxy*, edited by H. G. Schneider, R. Volker (VEB Deutscher Verlag für Grundstoffindustrie, Leipzig, 1971), pp. 183-217.
- Ogburn F., Paretzkin B., Peiser H. S., "Pseudopentagonal twins in electrodeposited copper dendrites," *Acta Crystallographica* **17**, 774-775 (1964).
- Ozaki Y., Ichihashi M., Kondow T., "Spheroidal and torsional vibrations of nearly spherical Ar clusters calculated by molecular dynamics," *Chemical Physics Letters* **188**, 555-559 (1992).
- Pashley D. W., Stowell M. J., Jacobs M. H., and Law T. J., "The growth and structure of gold and silver deposits formed by evaporation inside an electron microscope," *Philosophical Magazine* **10**, 127-158 (1964).
- Pashley D. W., "The nucleation, growth, structure and epitaxy of thin surface films," *Advances in Physics* **14**, 327-416 (1965).
- Patil A. N., Paithankar D. Y., Otsuka N., Andres R. P., "The minimum-energy structure of nanometer-scale gold clusters," *Zeitschrift für Physik* **D26**, 135-137 (1993).
- Penisson J. M., Renou A., "Structure of an icosahedral palladium particle," *Journal of Crystal Growth* **102**, 585-591 (1990).
- Pennycook S. J., Howie A., Shannon M. D., Whyman R., "Characterization of supported catalysts by high resolution STEM," *Journal of Molecular Catalysis* **20**, 345-355 (1983).

- Raoult B., Farges J., Feraudy M. F. De., Torchet G., "Comparison between icosahedral, decahedral and crystalline Lennard-Jones models containing 500 to 6000 atoms," *Philosophical Magazine* **B60**, 881-906 (1989).
- Reid. W. H, "The oscillations of a viscous liquid drop," *Quarterly applied mathematics* **18**, 86-89 (1960).
- Reimer L., *Transmission electron microscopy* (Springer-Verlag, New York, 1993).
- Reinhard D., Hall B. D., Ugarte D., Monot R., "Structure of free ultrafine silver particles, studied by electron diffraction: observation of large icosahedra ," *Zeitschrift fur Physik* **D26**, S76-78 (1993).
- Reinhard D., Berthoud P., Ugarte D., Hall B. D., Monot R., "Free clusters of Cu atoms: a study of structural size effects using high energy electron diffraction," *Physics of low dimensional structures* **1**, 59-66 (1994).
- Renou A., Gillet M., "Growth of Au, Pt and Pd particles in a flowing argon system: Observations of decahedral and icosahedral structures," *Surface Science* **106**, 27-34 (1981).
- Renou A., Rudra A., "Epitaxial growth of thin monocrystalline MgO substrates: Transmission electron microscope characterization of palladium deposits," *Surface Science* **156**, 69-84 (1985).
- Retchkiman. P. S., Gomez A., Polo G. V., Yacaman M. J., "Microdiffraction and lattice resolution studies of fivefold symmetry gold particles," *Journal of Vacuum Science and Technology* **A2**, 22-28 (1984).
- Rez P., Glaisher R. W., "Measurement of energy deposition in transmission electron microscopy," *Ultramicroscopy* **35**, 65-69 (1991).
- Rimai D. S., Demejo L. P., Bowen R. C., "Adhesion induced deformations of polymeric substrates: particle size dependence of the contact area," *Journal of Applied Physics* **66**, 3574-3578 (1989).
- Ross J., Andres R. P., "Melting temperature of small clusters," *Surface Science* **106**, 11-17 (1981).
- Saito Y., Yatsuya S., Mihama K., Uyeda R., "Multiply twinned particles of Germanium - A supplement to the formation of ultrafine particles by gas evaporation techniques," *Japan Journal of Applied Physics* **17**, 1149-1149 (1978).

- Samsavar A., Miller T., Chiang T.-C., "Determination of the bonding and growth of Ag on Si(100)-(2x1)," *Physical Review* **B38**, 9889-9894 (1988).
- Samsavar A., Hirschorn E. S., Leibsle F. M., Chiang T.-C., "Scanning-Tunnelling-Microscopy studies of Ag on Si(100)-(2x1)," *Physical Review Letters* **63**, 2830-2833 (1989).
- Saxton W. O., Smith D. J., "The determination of atomic positions in high resolution electron micrographs," *Ultramicroscopy* **18**, 39-48 (1985).
- Stephanopoulos M. F., Wong S., Schmidt L. D., "Surface Morphology of Platinum Catalysts," *Journal of Catalysis* **49**, 51-82 (1977).
- Searcy A. W., "The influence of molecular motions on the stabilities and shapes of solid particles," *Journal of Chemical Physics* **81**, 2489-2491 (1984).
- Self P. G., O'Keefe M. A., *High resolution transmission electron microscopy and associated techniques*, edited by P. R. Buseck, J. M. Cowley, L. Eyring (Oxford University Press, New York, 1988).
- Shirokoff J., Erb U., "The role of interfacial energy in the development of preferred orientations of silver on silicon," *Philosophical Magazine Letters* **58**, 255-260 (1988).
- Skriver H. L., Rosengaard N. M., "Surface energy and work function of elemental metals," *Physical Review* **B46**, 7157-7168 (1992).
- Smith D. J., Marks L. D., "Direct lattice imaging of small metal particles," *Philosophical Magazine* **A44**, 735-740 (1981).
- Smith D. J., Petford-Long A. K., Wallenberg L. R., Bovin J. O., "Dynamic atomic-level rearrangements in small gold particles," *Science* **233**, 872-875 (1986).
- Solliard C., Buffat Ph., Faes F., "Equilibrium structure of small gold crystals," *Journal of Crystal Growth* **32**, 123-125 (1976).
- Solliard C., "Structure and strain of the crystalline lattice of small gold and platinum particles," *Surface Science* **106**, 58-63 (1981).
- Solliard C., Flueli M., "Surface stress and size effect on the lattice parameter in small particles of gold and platinum," *Surface Science* **156**, 487-489 (1985).

- Spence J. C. H., *Experimental high-resolution electron microscopy* (Oxford University Press, Oxford, 1988).
- Stephanopoulos M. F., Schmidt L. D., "Morphology and etching processes on macroscopic metal catalysts," *Progress in Surface Science* **9**, 83-111 (1979).
- Stillinger F. H., Stillinger D. K., "Computational study of transition dynamics in 55-atom clusters," *Journal of Chemical Physics* **93**, 6013-6024 (1990).
- Sawada S., Sugano S., "Theory of the structural fluctuation of Au₅₅ clusters," *Zeitschrift für Physik* **D20**, 259-261 (1991).
- Takagi M., "Electron diffraction study of liquid-solid transition of thin metal films," *Journal of the Physical Society of Japan* **9**, 359-363 (1954).
- Takayanagi K., "Critical surface reconstruction of mesoscopic particles," *Progress of Theoretical Physics* **106**, 249-255 (1991).
- Tholen A. R., "Vibrations and martensitic transformation in small cobalt particles," *Surface Science* **106**, 70-78 (1981).
- Tholen A. R., "Martensitic transformation in small cobalt particles," *Philosophical Magazine* **A53**, 259-276 (1986).
- Trinh. E, Zwern. A, and Wang. T. G, "An experimental study of small-amplitude drop oscillations in immiscible liquid systems," *Journal of Fluid Mechanics* **115**, 453-474 (1982).
- Tsamopoulos J. A. and Brown R. A., "Nonlinear oscillations of inviscid drops and bubbles," *Journal of Fluid Mechanics* **127**, 519-537 (1983).
- Uppenbrink J., Wales D. J., "Structure and energetics of model metal clusters," *Journal of Chemical Physics* **96**, 8520-8534 (1992).
- Uyeda R., "Studies of ultrafine particles in Japan - Crystallography - Methods of preparation and technological applications," *Progress in Materials Science* **35** (1), 1-96 (1991).
- Valkealahti S., Manninen M., "Instability of cuboctahedral copper clusters," *Physical Review* **B45**, 9459-9461 (1992).
- Vlachos D. G., Schmidt L. D., Aris R., "Structures of small metal clusters. I. Low

- temperature behavior," *Journal of Chemical Physics* **96**, 6880-6889 (1992).
- Wales D. J., Berry R. S., "Melting and freezing of small argon clusters," *Journal of Chemical Physics* **92**, 4283-4295 (1990).
- Wales D. J., Berry R. S., "Freezing, melting, spinodals and clusters," *Journal of Chemical Physics* **92**, 4473-4482 (1990).
- Wales D. J., "Transition states for Ar₃₅," *Chemical Physics Letters* **166**, 419-424 (1990).
- Wallenberg L. R., Bovin J. O., Petford-Long A. K., Smith D. J., "Atomic-resolution study of structural rearrangements in small platinum crystals," *Ultramicroscopy* **20**, 71-76 (1986).
- Wallenberg L. R., *Atomic imaging in real time of small clusters: a high resolution electron microscopy study* (Lund University, Lund, 1987).
- Wang S. W., Falicov L. M., Searcy A. W., "The equilibrium shapes of small particles," *Surface Science* **143**, 609-625 (1984).
- Wang T., Lee C., Schmidt L. D., "Shape and orientation of supported Pt particles," *Surface Science* **163**, 181-197 (1985).
- Weeks J. D., Saarloos W. V., Bedeaux D., Blokhuis E., "Consistency of capillary wave theory in three dimensions: Divergence of the interface width and agreement with density functional theory," *Journal of Chemical Physics* **91**, 6494-6504 (1989).
- Weitering H. H., Sullivan J. P., Carolissen R. J., Graham W. R., Tung R. T., "Electrical characteristics of silver/silicon contacts," *Applied Surface Science* **70/71**, 422-427 (1993).
- Wentorf R. H., *The art and science of growing crystals* (Wiley, New York, 1963).
- Werfelmeier W., "Ein geometrisches modell des atomkerns," *Zeitschrift fur Physik* **107**, 332-346 (1937).
- Williams P., "Motion of small gold clusters in the electron microscope," *Applied Physics Letters* **50**, 1761-1763 (1987).
- Winau D., Itoh H., Schmid A. K., Ichinokawa T., "Reconstructions and growth of Ag on Si(001)(2x1)," *Surface Science* **303**, 139-145 (1994).

- Winterbottom W. L., "Equilibrium shape of a small particle in contact with a foreign substrate," *Acta Metallurgica* **15**, 303-310 (1967).
- Woltersdorf J., Nepijko A. S., Pippel E., "Dependence of the lattice parameters of small particles on the size of the nuclei," *Surface Science* **106**, 64-69 (1981).
- Wulff G., "Zur frage der geschwindigkeit des wachstums und der auflösung der krystallflächen," *Zeitschrift für Kristallographica* **34**, 449-531 (1901).
- Xu P., Dunn D., Zhang J. P., Marks L. D., "Atomic imaging of surfaces in plan view," *Surface Science Letters* **285**, L479-L485 (1993).
- Yacaman M. J., Heinemann K., Yang C. Y., and Poppa H., "The structure of small vapor deposited particles. II. experimental study of particles with hexagonal profile," *Journal of Crystal Growth* **47**, 187-195 (1979).
- Yacaman M. J., Dominguez J. M., "Characterization of small platinum particles supported on graphite by electron microscopy," *Journal of Catalysis* **64**, 213-222 (1980).
- Yacaman M. J., Herrera R., Tehuacanero S., and Retchkiman P. S., "Decagonal and hexagonal structures in small gold particles," *Surface Science* **237**, 248-256 (1990).
- Yagi K., Takayanagi K., Kobayashi K., Honjo G., "In-situ observations of growth processes of multiply twinned particles," *Journal of Crystal growth* **28**, 117-124 (1975).
- Yang C. Y., "Crystallography of decahedral and icosahedral particles. I. Geometry of twinning," *Journal of Crystal Growth* **47**, 274-282 (1979).
- Yang C. Y., Yacaman M. J., Heinemann K., "Crystallography of decahedral and icosahedral particles. II. High symmetry orientations," *Journal of Crystal Growth* **47**, 283-290 (1979).
- Yeongcheol K., Plass R., Doraiswamy N., (private communications).
- Yokozeiki A., Stein G. D., "A metal cluster generator for gas-phase electron diffraction and its application to bismuth, lead, and indium: Variation of the microcrystal structure with size," *Journal of Applied Physics* **49**, 2224-2232 (1978).
- Miki-Yoshida M., Tehuacanero S., Jose-Yacaman M., "On the high temperature

coalescence of metallic nanocrystals," *Surface Science Letters* **274**, L569-L576 (1992).



3 5556 025 840 927